Investigation of Neuropeptidomics and Proteomics by Multifaceted Approaches Coupled to Mass Spectrometry

by

Shan Jiang

A dissertation submitted in partial fulfillment of

the requirements for the degree of

Doctor of Philosophy

(Pharmaceutical Sciences)

at the

UNIVERSITY OF WISCONSIN-MADISON

2016

Date of final oral examination: 10/27/2016

The dissertation is approved by the following members of the Final Oral Committee:

Li, Lingjun, Professor, Pharmacy, Chemistry

Burnette, Ronald R, Professor, Pharmacy

Bugni, Timothy S, Associate Professor, Pharmacy

Smith, Lloyd, Professor, Pharmacy

Thorne, Robert G, Assistant Professor, Pharmacy

Acknowledgements

I would like to gratefully acknowledge my advisor Lingjun Li. Her expertise and enthusiasm in academic research have significantly inspired and encouraged me to explore on the unknown world of science. Dr. Li has given me the freedom and tremendous support to achieve my professional and future career goals. I would like to deeply thank her for taking me as a graduate student in her lab. I felt so lucky to had this opportunity to work for her and grow to be an independent scientist under her guidance. She has been incredibly supportive whenever I want to try new ideas or come across bottlenecks over the past five years. Not only mentoring me in the professional way, Dr. Li has also been considerate at a personal level. It has been an honor to work with Dr. Li, and hereby I thank with my heart for her support throughout my graduate career.

I would like to thank my thesis committee members: Prof. Ronald Burnette, Prof. Tim Bugni, Prof. Robert Thorne and Prof. Lloyd Smith, for spending time, providing feedbacks of my preliminary research, and assisting with my future career out of their busy schedules.

I would like to acknowledge my collaborators Aaron Zhang in Prof. Tom Martin's lab, Loren Stallop in Prof. David Beebe's lab and visiting scholar Prof. Wei Wang. Collaborating with people outside my department greatly broads my mindset. I would like to acknowledge the Li Lab collaborators: Dr. Zichuan Zhang, Dr. Zhidan Liang, and Ling Hao who have contributed to this thesis work. Special thanks to Dr. Zichuan Zhang, who trained me many lab techniques in my first year in the group. Other lab members Dr. Jingxin Wang, Dr. Erin Gemperline, Dr. Xuefei Zhong, Qing Yu, Bingming Chen and Jillian Johnson have provided training, discussion on problems, talking about ideas, and help making a good lab environment.

I would like to thank Dr. Cameron Scarlett and Molly Pellitteri-Hahn of Analytical Instrumentation Center in the School of Pharmacy for maintaining instruments and trouble shooting problems.

Finally, I would like to thank my family and friends for giving me unconditional love and support, especially my parents Zitao Jiang and Rong Li and my fiance Xingmin Zhang. Without their continuous love and emotional accompanies over these years I can't accomplish my graduate career. I am grateful for their love and encouragement and having all my family and friends in my life.

Table of Contents

Investigation of neuropeptidomics and proteomics by multifaceted approaches coupled to mass spectrometry

Shan Jiang

Under the supervision of Professor Lingjun Li

At the University of Wisconsin-Madison

Abstract

In recent decades, mass-spectrometry (MS)-based neuropeptidomics and proteomics has become an extremely powerful tool in the analytical field that enables identification and quantification of proteins and peptides in complex biological samples. The introduction of advanced MS instruments and bioinformatics tools has enabled the high-throughput and high-specificity analyses of thousands of proteins including their post-translational modifications in cultured cells, primary tissues, and body fluids. In this dissertation, efforts have been made to address challenges in MS-based neuropeptidomics and proteomics: from sample preparation, to MS instrumentation and finally to data processing and functional analysis. Monolithic stationary support has been conjugated with multiple types of affinity reagents for highly efficient sample preparation. With enzymes being immobilized onto monolithic bed, on-column digestion can be completed in minutes for proteomics studies. With specific antibodies immobilized onto the column, purification of targeted analytes from biological matrices has been achieved. In order to study *in vivo* neuropeptidomic changes, MALDI MS imaging platform has been introduced and developed. Furthermore, analysis and characterization of complex neuropeptide (NP) extraction from tissues have been explored as complementary approaches to MALDI MSI platform, providing enhanced coverage of neuropeptidome. Additionally, MALDI MSI platform has been integrated to live animal model for real time monitoring of signaling molecules *in vivo* during

animal behavior. Finally, quantitative proteomics and bioinformatics analysis was applied to study the exocytosis pathways from pancreatic cancer cells. In summary, this dissertation research provides comprehensive improvement in the overall process of MS-based neuropeptidomics and proteomics. Development of multi-faceted approaches enables more in-depth investigation on signaling molecules in several biological systems.

Chapter 1

Introduction: research overview and background information

1. Overview

Study of proteome provides diverse information about protein composition, abundances, modifications, dynamic variations, etc. in a particular biological system. Derived from proteomics, peptidomics is an emerging field of interest in biotechnology and pharmaceutical sciences owing to their significant roles in biofunctions and nervous systems [1]. Modern analytical, instrumental and computational technologies enabled highly efficient proteomic and peptidomic analysis in complex biological matrices. Mass spectrometry (MS) measures the mass-to-charge ratio (m/z) of its ions and fragmented ions to product ions, which has been widely applied in proteomic and peptidomic identification and quantification [2, 3]. Overall workflows of MS-based omics study can be divided into three major parts: sample preparation, instrumentation and bioinformatics/statistical analysis. Biological samples from tissues, body fluid, cell lysate, organelles, etc. are first dissected and extracted to obtain a mixture of proteins and peptides. To pre-cleanup sample mixtures, methods such as immunoprecipitation, fractionation, enrichment and affinity purification are commonly utilized. After sample preparation, the resulting mixture is separated by a multitude of separation strategies prior to MS analysis to reduce sample complexity and enable comprehensive identification. Separated mixture can then be analyzed by a variety of MS instruments to acquire information of each peptide sequence. With the development of bioinformatics and biostatistics, computational methods are used to assess large datasets and perform quantitative analysis. Therefore, in my thesis work, I aim to develop and address challenges in those three major parts: sample preparation, instrumentation and statistical/bio-functional deduction. To achieve fast and more streamlined sample preparation, Chapters 3 and 4 discussed how to apply monolithic stationary phase for high throughput proteomic digestion and affinity enrichment. Chapters 5 and 6

described the integration of MALDI MS imaging and *in vivo* microdialysis for real time monitoring of signaling molecules in animal models. Chapter 7 focused on further biological application of MS-based proteomics by using label-free quantification and computational approaches. Chapter 2 provided a review of recent advances in instrumentation area of coupling capillary electrophoresis (CE) separation to ESI and MALDI MS.

2. Brief background

2.1. Crustacean neuropeptide

Neuropeptides (NPs) are signaling molecules that released by neurons to communicate and regulate physiological processes [4, 5]. NPs were reported to mediate in many biological behaviors such as feeding, pain sensing and reproduction [6, 7]. Crustaceans have long been used for study of singling molecules in our group. It has a relatively simple nervous system compared to mammalian models and well-defined neurons which makes it an attractive model for neuropeptide study [8]. Crustacean central nervous system and stomatogastric nervous system secrete NPs to circulating body fluid. Major tissues such as sinus glands, brain, pericardial organs, etc. in crustacean nervous system are illustrated in Figure 1. Due to the wide dynamic range of neuropeptides existed in crustacean models, appropriate characterization methods are needed to improve detection sensitivity. Thus in this work, affinity approach was developed for NP enrichment from tissues. Monolithic affinity column was immobilized with anti-NP-antibody to enrich and separate specific NP family from complex tissue extractions.

2.2. Small molecule neurotransmitters and metabolites

Neurotransmitters (NTs) are endogenous messengers stored in synaptic vesicles which involve in signaling transduction [9, 10]. In the nervous system, neurotransmitters are one of the most diverse classes of chemical messengers that include amino acids, monoamines, purines, peptides, etc. Compared to NPs, small-molecule neurotransmitters and their metabolites are even more difficult to capture due to their rapid degradation rates and low *in vivo* concentrations [11]. Therefore, we utilized highly efficient and sensitive methods like capillary electrophoresis (CE) with sub-uL volume of sample consumption. With micro-scale separation, small molecule NTs and metabolites were successfully characterized in crustacean model [12].

2.3. Separation prior to MS

In this thesis work, separation techniques involve liquid chromatography (LC), capillary electrophoresis (CE) and ion mobility (IM). CE achieves separation based on size and charge of the analytes. While LC is a liquid-based separation where analytes are separated based on their retentions on the stationary phase [13]. In liquid phase separation, both chromatographic and electrophoretic separation techniques have been employed for peptide and protein studies followed by MS analysis. Nowadays, LC/MS is considered the most commonly used method for peptide mapping and large-scale shotgun proteomics. Whereas CE/MS serves an attractive alternative that provides different selectivity, which is especially capable for micro-scale analysis. Owing to their different separation mechanisms, CE/MS and LC/MS are highly complementary approaches. Thus, employing multi-dimensional separations results in significantly increased identification coverage [14, 15]. In gas phase separation, ion mobility, charged analytes are introduced to an IM drift tube and being differentiate based on their size and shape [16, 17]. Advantages of IM separation over liquid-phase separation techniques is the ability for conformation characterization, especially for structural isomers and small molecules [18-20].

2.4. Monolithic stationary phase

In recent years, monolithic materials has emerged to be a new generation of chromatographic stationary phase, due to its advantages of in-situ preparation, fast mass transfer, macroporous structure and high permeability [21-23]. Furthermore, as a class of functional materials, functional groups on the monolithic polymers are usually modified by chemical reactions for fabrication of responsive materials, which could be widely applied in various fields. Therefore, the construction of functional monolith can provide new opportunities for its development in analytical sciences [24, 25]. By performing covalent binding onto the surface of

monolithic materials, functional columns have been fabricated and applied in rapid on-column digestion prior to proteomics and affinity purification of analytes of interest.

2.5. Ionization source of MS

Ionization source is equipped on the mass spectrometers for absorbing molecules into the subsequent MS chambers. In order to be detected and analyzed by MS, molecules must first be added or removed charge(s). There are two main types of ionization sources used in MS-based proteomics: electrospray ionization (ESI) and matrix-assisted laser desorption/ionization (MALDI). ESI generates multiply charged molecules and is usually coupled with online separation techniques. Conversely, MALDI produces singly charged ions and provides spatial distribution of target analytes. In MALDI, samples or tissue slices are mixed with a matrix and allowed to co-crystallize on a sample plate or glass slides that is then introduced into a MALDI mass spectrometer. These two ionization techniques are complementary for MS-based bioanalysis. Therefore, my thesis research has employed both techniques to obtain a more comprehensive analysis of signaling molecules [12, 26, 27].

3. Conclusion of contribution and innovation

This doctoral thesis established advanced techniques in MS-based bio-analysis. Efforts have been made to develop functional monolithic stationary phase for enzyme reactor that significantly improved experimental efficiency of large-scale proteomic studies. Moreover, we designed monolithic affinity support to extract target analytes presented at low abundant. Affinity purification of signaling peptides at micro-scale sample consumption was accomplished for the first time in a timely manner. MS instrumentation was developed and I created MSI interface coupled to *in vivo* microdialysis (MD). The novel separation-enhanced MD-MSI platform enabled detection of circulatory neurotransmitters (NTs) and discovered more than two hundred small molecule NTs and metabolites. Integration of MS instrumentation with MD identified novel signaling molecules in crustacean hemolymph and was applied for real time monitoring of *in vivo* analysis. In addition to the study of signaling molecules, signaling vesicles and their secretion pathways were also investigated by the application of MS-orientated techniques. By employing quantitative proteomic and bioinformatics approaches, evidence of new secretion pathway was provided for further in-depth validation. Collectively, this work have established improved techniques and functional applications for the study of neuropeptidomics and proteomics.

References:

1. Dallas, D.C., et al., *Current peptidomics: Applications, purification, identification, quantification, and functional analysis.* Proteomics, 2015. **15**(5-6): p. 1026-1038.
2. Mann, R.A.M., *Mass spectrometry-based proteomics.* Nature, 2003. **422**: p. 198-207.
3. Bayés, A. and S.G.N. Grant, *Neuroproteomics: understanding the molecular organization and complexity of the brain.* Nature Reviews Neuroscience, 2009. **10**(9): p. 635-646.
4. OuYang, C., Z. Liang, and L. Li, *Mass spectrometric analysis of spatio-temporal dynamics of crustacean neuropeptides.* Biochimica et Biophysica Acta (BBA) - Proteins and Proteomics, 2015. **1854**(7): p. 798-811.
5. Dickinson, A.E.C.E.A.S.P.S., *Crustacean neuropeptides.* Cell. Mol. Life Sci., 2010. **67**: p. 4135-4169.
6. Buchberger, A., Q. Yu, and L. Li, *Advances in Mass Spectrometric Tools for Probing Neuropeptides.* Annual Review of Analytical Chemistry, 2015. **8**(1): p. 485-509.
7. Li, L. and J.V. Sweedler, *Peptides in the Brain: Mass Spectrometry–Based Measurement Approaches and Challenges.* Annual Review of Analytical Chemistry, 2008. **1**(1): p. 451-483.
8. Ye, H., et al., *Defining the Neuropeptidome of the Spiny LobsterPanulirus interruptusBrain Using a Multidimensional Mass Spectrometry-Based Platform.* Journal of Proteome Research, 2015. **14**(11): p. 4776-4791.
9. Werman, R., *A review — critical for idenctification of a central nervous system transmitter.* Comparative Biochemistry and Physiology, 1966. **18**: p. 745-766.

10. FISHMAN, M.C., *Sir Henry Hallett Dale and the Acetylcholine Story.* Yale Journal of Biology and Medicine, 1971. **45**: p. 104-118.

11. Gemperline, E., B. Chen, and L. Li, *Challenges and recent advances in mass spectrometric imaging of neurotransmitters.* Bioanalysis, 2014. **6**(4): p. 525-540.

12. Jiang, S., et al., *Investigation of signaling molecules and metabolites found in crustacean hemolymph via in vivo microdialysis using a multifaceted mass spectrometric platform.* Electrophoresis, 2016. **37**(7-8): p. 1031-8.

13. Bettina Sarg, K.F., Leopold Kremser, Bernhard Halfinger, Roberto Sebastiano and Herbert H. Lindner, *Comparing and combining capillary electrophoresis electrospray ionization mass spectrometry and nano-liquid chromatography electrospray ionization mass spectrometry for the characterization of post-translationally modified histones.* . Mol Cell Proteomics, 2013. **12**: p. 2640-56.

14. Zürbig, P., et al., *Biomarker discovery by CE-MS enables sequence analysisvia MS/MS with platform-independent separation.* Electrophoresis, 2006. **27**(11): p. 2111-2125.

15. Klein, J., et al., *Comparison of CE-MS/MS and LC-MS/MS sequencing demonstrates significant complementarity in natural peptide identification in human urine.* Electrophoresis, 2014. **35**(7): p. 1060-1064.

16. Francesco Lanucara, S.W.H., Christopher J. Gray and Claire E. Eyers, *The power of ion mobility-mass spectrometry for structural characterization and the study of conformational dynamics.* Nature Chemistry, 2014. **6**: p. 281-294.

17. Stauber, J., et al., *On-tissue protein identification and imaging by MALDI-Ion mobility mass spectrometry.* Journal of the American Society for Mass Spectrometry, 2010. **21**(3): p. 338-347.

18. McLean, J.A., et al., *Ion mobility–mass spectrometry: a new paradigm for proteomics.* International Journal of Mass Spectrometry, 2005. **240**(3): p. 301-315.

19. Jia, C., et al., *Site-Specific Characterization ofd-Amino Acid Containing Peptide Epimers by Ion Mobility Spectrometry.* Analytical Chemistry, 2014. **86**(6): p. 2972-2981.

20. Lietz, C.B., Q. Yu, and L. Li, *Large-Scale Collision Cross-Section Profiling on a Traveling Wave Ion Mobility Mass Spectrometer.* Journal of the American Society for Mass Spectrometry, 2014. **25**(12): p. 2009-2019.

21. Ladisch, M. and L. Zhang, *Fiber-based monolithic columns for liquid chromatography.* Analytical and Bioanalytical Chemistry, 2016. **408**(25): p. 6871-6883.

22. Nema, T., E.C.Y. Chan, and P.C. Ho, *Applications of monolithic materials for sample preparation.* Journal of Pharmaceutical and Biomedical Analysis, 2014. **87**: p. 130-141.

23. Nobuo Tanaka , H.K., Norio Ishizuka , Hiroyoshi Minakuchi , * ba a Kazuki Nakanishi , Ken Hosoya , Tohru Ikegami, *Monolithic silica columns for high-efficiency chromatographic separations.* Journal of Chromatography A, 2002. **965**: p. 35-49.

24. Q. Ching Wang, F.S., Jean M.J. FrCchet*, *Reversed-phase chromatography of small molecules and peptides on a continuous rod of macroporous poly(styrene-codivinylbenzene).* Journal of Chromatography A, 1994. **669**: p. 230-235.

25. Xu, L. and H.K. Lee, *Preparation, characterization and analytical application of a hybrid organic–inorganic silica-based monolith.* Journal of Chromatography A, 2008. **1195**(1-2): p. 78-84.

26. Zhang, Z., S. Jiang, and L. Li, *Semi-automated liquid chromatography-mass spectrometric imaging platform for enhanced detection and improved data analysis of complex peptides.* J Chromatogr A, 2013. **1293**: p. 44-50.

27. Zhong, X., et al., *Recent advances in coupling capillary electrophoresis-based separation techniques to ESI and MALDI-MS.* Electrophoresis, 2014. **35**(9): p. 1214-25.

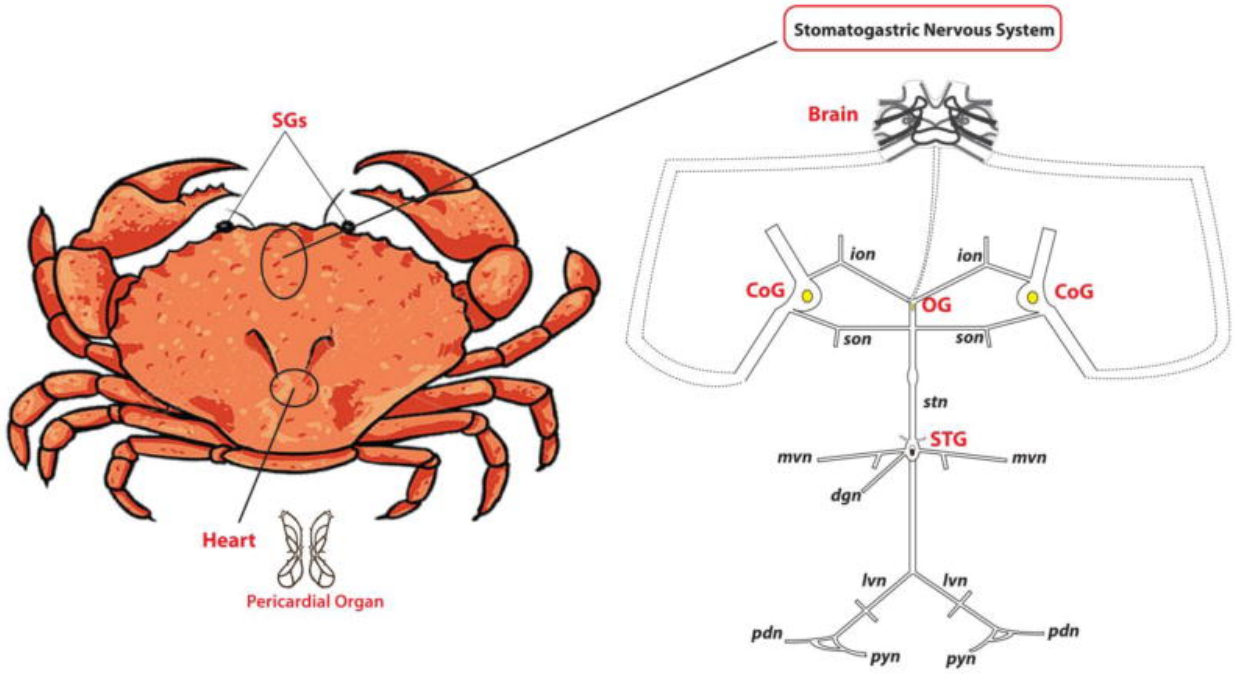

Figure 1. Schematic drawing of the stomatogastric nervous system (STNS) of Jonah crab, *Cancer borealis*.

The brain, sinus glands, and the pericardial organs constructed crustacean central nervous system and release hormones into the hemolymph chamber. The stomatogastric nervous system consists of the stomatogastric ganglion, oesophageal ganglion, paired commissural ganglia which are connected by motor nerves.

Adapted from OuYang et al. Biochim Biophys Acta. 2015 Jul; 1854(7): 798-811.

Chapter 2

Recent advances in coupling capillary electrophoresis based separation techniques to ESI and MALDI MS

Adapted from:

1. Zhong X., Zhang Z., **Jiang S.**, Li L., Recent advances in coupling capillary electrophoresis based separation techniques to ESI and MALDI MS. Electrophoresis. 2014; 35(9): 1214-1225.

Abstract

Coupling capillary electrophoresis (CE) based separation techniques to mass spectrometry creates a powerful platform for analysis of a wide range of biomolecules from complex samples because it combines the high separation efficiency of CE and the sensitivity and selectivity of MS detection. ESI and MALDI, as the most common soft ionization techniques employed for CE and MS coupling, offer distinct advantages for biomolecular characterization. This review is focused primarily on the technological advances in combining CE and chip-based CE with ESI and MALDI MS detection in the past five years. Selected applications in the analyses of metabolites, peptides, and proteins with the recently developed CE-MS platforms are also highlighted.

1. Introduction

Featuring minimum sample and solvent consumption, rapid separation speed, high resolving power, capillary electrophoresis (CE) finds extensive applications in the area of metabolomics [1, 2], bottom-up proteomics [3-7], as well as glycan [8] and intact protein analyses [9] when it is interfaced with versatile modes of mass spectrometry (MS) detection. A variety of soft ionization techniques have been employed for both on-line and off-line coupling of CE and MS, such as electrospray ionization (ESI), matrix-assisted laser desorption/ionization (MALDI), atmospheric pressure chemical ionization (APCI), atmospheric pressure photoionization (APPI) [10]. Among these ionization methods, ESI is the most popular approach for on-line CE-MS coupling due to the ease of implementation and the compatibility with a large category of molecules, from small metabolites to intact proteins. Off-line coupling of CE and MS by MALDI also attracts lots of interests because of the higher tolerance with salts, the sensitivity of specific category of analytes, and the versatility of separation modes and buffer choice. As ESI and MALDI are the two most prevalent ionization methods employed for biomolecule analysis and they offer distinct advantages in different applications, in this review, we focus discussion on the technical developments of CE-MS coupling with these two ionization methods in the recent five years.

2. On-line coupling of CE and ESI-MS

Although CE and ESI share some common properties, such as they both employ simple direct current (DC) circuits, and are both amenable to analysis of biomolecules, strategies for successful application of CE- ESI-MS must address several fundamental issues, including i) consolidation of the CE and ESI circuits; ii) stable electric contact at the CE outlet electrode; iii) proper emitter geometry for supporting stable electrospray ionization; iv) suitable electrolyte for separation and electrospray ionization. As scientists working in this area are pursuing better

sensitivity, physical robustness, reproducibility and stability, several improved CE-ESI-MS interfacing strategies emerged in recent years. Fundamentals and details of CE-ESI-MS interface designs were discussed in several previously published reviews [10-14]. The following discussions will be focused on the recent technological improvements of these CE-ESI-MS coupling strategies.

2.1. CE-ESI-MS interfaces employing sheath-flow or make-up flow liquid

The most common and commercially available sheath liquid interface uses a coaxial arrangement for three concentric tubing: the separation column, the straight metal tubing for sheath liquid delivery and the outer tubing for nebulizer gas [15]. The sheath liquid metal tubing functions as the CE outlet electrode and the electrospray emitter. The sheath liquid serves to establish electric contact between the metal tubing and the background electrolyte in the separation column, and to modify the components of the background electrolyte for improved ionization efficiency. The separation column usually extrudes out of the sheath liquid tubing by 1~2 millimeters to avoid any dead volume and obtain stable spray. As the dimension of the sheath liquid metal tubing must be large enough to accommodate the most frequently used silica capillary columns (360 μm OD), relatively larger flow rate of sheath liquid (usually 1~10 μL/min) is required to maintain stable electrospray ionization and a nebulising gas could be used to accelerate the solvent evaporation in the ion source. This interface design has been adopted by many researchers for years due to its robustness, ease of assembling, the versatile choice of background electrolyte (BGE) solution, and almost zero dead volume. However, two major weaknesses of this interface cannot be ignored. Firstly, the high-flow rate sheath liquid introduces significant dilution effect for the CE effluent. Secondly, nebulising gas causes a suction effect at the capillary outlet and induces parabolic flow inside the capillary, which decreases the separation efficiency. Although

this suction effect could be corrected by applying a negative pressure at the CE inlet vial, extra efforts are needed to determine the precise pressure to be applied at the inlet. Reducing the flow rate of sheath liquid becomes a key factor for improving the overall sensitivity of this type of interface and avoiding the use of a nebulising gas. Efforts towards going down to nanospray region have been made by several groups.

The Sweedler group used a scaled-down version of the conventional sheath liquid interface to achieve improved sensitivity [16-18]. In order to work in the sub-microliter per minute sheath liquid flow rate region, they reduced the OD and ID of the stainless steel (s.s) sheath liquid tubing to 260 μm and 130 μm respectively [17]. Accordingly, the separation column that goes through the s.s. tubing was also scaled down to 110 μm ID and 40 μm ID [17]. The separation capillary column end protruded 20−200 μm beyond the metal capillary tube for optimized spray [18]. In this configuration, sheath liquid infused at 0.75 to 1 μL/min by syringe pump was enough to support a stable Taylor cone for electrospray and nebulizer gas could be eliminated. With the reduced sheath liquid flow rate, this CE-ESI-MS interface provided enough sensitivity to investigate metabolites and neurotransmitters from single neurons on a Bruker MaXis Q-ToF platform [16-20].

Both Chen group [21] and Dovichi group [22] adopted the ‘junction-at-the-tip’ concept for the low-flow sheath liquid CE-ESI-MS interfaces. With this arrangement, the end of the CE separation column reaches as far as possible into a tapered outer tube that serves as the electrospray emitter. The separation column cannot protrude out of the emitter tip due to the gradual shrinking OD and ID of the tapered emitter tip, creating a liquid junction at the interior of the emitter tip where the sheath-liquid or make-up flow mixes with the CE effluent. The geometry of the emitter tip is the most critical factor that determines the optimal flow rate region

for stable electrospray. Different solutions were implemented by the two groups to achieve a minimum sheath liquid flow rate.

By evaluating the performance of a series of s.s. electrospray emitters with different tip sizes and shapes (Figure 1A), Chen and coworkers found that with similar tip size, asymmetrical emitter geometry can accommodate a wider flow rate range and offer better sensitivity compared to the blunt tapered symmetrical shape (Figure 1B) [23]. The emitter tip geometry with 35 degree beveled tip surface and 16 degree taper angle was chosen for their later interface configuration of CE-ESI-MS, which could accommodate a typical sheath liquid flow rate range of 100−500 nL/min. The shaft of the s.s. sprayer tube has a OD 720 μm of and ID of 412 μm, making it well suited for a conventionally used 360 μm OD fused silica capillary column. Compared with a commercial sheath-flow CE-MS interface, fivefold on average improvement of limit of detection of 18 amino acids was achieved by employing a relatively low sheath liquid flow [21].

While the s.s. emitter offers better mechanical strengths, Dovichi group employed borosilicate glass capillary to fabricate electrospray emitters with tip ID of 2~10 μm by micropipette puller [22]. In spite of higher risk of tip damage and blockage, such small tip can operate in the nanospray regime and give substantially increased signal-to-noise ratio, and it only needs a minimal amount of sheath liquid flow without mechanical pumping. As electrospray voltage could not be applied directly on the glass capillary emitter, high voltage was applied at the sheath liquid reservoir, which was connected to the spray emitter via another fused silica capillary and a PEEK cross union. By coupling this interface with an AB Sciex QTrap 5500 triple-quadrupole mass spectrometer, Li et al. demonstrated that the mass sensitivity of CE-ESI-multiple reaction monitoring (MRM) for absolute quantification of Leu-enkephalin in a complex mixture was improved by 10−20 fold compared to their previous study using nanoLC coupled

with MRM [24]. This CE-ESI-MRM method was further extended to detect three abundant proteins from 100 pg of cell lysate digest, which approximates protein content from a single cell [25]. The potential application of CE-ESI-MS in bottom-up proteomics was also investigated by interfacing this nanospray sheath-flow interface to an LTQ-Orbitrap Velo mass spectrometer, whose fast scan speed is more compatible with the short separation window of CE [26-31]. Suffering from small loading capacity, CE-ESI-MS/MS is more suitable for analyzing proteome samples of intermediate complexity, such as protein secretome prefractionated with HPLC [26]. It was also demonstrated that, CE-ESI-MS/MS favours detecting peptides with higher pI and lower hydrophobicity values compared to nanoLC-MS [26]. When the peptide sample loading amount goes below 10 ng, the number of unique peptides identified by a single CE-ESI-MS/MS run exceeds that identified by a single nanoLC-ESI-MS/MS run [31].

Another common concern associated with this type of 'junction-at-the-tip' configuration is the post-column band broadening caused by the dead volume formed at the interior of the tapered emitter tip. Both groups conducted computational simulation and experiments to evaluate this potential problem with their interfaces. Again, geometric dimension plays an important role in the band broadening effects. For the interface developed by the Chen group, the distance from separation column end to the emitter tip outlet was around 600 μm, making a total volume of the flow-through microvial close to 20 nL [32]. The simulated flow profile and mass transport process inside the tiny flow-through microvial showed that with proper sheath liquid flow rate, peak distortion and post-column band broadening can be minimized or become unnoticeable. These results were further confirmed by comparing the UV detected peaks and MS detected peaks under similar experimental conditions [32]. For the nanospray sheath-flow interface developed by the Dovichi group, the tapered length of the glass emitter was about 3 mm, and the

optimized spacing between the separation column end and the emitter tip was 1 mm [22]. The use of a 150 μm OD separation column rather than a 360 μm one reduced the dead volume enclosed by the emitter tip and the separation column end, as the 150 μm OD separation column could be inserted further into the tapered glass capillary emitter. It was demonstrated that a 2 mm gap between the separation column end and the emitter tip causes significant broader and lower amplitude peaks compared to the 1 mm gap.

Despite the concerns discussed above, the 'junction-at-the-tip' design forms a flow-through microvial at the CE outlet, which creates possibilities to perform CE separation in some special modes. One example demonstrated by Maxwell et al. [33] and Jayo et al. [34] is the separation of negatively charged carbohydrates with reversed polarity and electroosmotic flow (EOF) towards the inlet. The make-up flow solution in the flow-through microvial can back-fill the capillary to maintain a continuous EOF while providing a stable forward flow at the emitter tip surface to support electrospray. This flow-through microvial also enables interfacing on-line capillary isoelectric focusing (CIEF) with ESI-MS detection [35], since the microvial at the cathode end can supply basic catholyte solution during focusing stage and provide acidic mobilizer solution during the mobilization stage.

2.2. Sheathless interfaces for CE-ESI-MS

The sheathless CE-ESI-MS interfaces usually generates greater sensitivity since the analytes exiting the separation column does not suffer from dilution and the nanospray emitter gives fairly high ionization efficiency. However, eliminating sheath-flow liquid also restricts the choice of BGE, as BGE itself is used for nanospray without any further modification. In the absence of sheath-flow liquid, the most challenging problem is to establish stable and long-lasting electrical contact at the column outlet for completing the CE circuit and applying ESI voltage. Two

categories of designs are involved in the sheathless CE-ESI-MS interfaces: the one-piece interfaces which shape the separation column ends into nanospray emitters, and the two-pieces interfaces which employ replaceable nanospray emitters.

Among various strategies of creating electric contact employed in the one-piece CE-ESI-MS interface designs, such as applying metal coating on the emitter tip, or inserting an electrode into the column end [11, 12], the porous sprayer tip [36], originally developed by Moini et al. and later licensed by Beckman Coulter, has been widely practiced in the last few years. As shown in Figure 2, the electrical connection of this interface is achieved by inserting the porous capillary outlet into a metal sheath and filling metal sheath with background electrolyte [36, 37]. This porous sprayer tip, made from etching a segment of the capillary outlet by hydrofluoric solution, allows transporting of small ions across the porous wall [38] and accommodates flow rate as low as several nanoliter per minute [39, 40]. Compatibility with such ultra-low flow rate facilitates CE-MS applications using neutral coated capillaries that exhibit only an extremely low EOF, which greatly extends the use of this sheathless CE-ESI-MS interface in solving challenging separation problems such as glycoform profiling of glycopeptides [41] and intact biopharmaceutical proteins [42]. Evaluations of the system repeatability and sensitivity of this sheathless porous tip interface were conducted by several groups using various analytes. In general, the system repeatability (RSD of migration time and peak area) was considered to be suitable for quantitative analysis of small molecules [43-45], peptides [46] and intact proteins [47]. Compared to the conventional sheath-flow liquid interface, Ramautar et al. showed that the detection limits for 20 metabolite standards were decreased by 10−30 fold, leading to two fold increase of the coverage of human urine metabolome [45]; Haselberg et al. also found 50−140 fold improvement of detection limits for four intact protein standards [47]. With this sensitivity

and repeatability, CE-ESI-MS based on the sheathless porous tip interface has been used to solve a wide range of analytical problems, including study of protein-protein and protein-metal complexes under physiological conditions [48, 49], characterization of protein-drug conjugates [50], determination of amino acid racemization rates in ancient silk [51], forensic analysis of phosphorus-containing amino acid-type herbicides [52], metabolomic profiling of urine and cerebrospinal fluid samples [44, 45, 53], bottom-up proteomics [37, 54], and protein post-translation modifications [40-42, 55]. In order to improve the sample loading capacity, transient isotachophoresis (t-ITP) [39, 40, 45], and solid phase microextraction (SPME) combined with t-ITP [54] were integrated online with this sheathless interface in the applications of metabolomics and bottom-up proteomics studies. In comparison with reversed phase nanoLC-ESI-MS, it has been shown that, CE-ESI-MS is an important platform for bottom-up proteomics studies [37, 54], and especially for phosphoproteomics [40, 55]. Heemskerk et al. developed a t-ITP-CE-ESI-MS strategy that gave superior mass sensitivity and concentration sensitivity for phosphopeptide detection [40]. They also showed that this optimized CE-MS strategy has a better chance to identify multiphosphorylated peptides, which could not be detected by the nano-LC-MS even with a higher sample loading amount [40]. The most recent research on characterization of post-translationally modified histones [55], published by Sarg et al., also demonstrated that more modified peptides and more modification sites, mainly acetylation, phosphorylation, deamidation, were found by the ultra-low flow sheathless CE-ESI-MS with 2 orders of magnitude smaller sample loading amount compared to nanoLC-MS. Figure 3 shows a detailed comparison of the number of unmodified and modified histone H1 peptides identified by CE-ESI-MS and LC-ESI-MS/MS analysis.

Efforts on improving the two-piece sheathless interface designs have also been noted. In contrast to the one-piece design, the disposable emitter made from bare-fused silica capillary can be easily replaced if clogged or damaged, and it is relatively simple to coat the capillary inner surface for specific applications. The challenges of building robust two-piece sheathless interfaces lie in aligning the separation column end and emitter with minimum gap, and maintaining stable electric contact at the joint of the two pieces. In the design made by Park et al. [56, 57], two ports of a three-port plastic tee were used to secure the separation column and the emitter, and the third one was packed with Nafion, which formed a conductive polymer layer that allows cations moving through. A piece of sponge soaked with electrolyte was placed on top of the Nafion layer and voltage for electrospray was applied through a platinum wire wrapping around the tee. In another design constructed by Her et al. recently [58], a 1 mm long, 50 μm ID microchannel made inside a polydimethylsiloxane (PDMS) microdevice was employed to connect the separation column, the capillary emitter, and the microreservoir containing BGE where ESI voltage was applied. Although dead volume at the junction of the two capillaries still existed in both designs, the authors found that the separation efficiency was not significantly affected by the gap.

2.3. Chip based CE-ESI-MS

Interfacing commercially available CE instrument to ESI-MS usually requires a capillary column length above 65 cm due to the physical distance from the CE inlet electrode to the ion source, which might cause relatively longer separation time as the maximum voltage could be applied across the column is 30 kV. Performing CE on microfabricated devices can overcome this problem because the miniaturized chip can be incorporated into the ion source and the separation channels can be customized to the desired lengths for specific applications. To spray the effluent

from CE channel, either an external emitter is attached to the end of the micro-separation channel or an edge or a corner of the microdevice is shaped into a nanospray emitter. The Her group tried different methods of attaching external emitters to poly (methyl methacrylate) based CE chips. They first made a sheathless interface by fixing the back end of a conductive rubber coated capillary emitter to the outlet of the CE microchannel using epoxy resin [59], and later constructed a liquid junction interface by connecting the microchannel and the fused-silica capillary emitter with a 1.5 cm capillary and immersing this connecting capillary in a sheath liquid reservoir [60]. Integrated nanospray emitter on glass microchips were fabricated in different approaches. Belder et al. recently described a method to modify the channel outlet of an electrophoresis glass chip into a sheathless nanospray emitter. A 300 μm diameter cone machined concentrically around the channel opening on the glass edge was drawn into a sharp tip and then etched by hydrofluoric acid [61-63]. With the tip opening around 10 μm, the integrated glass chip emitter demonstrated performance similar to that achieved by commercial nanosprayer [62]. Rather than modifying a planar edge of the glass chip into a nanospray emitter, Ramsey group used the 90 degree rectangular corner of a 300 μm thick glass chip as the electrospray emitter [64]. The CE separation channel ended at the rectangular corner, where it met the end of electroosmotic pump channel that delivers a make-up flow. A positively charged surface coating was used to eliminate adsorption of protein/peptides on the separation channel and to generate anodic electroosmotic flow. High separation efficiency achieved in several minutes using this chip-CE-ESI-MS device was demonstrated in the analysis of protein digests [64] and single cell lysate [65].

Two-dimensional separation platforms are desired in comprehensive analysis of complex biological samples because they provide improved peak capacity and resolving power. As an

orthogonal separation mode to RPLC, on-chip CE is an ideal choice for the second separation dimension since its fast separation speed improves the sampling rate of the first dimension. Monolithic integration of 2D LC-CE-ESI on a glass microfluidic device [66] and coupling capillary UPLC with on-chip CE-ESI [67] (Figure 4) were recently reported by the Ramsey group. In both systems, effluent from RPLC was transferred to the CE separation channel by electrokinetically gated injections. With the large field strength (~1.1 kV/cm) for CE separation, the migration time scale for the second dimension was within only 22 seconds so that CE injections spaced 10 s apart could be used to sample peaks from the first dimension [66, 67]. At this stage, only full scan MS mode could be used to record chip-CE-ESI-MS data due to the extremely narrow CE peaks. To fully exploit the advantages of microfluidic devices for complex sample analysis, data sampling rates of mass spectrometers still need to be improved to acquire enough tandem MS spectra for structural elucidation and analyte identification [63].

3. Off-line coupling of CE and MALDI-MS

Coupling of CE with MALDI-MS detection provides an attractive alternative to CE-ESI-MS because it offers more choices for the BGE and allows for easier implementation of other separation modes besides zone electrophoresis. Most notably, MALDI-MS has better tolerance with salts compared to ESI-MS and the MALDI MS detection can be decoupled from CE separation, thus enabling independent optimization of CE separation and MS detection. Despite several reports on on-line coupling of CE and MALDI-MS [10], off-line coupling of CE with MALDI-MS detection is still more prevalent in the recent years since it does not require any modification of the MALDI source. Another advantage of off-line coupling is the number of spectra that could be acquired on the same sample spot is not limited by the data acquisition rate of the mass spectrometer or the elution time window of a transient peak. In this way, masses of

interest from full MS scan can be selected for MS/MS identification. The most critical issue for off-line CE-MALDI-MS coupling is to maintain the electric continuity while collecting the CE effluent at the capillary outlet. As both ESI-MS and MALDI-MS are post-column detection methods, some capillary outlet configurations used in CE-ESI-MS can be adapted for CE-MALDI-MS coupling, such as the coaxial sheath-flow liquid interfaces, the sheathless interfaces using metal coated capillary end, and the pressurized liquid junction interfaces. Another challenge for CE-MALDI-MS coupling is to collect the CE effluent with minimum loss of sensitivity, minimum perturbation to the separation process and maximum preserving of on-column resolution. Some commercially available MALDI spotter designed for nanoLC system can be used to collect discrete CE fractions directly on the MALDI target with precise control of the time interval for spotting and the volume of each fraction. Although the automated MALDI spotters can spot as fast as four seconds per fraction, separation resolution is still compromised and they have to be used with a sheath liquid flow. Recent development of CE-MALDI- mass spectrometry imaging (MSI) provides a viable solution to this problem. In addition, strategy of applying matrix is also crucial for generating homogeneous crystals and obtaining reproducible results. In this section, more effective off-line CE-MALDI-MS interfacing strategies and recent developments in combining different CE separation modes with MALDI-MS detection will be discussed and highlighted.

3.1. CE-MALDI-MS interfaces employing sheath-flow liquid

The sheath liquid employed in the CE-MALDI-MS interface mainly serves two purposes: 1) to keep the integrity of CE circuit by grounding the sheath liquid reservoir or the coaxial metal sheath tubing that delivers the sheath liquid; 2) to create droplet on the capillary end for easier sample deposition. The composition of sheath liquid solution can be the same as CE running

buffer or even matrix for MALDI detection as long as it does not affect the separation efficiency [68]. Helmja et al attempted to develop a universal CE fraction collector apparatus for different types of subsequent mass spectrometric detection using classical coaxial sheath-flow liquid interface configuration [69]. Gravity induced sheath liquid flow (~ 2.5 μL/s) formed droplets at the capillary tip, which can be detected by a light emitting diode droplet counter when falling from the capillary tip. The volume of each droplet largely depends on the capillary outer diameter. In this report, 12~18.5 μL per fraction/droplet, relatively large compared to the nanoliter volume of a CE peak, was collected in PCR tubes located on a moving x/y stage. Rather than continuously delivering sheath liquid, a 'drop on demand' sheath liquid CE-MALDI interface, employing a high-speed inkjet printer valve to dispense matrix sheath liquid to the capillary end in pulses, was developed by Vannatta and co-workers [70]. The distal end of CE separation capillary was inserted into a 190 μm ID nozzle through a tee, and the matrix flow was applied through another port of the tee and controlled by a dispensing valve. A CE fraction was deposited onto the MALDI plate fixed to a microscope x/y stage every 750 milliseconds. With this fast deposition rate, separation efficiency with up to 40 000 theoretical plates was achieved in less than 3 minute separation, and over 70% of sequence coverage was obtained for tryptic digested α-lactalbumin in the subsequent MALDI-ToF detection.

3.2. Sheathless interfaces for CE-MALDI-MS

Although sheathless interfaces can provide better sensitivity, more attention must be paid to preventing current breakdown during sample collection. A 'porous polymer joint' sheathless interface for CE-MALDI off-line coupling was constructed by Wang et al. [71, 72]. A fracture was opened near the outlet end of CE separation capillary and was covered with cellulose acetate membrane allowing ions to go through for electric conduction. This porous polymer joint was

immersed in buffer vial with grounded electrode, and the capillary column end went through the vial for sample deposition. The pressure-initiated capillary siphoning generated a low hydrodynamic flow (<100 nL/min), facilitating direct sample fraction deposition on Parafilm-coated MALDI target. CE separation of neuropeptides was driven in a reversed-polarity mode with acidic BGE. In conjunction with stable isotopic labelling, this off-line CE-MALDI-MS platform was further applied in the relative quantitation of crustacean peptidome in response to salinity stress [73].

Another sheathless interface introduced by the Girault group employs silver coated capillary column outlet for iontophoretic sample deposition on MALDI target (Figure 5) [74, 75]. Individual droplets of several microlitres were predeposited on the MALDI target to receive CE zones exiting the capillary end by electromigration and diffusion when the capillary tip dipped into these droplets. This approach allows using neutral capillary coating that eliminates EOF, and current breakdown during separation process could be avoided even without a sheath liquid flow or a bulk flow from inside of the capillary. The grounded capillary end was lifted from and dipped into a droplet at a relatively high frequency (~ 15 second per step), however, the electropherograms recorded by UV detector did not show a decrease in separation efficiency.

While most MALDI interfaces require mechanical motors to move the MALDI target to switch sample deposition position, Gorbatsova et al. used a digital microfluidic (DMF) board to manipulate the movement of collected droplets and send them to preset location [76]. In this setup, the positions of capillary column end and the microfluidic board were both fixed. Droplets of 3 μL volume, generated from a second 150 μm OD capillary tip positioned very close to the gold and silver coated separation column outlet, were responsible for maintaining electric continuity and carrying CE analytes onto a hydrophobic film covered DMF board. Operated

based on the electrowetting on dielectric (EWOD) phenomenon, the DMF board with a set of 14 electrodes transported the collected droplets to different positions on the film. The film was lifted off the board and affixed to a MALDI target after solvent evaporation.

3.3. CE-MALDI-MSI

For off-line CE-MALDI-MS coupling, the time interval among sample depositions determines the efficiency of transferring the on-column peak resolution to the on-target peak resolution. Although higher resolution could be retained on MALDI target by using a faster sample deposition rate, loss of on-column resolution always occurs by collecting discrete fractions. Collecting continuous CE traces on a moving target followed by MALDI-MS detection along the whole trace could alleviate this problem. This concept was first attempted by van Veeleen et al. in 1993 using a sheath liquid interface [77], and actually realized by Zhang et al. later employing a sheathless interface for depositing sample on a grounded s.s. target covered with cellulose membrane [78]. In that report, they used a 250 μm step size for acquiring mass spectra along the collected CE trace, which corresponded to 1 second online data sampling rate. The theoretical plate numbers of CE peaks from reconstructed electropherograms based on off-line MALDI detection were reported to be as high as 80−90% of those from on-line UV detection. With the development of MALDI-MSI hardware and software tools, nowadays it is possible to achieve step size as small as tens of microns on commercialized MALDI-ToF or MALDI-LTQ-Orbitrap instruments, which significantly improves the on-target electrophoretic peak resolution. Ideally, the on-column peak resolution could be fully retained by collecting continuous trace and using small enough raster step during imaging of collected trace. However, on-target sample dispersion during deposition and effluent sticking on the capillary outlet could also deteriorate the on-plate

peak resolution and peak shape. Hence, it is preferable to use interfaces without coaxial sheath liquid for continuous trace collection in CE-MALDI-MSI applications.

In order to collect the continuous CE flow efficiently for the following MALDI-MS detection, Amantonico et al. used a customized MALDI target coated with omniphobic polysilazane nanocoating, which was also incorporated with an array of parallel grooves acting as recipients of the CE effluent [79]. Before separation, matrix dissolved in organic solvents was channeled into the 400 μm wide and 100 μm deep grooves and formed homogeneous coverage due to the modified surface wettability. During the CE run, the circuit at the outlet was completed by keeping the column end in contact with the grounded MALDI target. The capillary outlet was secured by a polytetrafluoroethylene (PTEE) sleeve, whose hydrophobicity helped preventing droplets attaching on the column end. The parallel grooves enabled multiplexing experiments by conducting CE separations in parallel columns simultaneously. Analysis of metabolites from yeast cell lysate in both positive and negative ionization mode was demonstrated on this platform.

Further improvements on coupling CE with MALDI-MSI was reported by Li and co-workers [80, 81]. They first used a pressurized liquid junction interface combined with grooved MALDI target plate for continuous trace deposition [80]. A capillary section with a fracture near the outlet was immersed in a pressurized liquid reservoir that was grounded through a platinum electrode. The pressure in the liquid reservoir combined with EOF created steady flow for sample deposition in the grooves with matrix pre-applied by air brush. The groove width was narrowed down to 250 μm to reduce on-target radial dispersion, and the distal end of the 360 OD capillary column was etched to 150 μm by hydrofluoric acid to fit the width of the groove. With the target moving at a speed of 110 μm/s during sample collection and 100 μm spatial resolution

for MALDI-MSI detection, the reconstructed extracted ion electropherogram (Figure 6A) of several peptides showed similar separation efficiency as the UV detected electropherogram (Figure 6B). To avoid sample dilution introduced by the make-up flow from the liquid junction, another pressure assisted (PA) CE-MALDI-MSI interface (Figure 7A) [81] was constructed later based on the 'porous polymer joint' sheathless interface [71] developed earlier by our group. Gravity induced hydrodynamic flow, as well as EOF contributed to the bulk flow in the separation column, which was mixed with the matrix flow delivered by another capillary at the tip and immediately deposited on a moving ground s. s. MALDI plate without grooving. Capillary with smaller OD of 190 μm was used in this interface to minimize the sample dispersion on the target. Both CE-MALDI-MSI platforms were evaluated by relative quantification of peptide mixtures via isotopically labeled formaldehyde. Compared to CE-MALDI via discrete spot/fraction collection, improved peptidome coverage was achieved by CE-MALDI-MSI because of better preservation of separation efficiency on the MALDI target. 46 tryptic peptides from bovine serum albumin and 150 putative neuropeptides extracted from crustacean neural organs were observed with PACE-MSI (Figure 7B). Combined with reversed phase HPLC fractionation, this PACE-MSI platform demonstrated powerful separation efficiency in the analysis of orcokinin family neuropeptides from crude neural tissue extracts [82]. These innovations on CE-MALDI-MSI based techniques provide new approaches for the analysis of trace-level analytes from complex biological samples.

3.4. CIEF and GCE coupled with MALDI-MS

Off-line coupling of CIEF with MALDI-MS detection usually involves two steps: (1) isoelectric focusing, which could be performed with a conventional CE setup or a modified setup facilitating the subsequent sample collection; (2) mobilizing the focusing sample zones while

depositing them on a MALDI sample plate. Different approaches to accomplish these two steps were adopted by researchers. If the conventional CE apparatus is used for focusing, the voltage has to be stopped to remove the catholyte vial, and the capillary outlet could be directly used for sample deposition on a MALDI target [83, 84] or directed to a coaxial sheath liquid deposition device [85]. A more convenient way would be using the same setup for both CIEF focusing and mobilization/sample deposition. Lechner et al. used a spotting robot, which actually worked as a grounded coaxial sheath liquid interface, for electric connection and catholyte supply during the focusing and pressure mobilization process [86]. The catholyte sheath liquid helped creating droplets and the matrix was deposited by another capillary. The 'porous polymer joint', previously employed for pressure assisted CZE-MALDI-MS coupling [71], was also adopted by Cheng et al. in CIEF-MALDI-MS application [87]. Electrophoretic mobilization could be an option, but extra procedures would be involved to switch the catholyte solution to mobilizer solution at the beginning of mobilization. Therefore, most researchers still prefer to adopt pressure mobilization with voltage applied across the capillary during sample collection. In spite of technical challenges with the instrumentation, CIEF-MALDI-MS applications in examining the microheterogeneity of intact glycoproteins [88], discovering novel neuropeptides [83], characterizing glycopeptides and phosphopeptides [86] were demonstrated by several groups.

A major issue for CIEF-MALDI-MS coupling is the suppressed ionization efficiency caused by high concentration of carrier ampholytes, viscosity-increasing agents, and protein solubilising detergents. Systematical evaluation of MALDI signal suppression caused by these additives was performed by Silverland et al., and it was concluded that compromises have to be made between the separation efficiency and repeatability on one hand and MS signal intensity on the other [89]. Cheng et al. reported a special sample deposition method to alleviate the protein signal

suppression [87]. A rough on-target separation of proteins and additives was achieved by depositing 0.1 μL of CIEF fraction into a 1 μL water droplet on a MALDI plate. While the smaller additive molecules (carrier ampholytes, detergents, and salts) diffused faster toward the edge of water droplet, most protein molecules remained at the centre region. After solvent evaporation, 0.5 μL of matrix solution was added for co-crystallization. 2-10 fold of S/N ratio improvement in protein signals was reported; however, it may still suffer from limitations for analysis of smaller peptides due to similar molecular weight range as the carrier ampholytes. Another potential solution to this problem, coupling monolithic column based immobilized pH-gradient (IPG) CIEF with MALDI-MS, was proposed and demonstrated by Zhang et al. [90]. Instead of mixing with sample prior to focusing, carrier ampholytes were loaded into the separation capillary, pre-focused and linked to the epoxy groups on the monolith surface so that the pH gradient was immobilized. Enhanced MALDI MS signal intensities were observed due to the elimination of carrier ampholytes from sample. Choice of monolith fabrication material might be further optimized for avoiding hydrophobic interaction between monolith surface and peptides and proteins while retaining the rigidity of the monolith.

An additional advantage of off-line coupling is that post-separation sample treatment can be performed if necessary. A good example was demonstrated by coupling SDS-CGE and MALDI-TOFMS for protein separation and characterization [91]. A strip of stepping poly(tetrafluoroethylene) (PTEF) membrane immersed in outlet buffer reservoir was used to collect the CGE separated SDS-protein complexes. After sample collection, the membrane was washed with 0.40% Tergitol NP Type 40 at 40 °C for 60 minutes to remove the SDS bound to proteins. Then the PTEF membrane with SDS-free proteins was attached to MALDI target for MS detection.

3.5. Microfluidic device based CE-MALDI MS

Coupling microfluidic device-based CE to MALDI-MS is still facing difficulties, such as collecting the narrow peaks on chip, transferring the collected fraction from a microfluidic chip to a MALDI target efficiently. Only a limited number of reports described development in this area. A polydimethylsiloxane (PDMS) based microfluidic device, reported by Luo et al., was applied to on-chip CE separation and fractionation followed by MALDI-MS detection [92]. Instead of collecting sample zones at the capillary outlet end during an on-going run, the separated sample zones distributing along the separation channel were segmented and collected for MALDI-MS. After a brief voltage application, the separation was stopped and valves along the separation channels were closed to form segmented compartments. By actuating the pumps in the control layer, these in-channel fractionated sample segments were sent to individual micro reservoirs by pressure via a series of branched channels connected to the separation channel. Then the collected microliter volume fractions were transferred out of the microfluidic device by dispensing tools for the subsequent MALDI-MS detection. The separation resolution was significantly limited by the number of fractions that could be collected on the chip; and the detection sensitivity could also be compromised by the sample loss during transferring the microliter fractions from the microfluidic device to the MALDI target.

4 Concluding remarks

This review summarizes the recent technological advances in the development and application of interfacing CE based separation techniques with ESI and MALDI MS detection for biomolecule analysis. While LC-ESI-MS remains the most widely used platform for ‘omics’ research, growing interests in the application of CE-ESI-MS in the analysis of small molecules, peptides as well as proteins have been propelled by the evolving and ever-improving interface designs.

Improvements on interface robustness, ionization efficiency, signal stability and reproducibility make CE-ESI-MS a complementary or an even superior tool in specific applications, especially in the analyses of small hydrophilic metabolites, short peptides and post-translational modification of proteins. Although MALDI-MS is seldom used for label-free quantification, CE-MALDI-MS integrated with isotopic labelling [73, 80, 81] or iTRAQ labelling [93] has proven to be effective in multiplexed relative quantification of peptides or protein digests from complex biological samples. High spatial resolution of MALDI-MS imaging (MSI) enables almost complete retention of the on-column separation efficiency. The reconstructed electropherograms of isotopically labeled peptide pairs allow for quantitative analysis, making CE-MALDI-MSI a promising technique for samples that could not be well resolved or efficiently ionized by on-line CE-ESI-MS. With the fast development in CE-MS instrumentation, we envision that this analytical platform would find greater utility for many routine analyses in analytical laboratories and provide powerful tools to solve challenging biological problems.

5 References

[1] Ramautar, R., Somsen, G. W., de Jong, G. J., *Electrophoresis* 2013, *34*, 86-98.

[2] Kuehnbaum, N. L., Britz-McKibbin, P., *Chemical Reviews* 2013, *113*, 2437-2468.

[3] Zhao, S. S., Zhong, X. F., Tie, C., Chen, D. D. Y., *Proteomics* 2012, *12*, 2991-3012.

[4] Krenkova, J., Foret, F., *Proteomics* 2012, *12*, 2978-2990.

[5] Ramautar, R., Heemskerk, A. A. M., Hensbergen, P. J., Deelder, A. M., Busnel, J. M., Mayboroda, O. A., *J. Proteomics* 2012, *75*, 3814-3828.

[6] Fonslow, B. R., Yates, J. R., *J. Sep. Sci.* 2009, *32*, 1175-1188.

[7] Desiderio, C., Rossetti, D. V., Iavarone, F., Messana, I., Castagnola, M., *J. Pharm. Biomed. Anal.* 2010, *53*, 1161-1169.

[8] Mechref, Y., Novotny, M. V., *Mass Spectrometry Reviews* 2009, *28*, 207-222.

[9] Haselberg, R., de Jong, G. J., Somsen, G. W., *Electrophoresis* 2013, *34*, 99-112.

[10] Hommerson, P., Khan, A. M., de Jong, G. J., Somsen, G. W., *Mass Spectrometry Reviews* 2011, *30*, 1096-1120.

[11] Zamfir, A. D., *Journal of Chromatography A* 2007, *1159*, 2-13.

[12] Maxwell, E. J., Chen, D. D. Y., *Analytica Chimica Acta* 2008, *627*, 25-33.

[13] Klampfl, C. W., *Electrophoresis* 2009, *30*, S83-S91.

[14] Bonvin, G., Schappler, J., Rudaz, S., *Journal of Chromatography A* 2012, *1267*, 17-31.

[15] Smith, R. D., Barinaga, C. J., Udseth, H. R., *Anal. Chem.* 1988, *60*, 1948-1952.

[16] Lapainis, T., Rubakhin, S. S., Sweedler, J. V., *Anal. Chem.* 2009, *81*, 5858-5864.

[17] Nemes, P., Knolhoff, A. M., Rubakhin, S. S., Sweedler, J. V., *Anal. Chem.* 2011, *83*, 6810-6817.

[18] Nemes, P., Rubakhin, S. S., Aerts, J. T., Sweedler, J. V., *Nat. Protoc.* 2013, *8*, 783-799.

[19] Nemes, P., Knolhoff, A. M., Rubakhin, S. S., Sweedler, J. V., *ACS Chem. Neurosci.* 2012, *3*, 782-792.

[20] Knolhoff, A. M., Nautiyal, K. M., Nemes, P., Kalachikov, S., Morozova, I., Silver, R., Sweedler, J. V., *Anal. Chem.* 2013, *85*, 3136-3143.

[21] Maxwell, E. J., Zhong, X. F., Zhang, H., van Zeijl, N., Chen, D. D. Y., *Electrophoresis* 2010, *31*, 1130-1137.

[22] Wojcik, R., Dada, O. O., Sadilek, M., Dovichi, N. J., *Rapid Commun. Mass Spectrom.* 2010, *24*, 2554-2560.

[23] Maxwell, E. J., Zhong, X. F., Chen, D. D. Y., *Anal. Chem.* 2010, *82*, 8377-8381.

[24] Li, Y., Wojcik, R., Dovichi, N. J., Champion, M. M., *Anal. Chem.* 2012, *84*, 6116-6121.

[25] Sun, L., Li, Y., Champion, M. M., Zhu, G., Wojcik, R., Dovichi, N. J., *Analyst* 2013, *138*, 3181-3188.

[26] Li, Y., Champion, M. M., Sun, L., Champion, P. A. D., Wojcik, R., Dovichi, N. J., *Anal. Chem.* 2012, *84*, 1617-1622.

[27] Sun, L. L., Zhu, G. J., Li, Y. H., Wojcik, R., Yang, P., Dovichi, N. J., *Proteomics* 2012, *12*, 3013-3019.

[28] Wojcik, R., Li, Y., MacCoss, M. J., Dovichi, N. J., *Talanta* 2012, *88*, 324-329.

[29] Zhu, G., Sun, L., Yang, P., Dovichi, N. J., *Analytica Chimica Acta* 2012, *750*, 207-211.

[30] Sun, L. L., Zhu, G. J., Dovichi, N. J., *Anal. Chem.* 2013, *85*, 4187-4194.

[31] Zhu, G., Sun, L., Yan, X., Dovichi, N. J., *Anal. Chem.* 2013, *85*, 2569-2573.

[32] Zhong, X. F., Maxwell, E. J., Chen, D. D. Y., *Anal. Chem.* 2011, *83*, 4916-4923.

[33] Maxwell, E. J., Ratnayake, C., Jayo, R., Zhong, X. F., Chen, D. D. Y., *Electrophoresis* 2011, *32*, 2161-2166.

[34] Jayo, R. G., Li, J. J., Chen, D. D. Y., *Anal. Chem.* 2012, *84*, 8756-8762.

[35] Zhong, X. F., Maxwell, E. J., Ratnayake, C., Mack, S., Chen, D. D. Y., *Anal. Chem.* 2011, *83*, 8748-8755.

[36] Moini, M., *Anal. Chem.* 2007, *79*, 4241-4246.

[37] Faserl, K., Sarg, B., Kremser, L., Lindner, H., *Anal. Chem.* 2011, *83*, 7297-7305.

[38] Tie, C., Zhang, D. W., Chen, H. X., Song, S. L., Zhang, X. X., *J. Mass Spectrom.* 2012, *47*, 1429-1434.

[39] Busnel, J. M., Schoenmaker, B., Ramautar, R., Carrasco-Pancorbo, A., Ratnayake, C., Feitelson, J. S., Chapman, J. D., Deelder, A. M., Mayboroda, O. A., *Anal. Chem.* 2010, *82*, 9476-9483.

[40] Heemskerk, A. A. M., Busnel, J. M., Schoenmaker, B., Derks, R. J. E., Klychnikov, O., Hensbergen, P. J., Deelder, A. M., Mayboroda, O. A., *Anal. Chem.* 2012, *84*, 4552-4559.

[41] Heemskerk, A. A. M., Wuhrer, M., Busnel, J. M., Koeleman, C. A. M., Selman, M. H. J., Vidarsson, G., Kapur, R., Schoenmaker, B., Derks, R. J. E., Deelder, A. M., Mayboroda, O. A., *Electrophoresis* 2013, *34*, 383-387.

[42] Haselberg, R., de Jong, G. J., Somsen, G. W., *Anal. Chem.* 2013, *85*, 2289-2296.

[43] Bonvin, G., Veuthey, J. L., Rudaz, S., Schappler, J., *Electrophoresis* 2012, *33*, 552-562.

[44] Hirayama, A., Tomita, M., Soga, T., *Analyst* 2012, *137*, 5026-5033.

[45] Ramautar, R., Busnel, J. M., Deelder, A. M., Mayboroda, O. A., *Anal. Chem.* 2012, *84*, 885-892.

[46] Whitmore, C. D., Gennaro, L. A., *Electrophoresis* 2012, *33*, 1550-1556.

[47] Haselberg, R., Ratnayake, C. K., de Jong, G. J., Somsen, G. W., *Journal of Chromatography A* 2010, *1217*, 7605-7611.

[48] Nguyen, A., Moini, M., *Anal. Chem.* 2008, *80*, 7169-7173.

[49] Moini, M., *Rapid Commun. Mass Spectrom.* 2010, *24*, 2730-2734.

[50] Haselberg, R., Harmsen, S., Dolman, M. E. M., de Jong, G. J., Kok, R. J., Somsen, G. W., *Analytica Chimica Acta* 2011, *698*, 77-83.

[51] Moini, M., Klauenberg, K., Ballard, M., *Anal. Chem.* 2011, *83*, 7577-7581.

[52] Kawai, M., Iwamuro, Y., Iio-Ishimaru, R., Chinaka, S., Takayama, N., Hayakawa, K., *Anal. Sci.* 2011, *27*, 857-860.

[53] Ramautar, R., Shyti, R., Schoenmaker, B., de Groote, L., Derks, R. J. E., Ferrari, M. D., van den Maagdenberg, A., Deelder, A. M., Mayboroda, O. A., *Anal. Bioanal. Chem.* 2012, *404*, 2895-2900.

[54] Wang, Y., Fonslow, B. R., Wong, C. C. L., Nakorchevsky, A., Yates, J. R., *Anal. Chem.* 2012, *84*, 8505-8513.

[55] Sarg, B., Faserl, K., Kremser, L., Halfinger, B., Sebastiano, R., Lindner, H. H., *Mol Cell Proteomics* 2013, *12*, 2640-2656.

[56] Shi, L. H., Jin, Y. X., Moon, D. C., Kim, S. K., Park, S. R., *Electrophoresis* 2009, *30*, 1661-1669.

[57] Jeong, J. S., Kim, S. K., Park, S. R., *Electrophoresis* 2012, *33*, 2112-2121.

[58] Huang, J. L., Hsu, R. Y., Her, G. R., *Journal of Chromatography A* 2012, *1267*, 131-137.

[59] Li, F. A., Wang, C. H., Her, G. R., *Electrophoresis* 2007, *28*, 1265-1273.

[60] Li, F. A., Huang, J. L., Her, G. R., *Electrophoresis* 2008, *29*, 4938-4943.

[61] Hoffmann, P., Hausig, U., Schulze, P., Belder, D., *Angew. Chem.-Int. Edit.* 2007, *46*, 4913-4916.

[62] Hoffmann, P., Eschner, M., Fritzsche, S., Belder, D., *Anal. Chem.* 2009, *81*, 7256-7261.

[63] Fritzsche, S., Hoffmann, P., Belder, D., *Lab Chip* 2010, *10*, 1227-1230.

[64] Mellors, J. S., Gorbounov, V., Ramsey, R. S., Ramsey, J. M., *Anal. Chem.* 2008, *80*, 6881-6887.

[65] Mellors, J. S., Jorabchi, K., Smith, L. M., Ramsey, J. M., *Anal. Chem.* 2010, *82*, 967-973.

[66] Chambers, A. G., Mellors, J. S., Henley, W. H., Ramsey, J. M., *Anal. Chem.* 2011, *83*, 842-849.

[67] Mellors, J. S., Black, W. A., Chambers, A. G., Starkey, J. A., Lacher, N. A., Ramsey, J. M., *Anal. Chem.* 2013, *85*, 4100-4106.

[68] Huck, C. W., Bakry, R., Huber, L. A., Bonn, G. K., *Electrophoresis* 2006, *27*, 2063-2074.

[69] Helmja, K., Borissova, M., Knjazeva, T., Jaanus, M., Muinasmaa, U., Kaljurand, M., Vaher, M., *Journal of Chromatography A* 2009, *1216*, 3666-3673.

[70] Vannatta, M. W., Whitmore, C. D., Dovichi, N. J., *Electrophoresis* 2009, *30*, 4071-4074.

[71] Wang, J., Ma, M., Chen, R., Li, L., *Anal. Chem.* 2008, *80*, 6168-6177.

[72] Wang, J. H., Jiang, X. Y., Sturm, R. M., Li, L. J., *Journal of Chromatography A* 2009, *1216*, 8283-8288.

[73] Wang, J., Zhang, Y., Xiang, F., Zhang, Z., Li, L., *Journal of Chromatography A* 2010, *1217*, 4463-4470.

[74] Pourhaghighi, M. R., Busnel, J. M., Girault, H. H., *Electrophoresis* 2011, *32*, 1795-1803.

[75] Busnel, J. M., Josserand, J., Lion, N., Girault, H. H., *Anal. Chem.* 2009, *81*, 3867-3872.

[76] Gorbatsova, J., Borissova, M., Kaljurand, M., *Electrophoresis* 2012, *33*, 2682-2688.

[77] Vanveelen, P. A., Tjaden, U. R., Vandergreef, J., Ingendoh, A., Hillenkamp, F., *Journal of Chromatography* 1993, *647*, 367-374.

[78] Zhang, H. Y., Caprioli, R. M., *J. Mass Spectrom.* 1996, *31*, 1039-1046.

[79] Amantonico, A., Urban, P. L., Zenobi, R., *Analyst* 2009, *134*, 1536-1540.

[80] Wang, J. H., Ye, H., Zhang, Z. C., Xiang, F., Girdaukas, G., Li, L. J., *Anal. Chem.* 2011, *83*, 3462-3469.

[81] Zhang, Z. C., Ye, H., Wang, J. H., Hui, L. M., Li, L. J., *Anal. Chem.* 2012, *84*, 7684-7691.

[82] Zhang, Z. C., Jia, C. X., Li, L. J., *J. Sep. Sci.* 2012, *35*, 1779-1784.

[83] Hui, L. M., Cunningham, R., Zhang, Z. C., Cao, W. F., Jia, C. X., Li, L. J., *J. Proteome Res.* 2011, *10*, 4219-4229.

[84] Zhang, Z. C., Wang, J. H., Hui, L. M., Li, L. J., *Journal of Chromatography A* 2011, *1218*, 5336-5343.

[85] Weiss, N. G., Zwick, N. L., Hayes, M. A., *Journal of Chromatography A* 2010, *1217*, 179-182.

[86] Lechner, M., Seifner, A., Rizzi, A. M., *Electrophoresis* 2008, *29*, 1974-1984.

[87] Cheng, C. A., Lu, J. A. J., Wang, X. Y., Roberts, J., Liu, S. R., *Electrophoresis* 2010, *31*, 2614-2621.

[88] Weiss, N. G., Jarvis, J. W., Nelson, R. W., Hayes, M. A., *Proteomics* 2011, *11*, 106-113.

[89] Silvertand, L. H. H., Torano, J. S., de Jong, G. J., van Bennekom, W. P., *Electrophoresis* 2009, *30*, 1828-1835.

[90] Zhang, Z. C., Wang, J. H., Hui, L. M., Li, L. J., *Electrophoresis* 2012, *33*, 661-665.

[91] Lu, J. J., Zhu, Z. F., Wang, W., Liu, S. R., *Anal. Chem.* 2011, *83*, 1784-1790.

[92] Luo, Y. Q., Xu, S. Y., Schilling, J. W., Lau, K. H., Whitin, J. C., Yu, T. T. S., Cohen, H. J., *Jala* 2009, *14*, 252-261.

[93] Zuberovic, A., Wetterhall, M., Hanrieder, J., Bergquist, J., *Electrophoresis* 2009, *30*, 1836-1843.

Figures

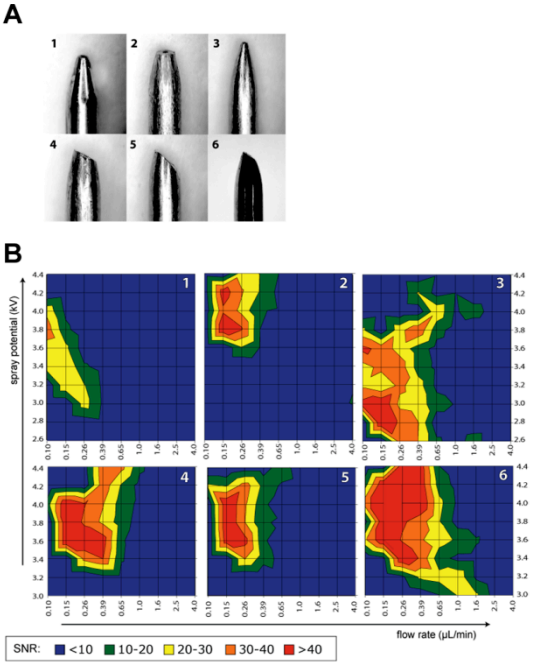

Figure 1(A) Different shapes of stainless steel electrospray emitters investigated for optimal ESI performance: symmetrically tapered electrospray needle (**1**), blunt tapered tip (**2**), sharp tapered needle (**3**), 30° bevel tip made from **2** (**4**), 45° bevel tip made from **2** (**5**), 35° bevel tip with a smaller surface area (**6**). (B) Average signal-to-noise ratio of arginine as a function of flow rate and electrospray potential. Emitter geometry for each plot is indicated in the top right corner. Sample: 20 μM each of proline, threonine, isoleucine, and arginine in 0.2% formic acid and 50% methanol. Reprinted with permission from Ref [23]. Copyright American Chemical Society 2010.

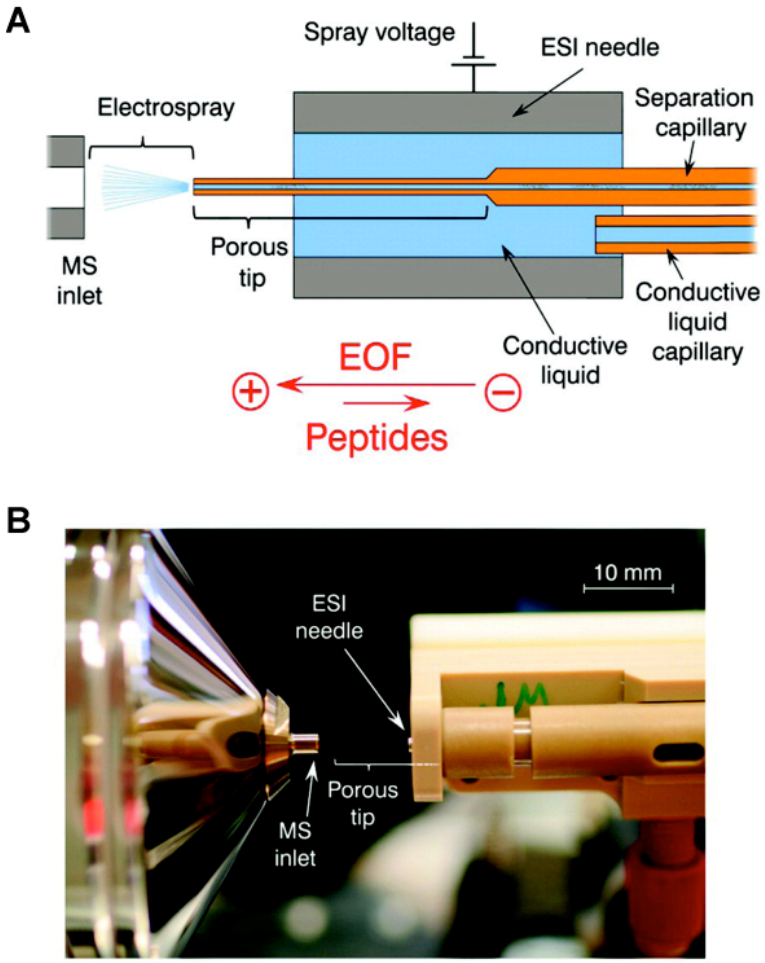

Figure 2 The high-sensitivity porous sprayer interface (A) schematic and (B) photograph of the prototype interface. Reprinted with permission from Ref [37]. Copyright American Chemical Society 2011.

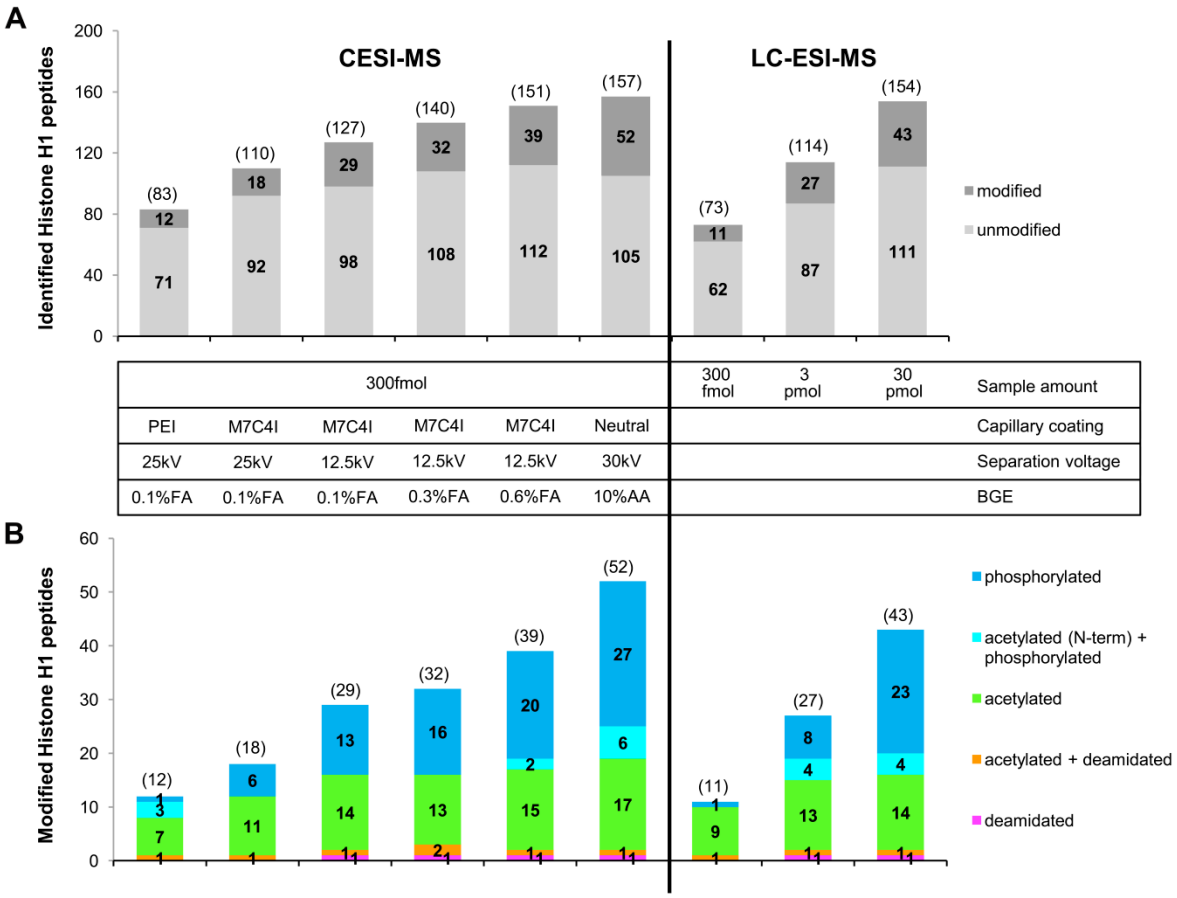

Figure 3 Number of unmodified and modified histone H1 peptides identified by CE- and LC-ESI-MS/MS analysis. (A) Number of identified histone H1 peptides (modified and non-modified) were merged from triplicate analyses. (B) Within each column the total number of modified peptides as well as the distribution of specific types of modifications is shown. The numbers presented in the diagram are the sum of unique modified peptides found in triplicate runs. Overlap of peptides identified with CE-ESI-MS ranges from 75.0% - 84.1%, with LC-ESI-MS from 65.8% - 71.4%. Reprinted with permission from Ref [55]. Copyright American Society for Biochemistry and Molecular Biology 2013.

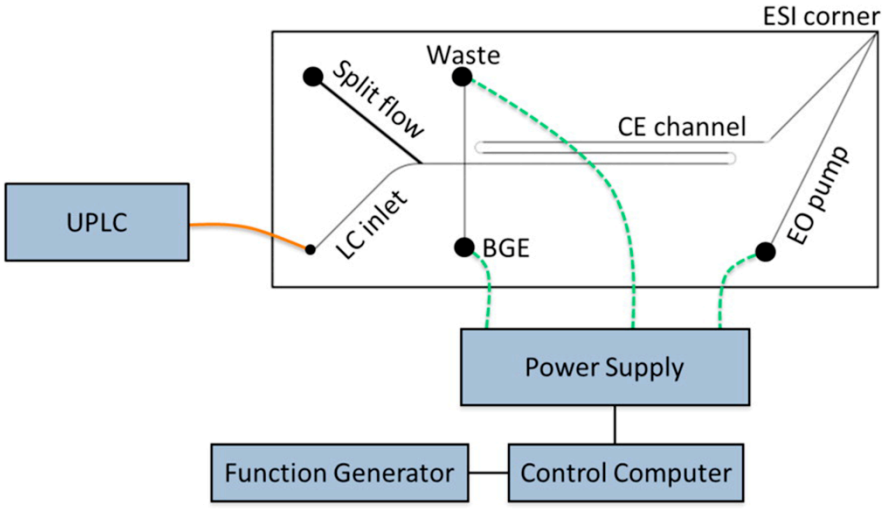

Figure 4 Schematic of the hybrid capillary LC microchip CE-ESI experimental setup. The orange line represents a transfer capillary connecting the LC column to the microfluidic device. The dashed green lines represent electrical connections between the high voltage power supply and the microfluidic reservoirs. The device was positioned with the ESI corner approximately 5 mm from the mass spectrometer inlet. Reprinted with permission from Ref [67]. Copyright American Chemical Society 2013.

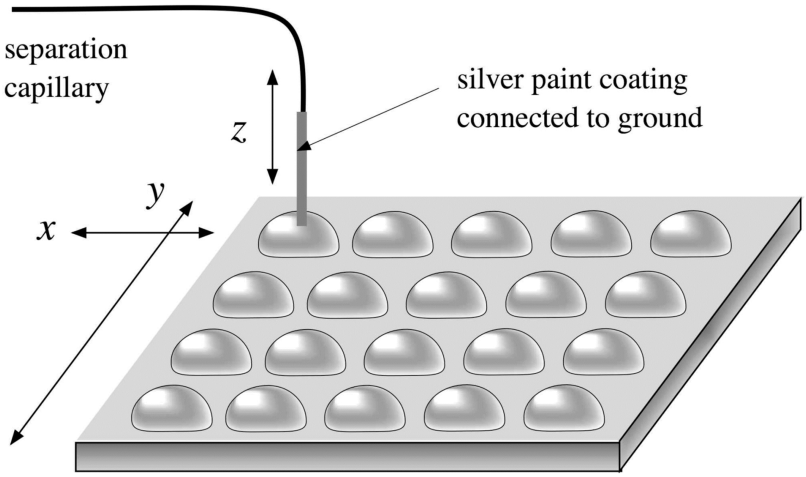

Figure 5 CE-MALDI-MS interface by iontophoretic fraction collection. A separation capillary silver-coated at the tip was dipped into droplets predeposited on the MALDI plate mounted on an x-y stage. Fractions were collected based on electro-migration and diffusion. Reprinted with permission from Ref [75] Copyright American Chemical Society 2009.

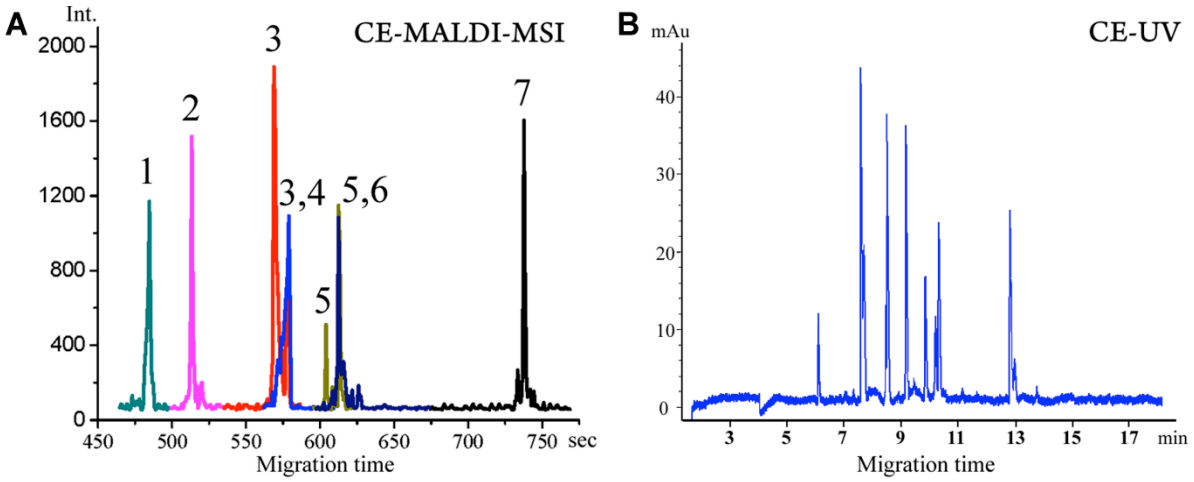

Figure 6 (A) Reconstructed CE electropherogram from MALDI TOF/TOF-MSI of seven peptide standards. The peak IDs are (1) GAHKNYLRF, *m/z* 1105.59 (0.70 µM), (2) IARRHPYFL, *m/z* 1172.67 (0.75 µM), (3) SGGFAFSPRLamide, *m/z* 1037.55 (0.65 µM), (4) CYFQNCPRGamide, *m/z* 1084.45 (0.37 µM), (5) APSGAQRLYGFGLamide, *m/z* 1335.72 (0.25 µM), (6) AGCKNFFWKTFTSC, *m/z* 1637.72 (0.55 µM), (7) PFCNAFTGCamide, *m/z* 956.37 (0.5 µM). (B) CE-UV electropherogram. Reprinted with permission from Ref [80] Copyright American Chemical Society 2011.

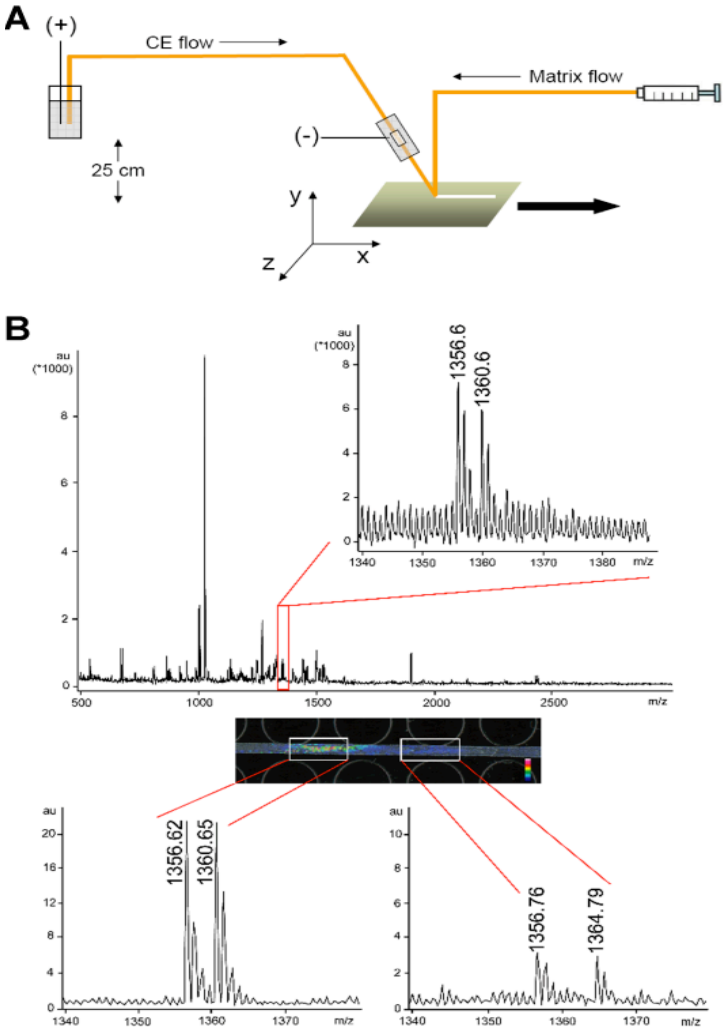

Figure 7 Interface for pressure assisted CE-MALDI-MSI coupling. (A) CE flow and matrix flow are collected on a ground stainless steel MALDI plate. (B) Image-based analysis of isotopic labeled peptide peak pairs (1:1 concentration ratio) showing enhanced signal-to-noise ratios and improved quantitation accuracy. Reprinted with permission from Ref [81]. Copyright American Chemical Society 2012.

Chapter 3

A One-Step Preparation Method of Monolithic Enzyme Reactor for Highly Efficient Sample Preparation Coupled to Mass Spectrometry-Based Proteomics Studies

Adapted from:

1. **Jiang S.**, Zhang Z., Li L., A one-step preparation method of monolithic enzyme reactor for highly efficient sample preparation coupled to mass spectrometry-based proteomics studies. *J chromatogr A.* 2015 (1412) 75-81.

Abstract

Mass spectrometry (MS) coupled to sample preparation and separation techniques has become a primary tool for proteomics studies. However, due to sample complexity, it is often challenging to achieve fast and efficient sample preparation prior to MS analysis. In recent decades, monolithic materials have been developed not only as chromatographic media, but also as efficient solid supports for immobilizing multiple types of affinity reagents. Herein, the N-acryloxysuccinimide-co-acrylamide-co-N,N'-methylenebisacrylamide (NAS-AAm-Bis) monolith was fabricated within silanized 200 μm i.d. fused-silica capillaries and was used as an immobilized enzyme reactor (IMER). The column was conjugated with trypsin/Lys-C and Lys-N enzymes to allow enzymatic digestions to occur while protein mixture was loaded onto the IMER column followed by MS-based proteomics analysis. Similar MS signal and protein sequence coverage were observed using protein standard bovine serum albumin (BSA) compared to in-solution digest. Furthermore, mouse serum, yeast, and human cell lysate samples were also subjected to enzymatic digestion by both IMER (in seconds to minutes) and conventional in solution digestion (overnight) for comparison in large-scale proteomics studies. Comparable protein identification results obtained by the two methods highlighted the potential of employing NAS-based IMER column for fast and highly efficient sample preparation to MS analysis in proteomics studies.

1. Introduction

Proteomics is the large-scale study of proteins which can provide global information of protein identification, characterization, and quantification. Proteomics increasingly plays an important role in major research areas including protein interaction studies, biomarker discovery, cancer remediation, drug treatment, and disease-screening medical diagnostics [1-3]. Mass spectrometry (MS) has become the method of choice for proteomics analysis. Analytes from complex samples can be resolved, fragmented, identified and quantified in various biological samples. Numerous applications have been reported in the field of MS-based peptide and protein analysis [4, 5].

Among various approaches in proteomics study, bottom-up proteomics remains the most widely applied method. In the bottom-up approach, proteins are digested into smaller peptide fragments that are often easier to ionize and detect by liquid chromatography-electrospray ionization mass spectrometry (LC-ESI-MS) and matrix-assisted laser desorption/ionization mass spectrometry (MALDI-MS) [6-8]. The classic workflow for MS-based proteomics mainly involves protein solubilization/denaturation, reduction, alkylation, and enzymatic digestion. One of the most time-consuming steps is protein digestion, taking as much as 12h or longer for complex sample digestion. In addition, the introduction of salt requires extra clean up steps in sample preparation, which cause sample loss and higher likelihood of degradation [9, 10]. To address this bottleneck in protein identification, characterization and quantification, protein digestion has been improved through the development of novel techniques in order to increase throughput and reproducibility. Over the years, researchers have established various approaches to assist digestion such as microwave irradiation, infrared energy, organic and detergent-assisted methods, power ultrasound with elevated pressure and temperature, etc [11-15]. The improved

throughput in protein digestion is also achieved by immobilization of the protease onto a solid support leading to reduced autolysis of enzyme and enhanced digestion efficiency [16, 17].

Immobilized enzyme reactors (IMERs) have the ability to increase the throughput and efficiency of sample preparation [18]. Multiple types of solid support have been applied in IMERs fabricated into different formats such as capillary, microchip, pipette tips, etc [19-22]. Monolithic materials that possess a continuous macroporous channel, which features both large surface area and low backpressure, have been demonstrated as an efficient solid support suitable for multiple types of binding ligands [23]. A variety of monoliths have been reported for manufacturing micro-reactors used in proteolysis reaction of proteins into peptides. With active functional groups or leaving groups on the monolithic structure, proteins can be covalently linked to the monolithic surface while retaining their biological activities. Multiple types of monoliths have been employed for protein conjugation including poly(glycidy methacrylate-co-ethylene dimethacrylate), (GMA-EDMA), agarose, cryogel, and silica monoliths [24, 25]. The functional groups of monolithic materials make them ideal for multiple immobilization strategies with various ligands. Although monolithic supports feature fast and highly efficient on-column reactions, the covalent-binding reaction cannot be performed under harsh conditions like high temperature in order to retain the bio-activity of enzymes. Typically, excessive amounts of ligands are required for hours or days long reaction to ensure complete binding of enzyme with functional groups [26].

Despite the attractive features of applying fast and highly efficient sample preparation strategies using monolithic support for protein sample preparation, challenges still exist and require technical improvement to enable analysis of low-level samples or limited ligand amount. Herein, we constructed an IMER incorporated with multi-proteases in an open-tubular type

column and employed that for comprehensive identification in complex cell lysate. The inter-connected channel of monolithic materials enables high reaction speed between stationary phase and mobile phase, while the open-tubular structure ensures fast flow through rate in the meantime. We immobilized multiple proteases, trypsin/Lys-C mixture and Lys-N onto monolithic column so that proteins can be on-column digested in minutes and delivered to a mass spectrometer for subsequent analysis. Proof-of-concept experiments were performed to demonstrate the significant improvement in sample preparation efficiency and in reduction of experimental time with similar protein sequence coverage and protein identification compared to in-solution digestion. Furthermore, IMERs were utilized in large-scale proteomic studies using mouse serum, human and yeast cell lysates. These experiments showed comparable performance to the traditional overnight in-solution digestion method and great potential in micro-scale proteomics analysis.

2. Experimental section

2.1. Reagents and Materials.

Sodium chloride, sodium bicarbonate, ammonium hydroxide, acetone, acetonitrile, methanol, ammonium bicarbonate (AB), benzophenone (BP) and urea were purchased from Fisher Scientific (Pittsburgh, PA). Acrylamide (AAm, 99%), N, N'-methylenebisacrylamide (Bis, 99%), ammonium persulfate (APS, 98%), glycidyl methacrylate (GMA, 97%), ethylene dimethacrylate (EDMA, 98%), 3-(trimethoxysilyl) propyl ethacrylate (bind-silane, 98%), 1-propanol (99.5%), 1,4-butandiol (99%), 2,2′-Azobis(2-methylpropionitrile) (AIBN, 98%), polyethylene glycol (PEG 6000), N,N,N′,N′-Tetramethylethylenediamine (TEMED, 99%), dimethyl sulfoxide (DMSO), trifluoroacetic acid (TFA), iodoacetamide (IAA), α-Cyano-4-hydroxycinnamic acid (CHCA, 99%), mouse serum standard, and bovine serum albumin (BSA)

were from Sigma-Aldrich (St. Louis, MO). D/L-dithiothreitol (DTT), trypsin/Lys-C mix, yeast, and human lysate were from Promega (Madison, WI). N-acryloxysuccinimide (NAS) was got from Tokyo Chemical Industry (Tokyo, Japan). Lys-N was provided from Thermo Scientific (Rockford, IL). All water used in this study was doubly distilled on a Millipore filtration system (Bedford, MA). Fused-silica capillary with 200 μm i.d. and 360 μm o.d. was purchased from Polymicro Technologies (Phoenix, AZ).

2.2. Apparatus.

An ultrafleXtreme MALDI-TOF/TOF from Bruker Daltonics and MALDI LTQ Orbitrap spectrometer from Thermo Scientific were utilized for IMER column optimization and performance evaluation of standard protein BSA. An UtrafleXtreme MALDI-TOF/TOF (Bruker Daltonics, Bremen, Germany) equipped with a 1000 Hz Smartbeam 2 laser was used for IMER column optimization. The mass spectra were acquired in a positive ion reflectron mode with ion source 1 voltage 25.0 kV, ion source 2 voltage 22.0 kV, reflector 1 voltage 26.6 kV, reflector 2 voltage 13.6 kV and lens voltage 6.0 kV. 500 laser shots were accumulated and all the mass spectra were recorded from *m/z* 500 to *m/z* 2500. External calibration was performed by using a standard peptide mixture provided by Bruker Daltonics, including angiotensin II ($[M+H]^+$ 1046.54), angiotensin I ($[M+H]^+$ 1296.68), substance P ($[M+H]^+$ 1347.74), bombesin ($[M+H]^+$ 1619.82), ACTH clip 1-17 ($[M+H]^+$ 2093.09), ACTH clip 18-39 ($[M+H]^+$ 2465.20) and somatostatin ($[M+H]^+$ 3147.47). For evaluating digestion performance of standard protein BSA, the high resolution orbitrap detection was performed with a MALDI-LTQ-Orbitrap XL from Thermo Scientific (Waltham, MA). 10 scans were recorded for each spot with 2 micro-scans each step under the survey CPS (Crystal Positioning System) mode. Mass spectra in positive ion mode from *m/z* 400 to *m/z* 3000 were recorded at a resolution of 70,000 at *m/z* 400. ProteoMass

MALDI calibration kit from Sigma-Aldrich (St. Louis, MO) was used for instrument to achieve high mass accuracy of ±5 ppm.

A Waters nanoAcquity UPLC system (Milford, MA) coupled to a Thermo Scientific Q-Exactive hybrid quadrupole-Orbitrap mass spectrometer was employed for proteomic analysis of complex biological samples. A 75 μm × 100 mm BEH130 C_{18} column from Waters was used in LC separation using a gradient at 350 nL/min. Mobile phase A was composed of water and 0.1% formic acid. Mobile phase B was composed of ACN and 0.1% formic acid. Separation was performed by ramping solvent B from 3% to 10% over 5 min, then to 40% in the next 60 min, and finally to 95% during the following 10 min. MS spectra were acquired in positive ion mode over *m/z* 200-2000 at 70,000 resolution (*m/z* 200) with an AGC target of 1×10^6 and maximum injection time of 250 ms. Data dependent acquisition selected the top 10 most abundant precursor ions for tandem MS by HCD fragmentation using an isolation width of 2.0 Da, a normalized collision energy of 30, a resolution of 17,500, an AGC target of 2×10^5, a maximum injection time of 250 ms and a lower mass limit of *m/z* 100.

2.3. In Solution Protein Digestion.

The in solution protein digestion was performed as a comparison to IMER digestion. Briefly, 30 μg of protein mixture was dissolved in 20 μL of 8 M urea (0.96 g urea in 2.0 mL of 25 mM AB buffer). 1 μL of DTT (1M in 25 mM AB) was added to the tube followed by gentle vortex for reduction of disulfide bonds. After reduction at 37 ^{o}C for 1 h, 20 μL of IAA (200 mM in 25 mM AB) was added to the tube for alkylation for 1 h at room temperature in the dark. To consume residual alkylating reagent, 4 μL of DTT was added followed by 120 μL of 25 mM ammonium bicarbonate solution to dilute urea. In solution digestion was performed overnight at 37 ^{o}C after adding 1 μg of trypsin. The next morning, 1 μL of formic acid was added to quench the reaction

along with gentle vortexing. The digested 30 μg of BSA was divided into six aliquots and stored at -80 ^{o}C. Before usage, one aliquot was dried and reconstituted in 10 μL of 0.1% TFA and desalted with a Ziptip C18 pipette tip to final volume of 17 μL.

2.4. NAS-Based Monolithic Column Fabrication and Ligand Immobilization.

A 20 cm fused-silica capillary (200 μm i.d.) was flushed with 1M NaOH for 30 min, followed by water, 0.1M HCl for 30 min, water, and finally acetone. 50% (v/v) of bind-silane in acetone was flushed through the column for 40 min for silanization. The capillary was then rinsed with acetone and water, respectively. IMER column fabrication was derived from a previous report [27]. We modified and improved the polymerization method to reduce ligand consumption. Briefly, a mixture containing 20mg acrylamide, 30mg N, N'-methylenebisacrylamide and 30mg PEG in 1 mL of 0.2 M sodium bicarbonate/0.5 M sodium chloride buffer was heated at 55-60 °C for 15min. Then, 4 μL of 20% (v/v) TEMED was added to the above-mentioned solution and followed by nitrogen de-gassing. 5 μL N-Acryloxysuccinimide (NAS) (140 mg/mL dissolved in DMSO) was then added on top of the solution, and after 1min, 2 μL of 20% (w/v) ammonium persulfate (APS) was added to initiate polymerization. After 30s, 18 μL aliquot of this solution was quickly mixed with 2 μL of ligand solution (1 mg/mL enzyme containing 0.1 M benzamidine) and was pumped through the pre-treated capillary. Therefore, polymerization of IMER column was carried out in parallel with protease conjugation. The entire reaction can be completed within 30 min at room temperature. After reaction, the column was washed with 25 mM ammonium bicarbonate before sample loading.

2.5. On-Column Protein Digestion with IMER-MALDI-MS and IMER-LC-ESI-MS.

Before IMER digestion, the protein sample (BSA, mouse serum, yeast lysate, or human lysate dissolved in 25 mM ammonium bicarbonate) was reduced with DTT and alkylated with IAA for

10 min, respectively. The IMER column was conditioned with 25 mM ammonium bicarbonate solution. 10 μL protein sample of 0.3 mg/mL was then loaded and flushed through the column at 1μL/min and collected to a vial from the outlet end of the column. The collected digested sample was then analyzed with either MALDI-MS or LC-ESI-MS without further processing.

2.6. Monolithic stage tips

Plastic materials like polypropylene have a hydrophobic, chemically inert surface and the tips were for that reason surface modified using a solution with methanol and BP before use (5 wt%) [19-21, 23]. Poly(GMA-EDMA) monolith was prepared at 70°C from a polymerization mixture composed of EDMA and GMA as monomers, 1-propanol, 1.4-butanediol and water as porogenic solvents. Initiator BP concentration was 1.5 wt% with respect to monomers [24-26, 28]. Ratios of each component in the mixture was outlined in Figure 7. Monolithic stage tips was fabricated in 200 uL and 20 uL volume. After polymerization, trypsin was immobilized onto the stage tips by pipetting for 3 cycles manually. BSA of 0.3 ug/uL was digested by this enzymatic stage tip by 20 cycles pipetting followed by LC-MS/MS analysis.

3. Results and discussion

3.1. Optimization of Monolithic Column.

The condition for immobilizing ligands to NAS-AAm-Bis monolith is milder and follows a one-step reaction at room temperature. The electron pair on the N-terminals attacked the carbon of the carbonyl group causing the breaking of the carbon-oxygen bond which led to leaving of the succinimide group. The monomers, porogen, initiator and ligands were mixed in buffer and then filled into silanized capillary. The reactions including both polymerization and immobilization were conducted simultaneously at room temperature for 30 min, and no clean up procedure was needed except conditioning before usage (Figure 1). Compared with other types of monolithic

columns, ligand consumption was much lower and the short reaction time without heating greatly preserves the bioactivity for enzymes. The microscopic images of the NAS-based monolithic column are shown in Figure 2. An open tubular column was fabricated with highly uniform NAS-based monolith attached to the silanized capillary inner wall (Figure 2A and 2C), and mass transfer occurred between analytes and the monolith through the pores (Figure 2B). Three different internal dimensions of capillary columns have been tested and each MS profile was summed by three scans. As shown in supplemental Figure S1, enzyme-reactor fabricated in 200 μm i.d. produced higher digestion efficiency, as it provided larger space for monolithic stationary phase and produced the highest available monolithic surface area with intermediate pore size.

3.2. Evaluation of IMER Digestion with BSA.

We immobilized trypsin onto the monolith as an IMER and compared its performance with in solution digestion via MALDI-MS detection. The same concentration (5 μM) of BSA was digested by in-solution method and IMER columns of different lengths, including 10 cm, 30 cm, and 60cm. A 60 cm column had higher backpressure and longer distance for flowing through which gave rise to increased collection time of digested peptides from IMER. Therefore, we balanced digestion time with peptides intensity and sequence coverage which demonstrated 30 cm to be most efficient. As outlined in Figure 3C, the 30 cm IMER column yielded signal intensity above 1×10^5 and a sequence coverage at 50% while keeping digestion time within 5 min to produce sufficient amount of peptides for MALDI MS detection. Figure 3A and 3B show the mass spectral comparison between in solution and IMER digestion with MALDI-LTQ-Orbitrap detection. MALDI MS spectra were averaged by 20 scans and full MS were subjected to Mascot fingerprint search. Carbamidomethyl (C) and oxidation (M) were set as variable

modifications, peptide mass tolerance for precursor was set as 25 ppm, and one missed cleavage was allowed in database search. Similar protein coverage at 48-52% was observed for both methods while slightly higher MS signal intensity was obtained with IMER digestion. Compared to other IMERs, this one-step polymerized IMER features minimized preparation time of enzyme reactor with reduced proteases consumption, in the meantime retains good sequence coverage. Considering the significantly reduced digestion time (within 5 min for IMER *vs.* overnight for in solution digestion) and the capability for online coupling to other preparation/separation dimensions, IMER digestion provides a new avenue for fast and efficient proteomics sample preparation.

3.3. IMER Digestion of Mouse Serum, Yeast Cell Lysate and Human Cell Lysate Samples. Compared to other previously published work on IMER columns, the NAS-AAm-Bis column features mild fabrication condition and an open tubular inner structure with higher protein sequence coverage as observed with BSA analysis [29, 30]. We further applied IMER digestion to more complex samples followed by LC-ESI-Orbitrap detection to test if IMER digestion can be applied to large-scale proteomics studies. As outlined in Figure 4, the mouse serum, yeast and human cell lysate samples with final concentration of 0.3μg/μL were dissolved in ammonium bicarbonate buffer for reduction and alkylation for 10 min each, and then loaded onto a 30-cm IMER column for on-column digestion. The flow-through was collected without any further cleaning step. Alternatively, the protein mixtures were also digested by conventional in solution method overnight followed by drying, reconstitution, and desalting. The digested samples using both methods were loaded onto the LC column and analyzed with high resolution Q-Exactive Orbitrap mass analyzer, respectively.

The comparison of LC chromatograms from IMER and conventional in-solution digestion is shown in Figure 5. Immobilized enzymes exhibited similar digestion efficiency as free enzymes. Peptides digested by IMER showed a clean chromatogram, indicating no extra clean-up step was needed and complex protein mixtures were completely digested compared to in solution digestion. Raw data files were processed through Mascot MS/MS ion search and Proteome Discoverer 1.4 (PD) using Sequest HT algorithm. By using Mascot MS/MS ion search for mouse serum, 106 proteins with significant scores ($p<0.05$) have been matched with IMER digestion, while 137 matches were observed from the digestion in solution plus sample cleaning. Data analysis for yeast and human cell lysates using PD also showed a comparable performance for IMER and in-solution digestion in terms of total identified protein numbers. With a precursor mass tolerance of 25 ppm and a fragment mass tolerance of 0.02 Da, identified peptides were additionally filtered with a false discovery rate (FDR) better than 1% as high confident peptides. As summarized in Table 1, 445 protein groups (with 5072 merged proteins and 12922 peptides) were identified in yeast lysate sample by IMER and 487 protein groups (with 5697 merged proteins and 10021 peptides) for in-solution method, while 216 protein groups (with 33846 merged proteins and 18052 peptides) were observed from human cell lysate samples by IMER and 207 protein groups (with 39010 merged proteins and 20696 peptides) by conventional method. As expected, the majority of the proteins identified are commonly shared while each digestion method also obtained unique protein IDs as shown in the Venn diagram in Figure 6, indicating its ability in improving complementary protein identifications as well as being an attractive alternative for global analysis of peptides and proteins from complicated biological matrix.

3.4. Comprehensive Protein Identification Using Multi-IMERs.

Unlike trypsin which cleaves at the carboxyl side of lysine and arginine, LysN protease cleaves at the amino-terminus of lysine residues. As a result, the peptides generated by LysN are longer than those generated by trypsin and have more prevalent charged amino terminal peptide fragments. Thus, the combination of using two types of enzymes greatly improved the peptide coverage and protein identification. A complementary identification of yeast lysate was performed using two types of IMER immobilized with trypsin/Lys-C mixture and Lys-N, respectively. The digested peptides were further injected onto LC-ESI-Orbitrap and the resulting data were processed through Mascot MS/MS ion search. As a result of complementary digestion, 559 proteins were matched in total, whereas 220 proteins were overlapped by both IMERs. In comparison to previous IMER studies, we demonstrated highly efficient one-step preparation of open-tubular IMER which accomplished polymerization and enzyme conjugation in 30 min. On-column digestion time was reduced to 5 min and acquired comparable sequence coverage without excessive amount of enzyme or immobilization time. Additionally, the combination of multiple proteases on IMER improves the analysis of different sub-groups of peptides, thus enhance identifications for “shotgun” proteomics.

3.5. In-tip digestion

Enzyme immobilized monolithic stage tips was illustrated in Figure 7. In-tip digestion of BSA took less than 2 min. The digested peptide mixture was injected into the Q Exactive mass spectrometer for top 10 DDA analysis. The acquired data was then searched against PEAKS software for peptide identification and calculation of protein coverage. A descent LC chromatogram of BSA in-tip digestion was shown Figure 8A. BSA sequence was used for peptide mapping in Figure 8B, amino acids that highlighted in grey were covered by tryptic peptides digested in-tip resulting in a sequence coverage of 91%. With nano-scale sample

consumption, in-tip digestion significantly improved efficiency and throughput without loss of digestion completion. These findings demonstrated the great potential and ability of applying monolithic stationary phase for manufacturing of functional pipette tips.

4. Conclusions

In this work, the NAS-AAm-Bis monolithic enzyme reactor has been developed as well as its offline coupling to MALDI-TOF/TOF, MALDI-LTQ-Orbitrap for feasibility evaluation using protein standard, and ESI-Orbitrap for proteomics study. The results showed that monolithic support enables highly specific and effective enzymatic reactions between analytes and immobilized enzymes with improved reproducibility and throughput. By comparison with conventional protein digestion in solution, IMER exhibits similar protein and peptide coverage but with significantly reduced reaction time and sample loading amount. In addition, no extra steps for cleaning are needed, highlighting the great potential for online coupling to MS analysis. The present work demonstrated the advantages of applying monolithic affinity support to complex peptidomics and proteomics studies.

Acknowledgements

This work is supported by National Institutes of Health grants (1R01DK071801 and S10RR029531). The authors thank Thermo Pierce for providing LysN enzyme. We also thank the Biological and Biomaterials Preparation, Imaging and Characterization Facility at UW-Madison for taking scanning electron microscope image.

References:

1. Cheng, G., et al., *Immobilization of trypsin onto multifunctional meso-/macroporous core-shell microspheres: A new platform for rapid enzymatic digestion.* Analytica Chimica Acta, 2014. **812**: p. 65-73.
2. Yamaguchi, H. and M. Miyazaki, *Enzyme-immobilized reactors for rapid and efficient sample preparation in MS-based proteomic studies.* Proteomics, 2013. **13**(3-4): p. 457-466.
3. Switzar, L., M. Giera, and W.M.A. Niessen, *Protein Digestion: An Overview of the Available Techniques and Recent Developments.* Journal of Proteome Research, 2013. **12**(3): p. 1067-1077.
4. Chiou, S.-H., et al., *Clinical proteomics: Current status, challenges, and future perspectives.* The Kaohsiung Journal of Medical Sciences, 2011. **27**(1): p. 1-14.
5. Boonen, K., et al., *Peptidomics: The integrated approach of MS, hyphenated techniques and bioinformatics for neuropeptide analysis.* Journal of Separation Science, 2008. **31**(3): p. 427-445.
6. Yamaguchi, H., et al., *Multidigestion in continuous flow tandem protease-immobilized microreactors for proteomic analysis.* Analytical Biochemistry, 2010. **407**(1): p. 12-18.
7. Xu, X., et al., *Trypsin entrapped in poly(diallyldimethylammonium chloride) silica sol-gel microreactor coupled to matrix-assisted laser desorption/ionization time-of-flight mass spectrometry.* Rapid Communications in Mass Spectrometry, 2008. **22**(8): p. 1257-1264.
8. Duan, J., et al., *Rapid protein identification using monolithic enzymatic microreactor and LC-ESI-MS/MS.* Proteomics, 2006. **6**(2): p. 412-419.

9. López-Ferrer, D., et al., *Sample treatment for protein identification by mass spectrometry-based techniques.* TrAC Trends in Analytical Chemistry, 2006. **25**(10): p. 996-1005.

10. Capelo, J.L., et al., *Overview on modern approaches to speed up protein identification workflows relying on enzymatic cleavage and mass spectrometry-based techniques.* Analytica Chimica Acta, 2009. **650**(2): p. 151-159.

11. Shin, S., et al., *Effects of temperature on ultrasound-assisted tryptic protein digestion.* Analytical Biochemistry, 2011. **414**(1): p. 125-130.

12. Vale, G., et al., *An assessment of the ultrasonic probe-based enhancement of protein cleavage with immobilized trypsin.* Proteomics, 2011. **11**(19): p. 3866-3876.

13. Pramanik, B.N., et al., *Microwave-enhanced enzyme reaction for protein mapping by mass spectrometry: A new approach to protein digestion in minutes.* Protein Science, 2009. **11**(11): p. 2676-2687.

14. Wang, S., et al., *Infrared-assisted tryptic proteolysis for peptide mapping.* Proteomics, 2008. **8**(13): p. 2579-2582.

15. Li, F., C.M. Schmerberg, and Q.C. Ji, *Accelerated tryptic digestion of proteins in plasma for absolute quantitation using a protein internal standard by liquid chromatography/tandem mass spectrometry.* Rapid Communications in Mass Spectrometry, 2009. **23**(5): p. 729-732.

16. Girelli, A.M. and E. Mattei, *Application of immobilized enzyme reactor in on-line high performance liquid chromatography: A review.* Journal of Chromatography B, 2005. **819**(1): p. 3-16.

17. Massolini, G. and E. Calleri, *Immobilized trypsin systems coupled on-line to separation methods: Recent developments and analytical applications.* Journal of Separation Science, 2005. **28**(1): p. 7-21.

18. Long, Y. and T.D. Wood, *Immobilized Pepsin Microreactor for Rapid Peptide Mapping with Nanoelectrospray Ionization Mass Spectrometry.* Journal of The American Society for Mass Spectrometry, 2014. **26**(1): p. 194-197.

19. P. Castell, M.W., 2 G. de With,1 H. Fischer,3 F. Huijs, *Surface Modification of Poly(propylene) by Photoinitiators: Improvement of Adhesion and Wettability.* Journal of Applied Polymer Science, 2003. **92**: p. 2341-2350.

20. Skoglund, C., F. Bassyouni, and M. Abdel-Rehim, *Monolithic packed 96-tips set for high-throughput sample preparation: determination of cyclophosphamide and busulfan in whole blood samples by monolithic packed 96-tips and LC-MS.* Biomedical Chromatography, 2013. **27**(6): p. 714-719.

21. Krenkova, J. and F. Foret, *Nanoparticle-modified monolithic pipette tips for phosphopeptide enrichment.* Analytical and Bioanalytical Chemistry, 2012. **405**(7): p. 2175-2183.

22. *<In-tip-digestion.pdf>*.

23. Ueda, K., et al., *Antibody-coupled monolithic silica microtips for highthroughput molecular profiling of circulating exosomes.* Scientific Reports, 2014. **4**: p. 6232.

24. Kleifeld, O., et al., *Identifying and quantifying proteolytic events and the natural N terminome by terminal amine isotopic labeling of substrates.* Nature Protocols, 2011. **6**(10): p. 1578-1611.

25. Altun, Z., et al., *Surface modified polypropylene pipette tips packed with a monolithic plug of adsorbent for high-throughput sample preparation.* Journal of Separation Science, 2007. **30**(12): p. 1964-1972.

26. Rappsilber, J., M. Mann, and Y. Ishihama, *Protocol for micro-purification, enrichment, pre-fractionation and storage of peptides for proteomics using StageTips.* Nature Protocols, 2007. **2**(8): p. 1896-1906.

27. Palm, A.K. and M.V. Novotny, *Analytical characterization of a facile porous polymer monolithic trypsin microreactor enabling peptide mass mapping using mass spectrometry.* Rapid Communications in Mass Spectrometry, 2004. **18**(12): p. 1374-1382.

28. Altun, Z., C. Skoglund, and M. Abdel-Rehim, *Monolithic methacrylate packed 96-tips for high throughput bioanalysis.* Journal of Chromatography A, 2010. **1217**(16): p. 2581-2588.

29. Liang, Y., et al., *Hydrophilic monolith based immobilized enzyme reactors in capillary and on microchip for high-throughput proteomic analysis.* Journal of Chromatography A, 2011. **1218**(20): p. 2898-2905.

30. Celebi, B., A. Bayraktar, and A. Tuncel, *Synthesis of a monolithic, micro-immobilised enzyme reactor via click-chemistry.* Analytical and Bioanalytical Chemistry, 2012. **403**(9): p. 2655-2663.

Table 1. Summary of the performance of IMER and in-solution digestion using complex protein mixture.[a]

Protein mixture	***Number of proteins groups identified with in-solution digestion***	***Number of proteins groups identified with IMER***	***Enzyme immobilized***	***Database search engine***
Mouse serum std	137	106	Trypsin/LysC	Mascot
Yeast lysate	487	445	Trypsin/LysC	PD
Yeast lysate	473	368	LysN	Mascot
Human lysate	207	216	Trypsin/LysC	PD

a. IMER digestion time was 5 min at room temperature. LC-MS/MS analysis for in-solution and IMER digestion was identical and parameters were described in apparatus session with same protein loading amount of 300 ng.

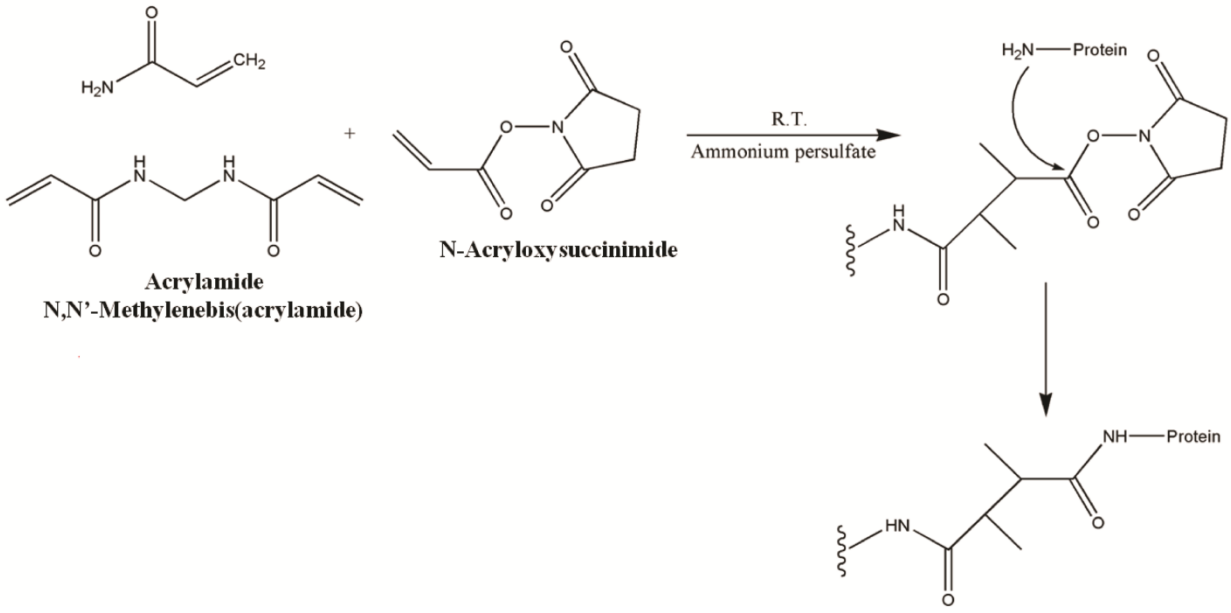

Figure 1. Synthesis of NAS-AAm-Bis monolithic column with immobilized ligand.

NAS, AAm and Bis were mixed with PEG and initiator. The ligand immobilization was conducted simultaneously with polymerization at room temperature for 30 min.

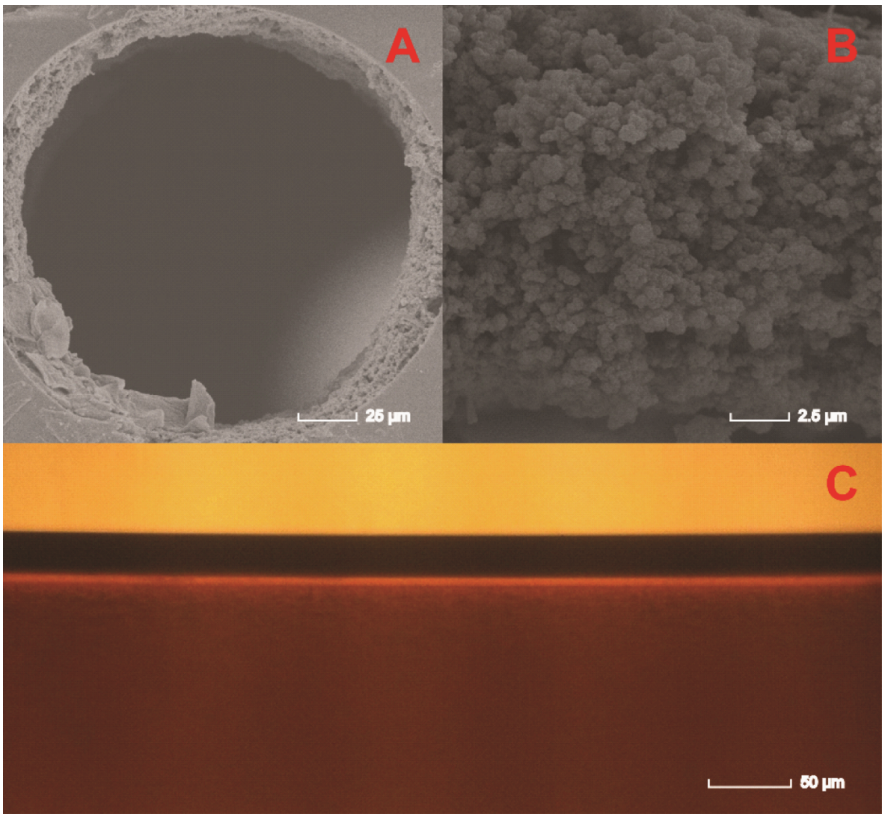

Figure 2. Microscopic images of NAS-AAm-Bis monolith fabricated within 200 µm i.d. capillary.

A: A scanning electron microscopic (SEM) image showing the NAS-AAm-Bis monolith fabricated within a 200 µm silanized capillary. An open tubular column was formed with a uniform layer of monolith attached to the capillary inner wall. B: A zoom-in of the SEM image to show the detailed structure of NAS-based monolith. C: An optical microscopic image taken from outside of the column showing the capillary wall (upper) and monolith (lower).

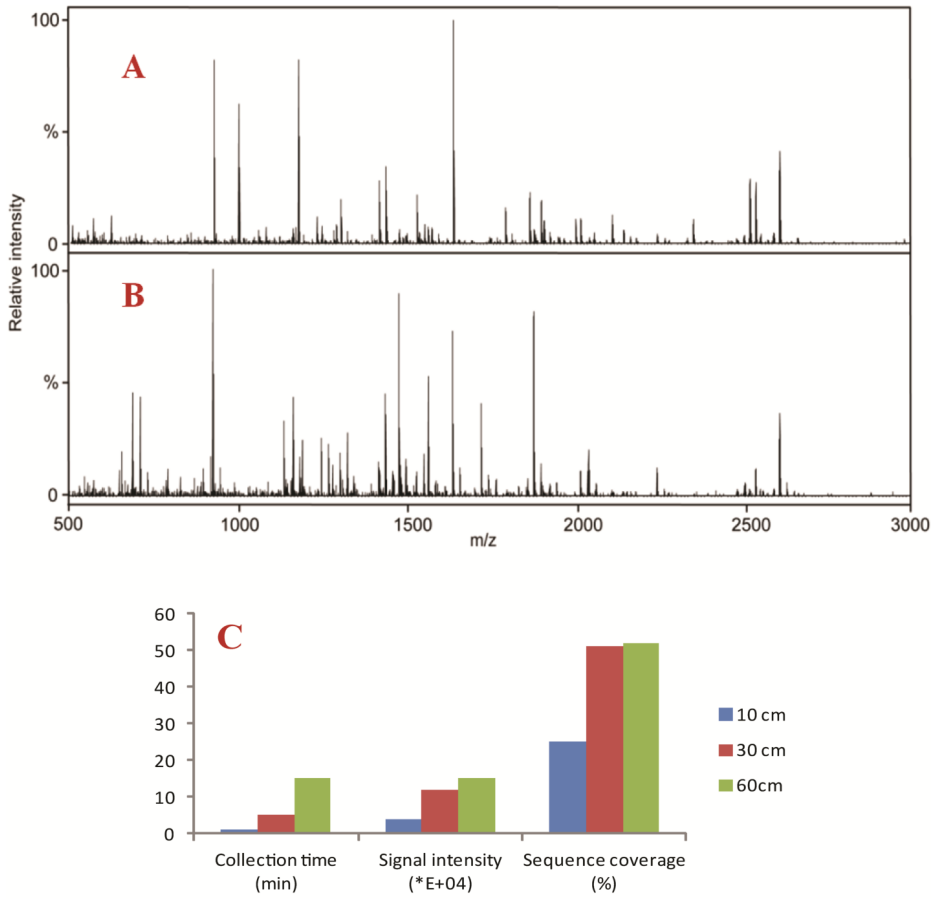

Figure 3. Mass spectral comparison between in solution digestion and IMER digestion with MALDI-MS detection.

A: Mass spectra generated from MALDI-LTQ-Orbitrap with BSA tryptic peptides via in solution digestion. B: Mass spectra generated from MALDI-LTQ-Orbitrap with BSA tryptic peptides via IMER digestion. C: Histogram showed optimized IMER condition of BSA digestion. The blue column represented that a 10 cm IMER yielded 25% sequence coverage of BSA and signal intensity of 4.00×10^4 [a.u.] over 1 min sample collection time. The red column represented that a 30 cm IMER yielded 51% sequence coverage of BSA and signal intensity of 1.20×10^5 [a.u.] over 5 min sample collection time. The green column represented that a 60 cm IMER yielded 52% sequence coverage of BSA and signal intensity of 1.50×10^5 [a.u.] over 15 min sample collection time.

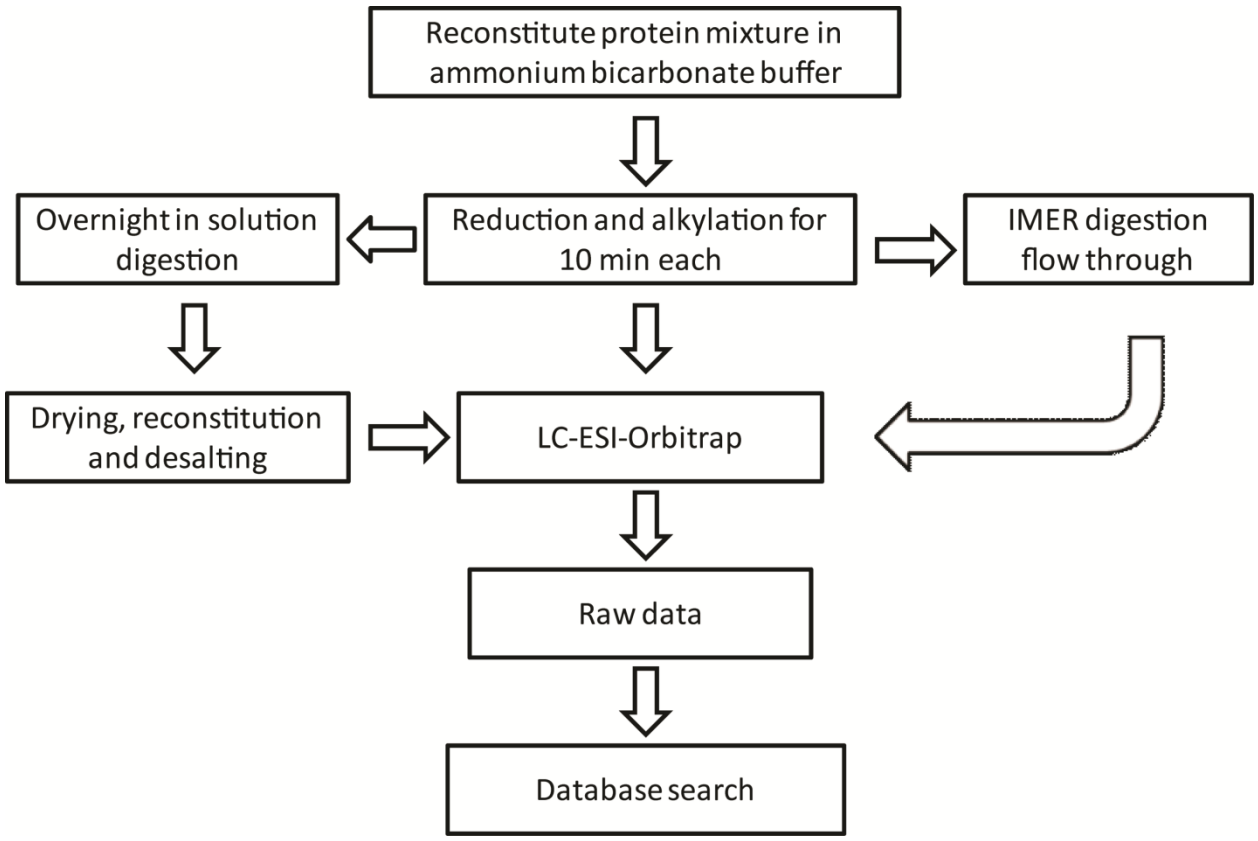

Figure 4. Scheme of offline coupling IMER digestion and conventional in solution digestion to LC-MS for large-scale proteomics studies.

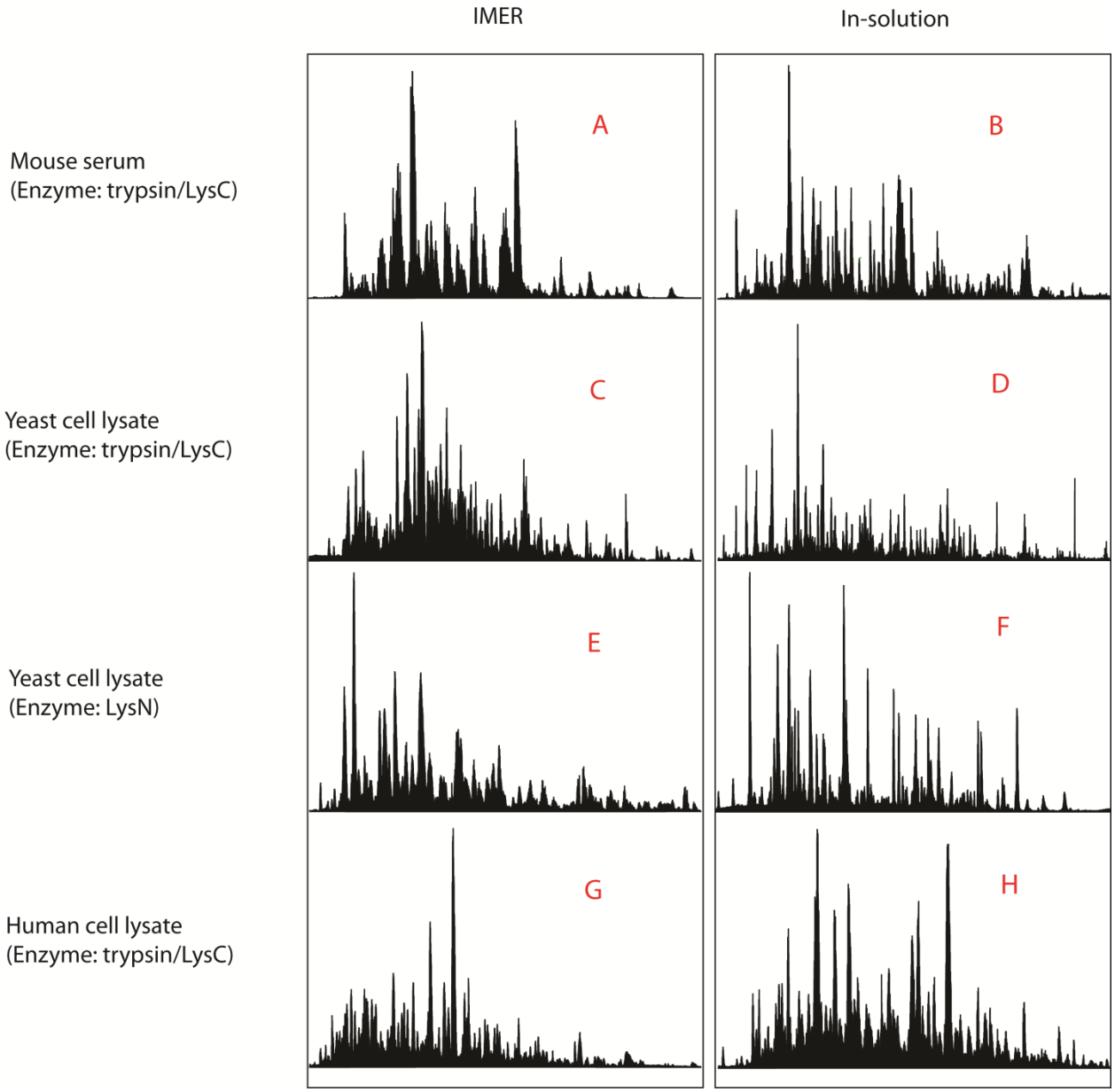

Figure 5. LC chromatograms of IMER and in-solution digestion prior to large-scale proteomics studies.

A, C, E and G: LC chromatograms for IMER digestion of mouse serum standard, yeast cell lysate (immobilized with trypsin/LysC and LysN) and human cell lysate, respectively. B, D, F, H: LC chromatograms of mouse serum standard, yeast and human cell lysate generated by traditional in-solution method.

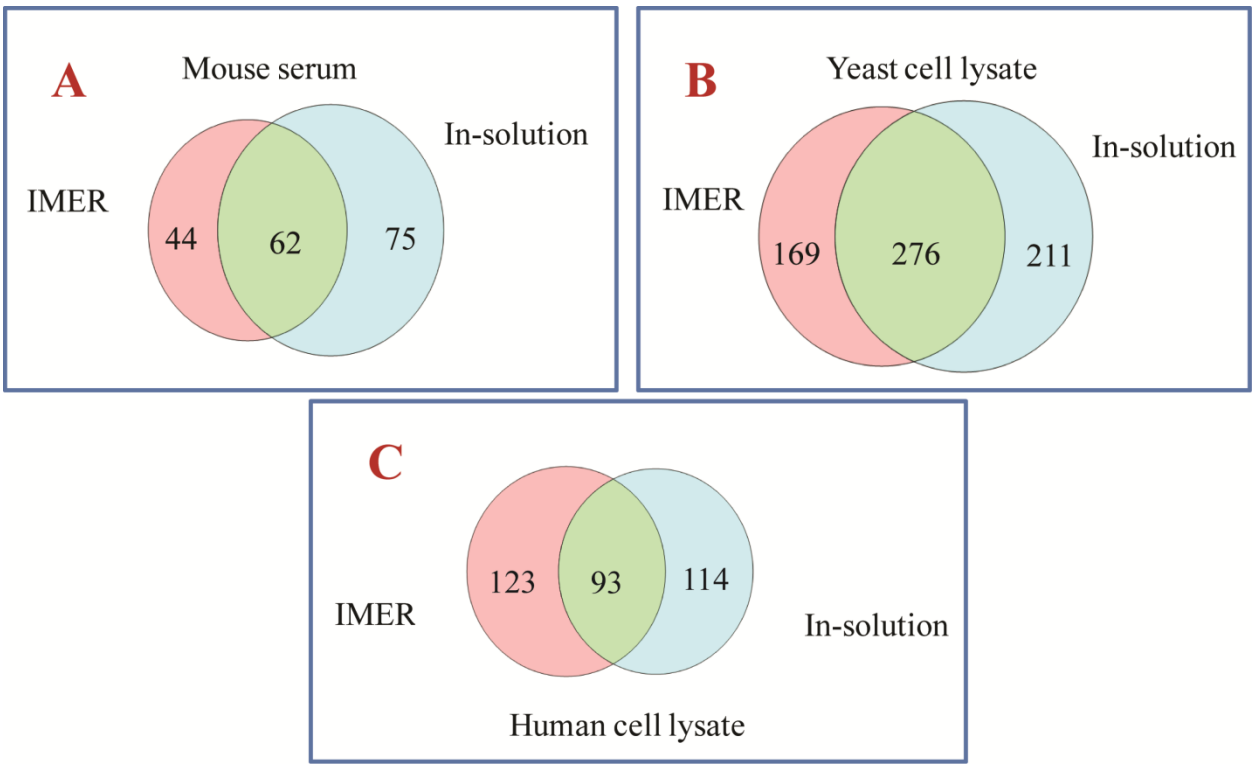

Figure 6. Comparisons between proteins identified by IMER and in-solution digestion for different biological samples.

A: Comparison of the number of proteins detected by IMER and in-solution digestion of mouse serum standard. B: Comparison of the number of proteins detected by IMER and in-solution digestion of yeast cell lysate. C: Comparison of the number of proteins detected by IMER and in-solution digestion of human cell lysate.

	GMA	EDMA	1-Propanol	1,4-Butadiol	AIBN
W (ug)	240	160	400	200	6 mg
V (uL)	230.3	152.2	497.5	196.7	NA

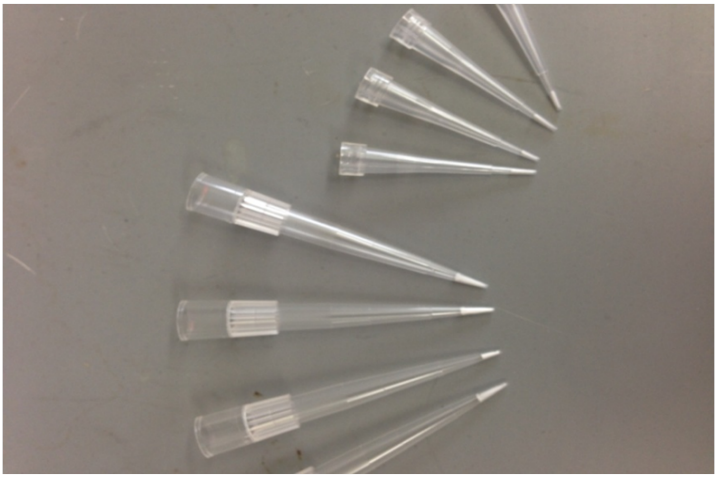

Figure 7. Composition of monolithic stage tips.

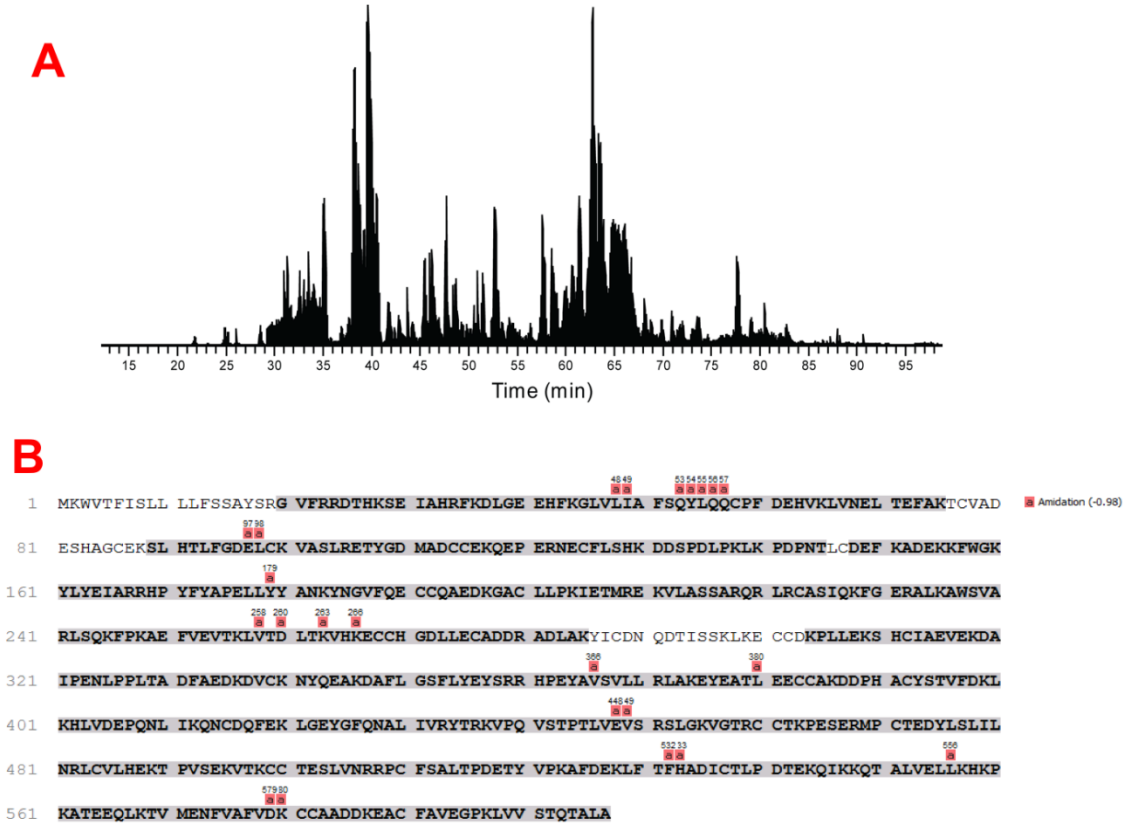

Figure 8. In-tip digestion of BSA analyzed by LC-MS/MS.

A. LC chromatogram of in-tip digestion of BSA. B. Tryptic peptides identified and sequence coverage of BSA.

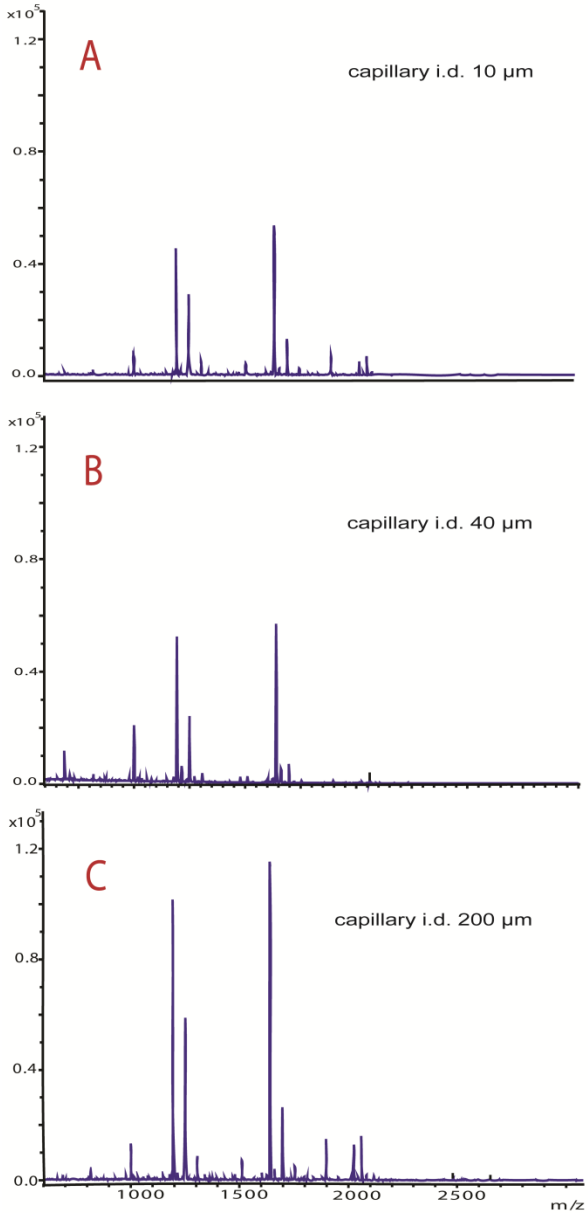

Figure S1. Comparison of digestion efficiency via two IMERs polymerized in columns with different inner diameters.

A: Spectrum of digested BSA by a 10 μm × 100 mm IMER column. B: Spectrum of digested BSA by a 40 μm × 100 mm IMER column. C: Spectrum of digested BSA by a 200 μm × 100 mm IMER column.

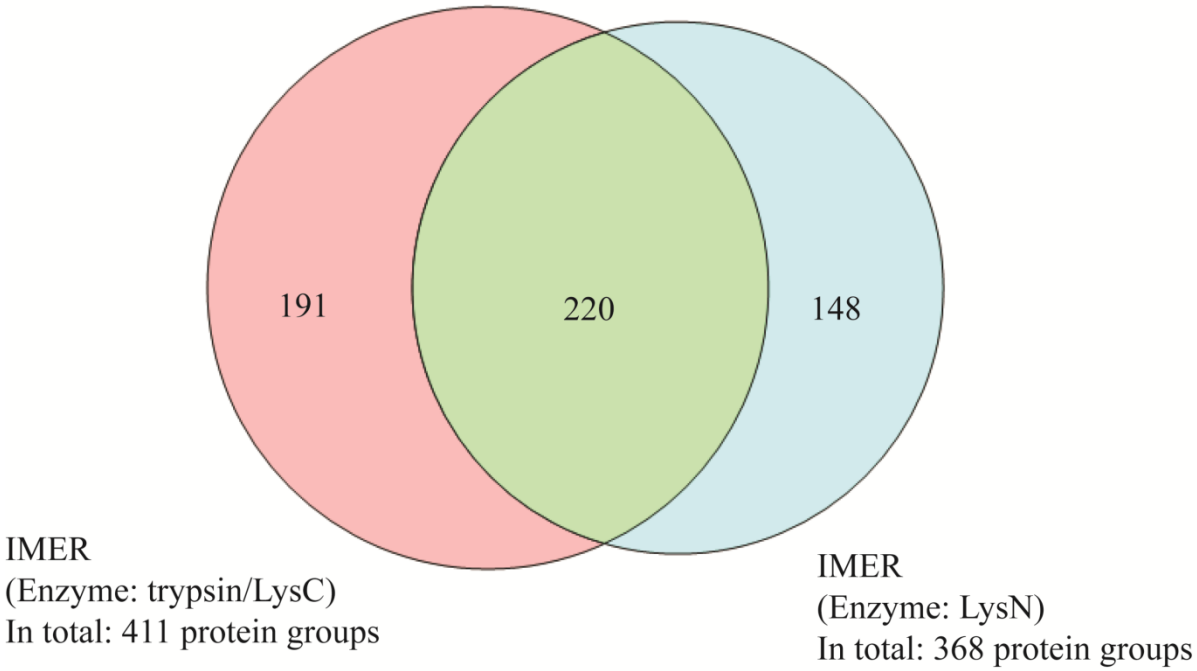

Figure S2. Complementary protein identification of yeast cell lysate via multi-IMERs.

As a result of complementary digestion by multi-proteases, 559 proteins were matched in total, while 220 proteins were overlapped by both IMERs.

Chapter 4

Application of monolithic affinity chromatography in peptidomics and proteomics studies

Adapted from:

1. **Jiang S.,** Zhang Z., Li L. Monolithic affinity chromatography for highly efficient purification and enrichment of target peptides from complex biological samples. *J. Chromatograph. A.* In preparation.

Abstract

Mass spectrometry coupling to sample preparation and separation techniques has become a primary tool for peptidomics and proteomics studies. Due to the wide dynamic range of analytes of interest, challenges still exist on how to improve detection limit and perform sample enrichment prior to mass spectrometry analysis. In recent decades, monolithic materials have been developed as both chromatographic media and affinity support for immobilizing multiple types of affinity reagents. Herein, we incorporated N-acryloxysuccinimide-co- acrylamide-co-N,N'-methylenebisacrylamide (NAS-AAm-Bis) monolith columns with specific antibodies for affinity purification. By immobilization of anti-FMRFamide antibody, RFamide-like neuropeptides were specifically isolated and enriched from other families. The monolithic column was further optimized for targeted capture of individual neuropeptide arginine vasopressin from mouse pituitary gland. Significant improvements on sample preparation efficiency and reduction of experimental time were achieved, highlighting great potential to integrate monolithic material in peptide and protein sample preparation.

1. Introduction

Affinity chromatography is an important separation and purification approach for analyzing target compounds in complex samples. This technique utilizes unique affinity between an antigen and an antibody or other specific molecular recognition events in biological systems [1, 2]. In affinity chromatography, stationary phase is immobilized with antibodies to capture compounds of interest. Purification of target molecules is achieved by specific and reversible binding that is present in many biological systems. Chromatography based on affinity interactions can be used alone or in combination with other types of separation strategies depending on the type of the target analytes and the level of purity that is needed. Due to the high selectivity of affinity columns, the technology has been used in various applications in separation science, biochemistry, biomedical development, drug discovery, etc. [3-7].

In recent decades, monolithic stationary phase becomes an attractive alternative due to its fast fabrication process and the ability of performing on-column chemical reactions. The monolithic bed contains large pores that allows the mobile phase to easily travel through the stationary phase [2]. Cryogel is a type of inorganic monolith that has been largely applied in bio-affinity chromatography. These supports can have good chemical and physical stability and have been reported to be cost-effective to use [8-10]. Cryogels are gel matrices that are formed in the presence of moderately frozen solutions of monomeric or polymeric precursors. These conditions can provide interconnected macro-pores that allow for relatively fast diffusion as analytes pass through this type of material. Cryogel materials can be prepared in the form of either columns or membranes [11]. Monolithic cryogels allow the use of high flow rates, making it possible to pass through large sample volumes in a short amount of time [12]. Cryogel monoliths have been used in separations and sample preparations involving plasmids, proteins and even cells [11].

Antibodies, concanavalin A, dyes, and metal-ion chelates have all been coupled to cryogel monoliths and used in applications such as the purification and depletion of proteins and enzymes from samples [9, 10].

For micro-scale sample analysis, it is often challenging to detect low abundance molecules in complex biological environment. Thus, techniques have been developed to improve detection limit and sensitivity, including sample purification and separation prior to downstream detection [13-15]. Mass spectrometry (MS)-based proteomics has become an important tool in protein identification and quantitation, elucidating biomarkers and underlying mechanisms of disease pathogenesis. MS has become an integral part of biological research primarily due to the established techniques of matrix-assisted laser desorption/ionization (MALDI) and electrospray ionization (ESI) [16, 17]. High throughput MALDI MS generates singly charged ions without LC separation thus enable rapid profiling of molecular species. ESI MS coupled to LC generates multiply charged ions and offers better fragmentation efficiency, thus enabling more in-depth proteomic identification and quantification. In this chapter, both MALDI and ESI MS approaches were employed to couple with monolithic affinity purification. Monolithic affinity column was fabricated and used for enrichment of specific neuropeptide family and extraction of target biomarkers from tissue and biofluid samples. Performance of affinity purification was evaluated by comparing samples before and after enrichment. Furthermore, quantitative proteomics was performed after affinity enrichment which showed good reproducibility and great potentials for future application.

2. Materials and methods

2.1. Reagents and materials

Acetic acid, sodium hydroxide, sodium chloride, sodium bicarbonate, ammonium hydroxide, acetone, acetonitrile, methanol, ammonium bicarbonate, phosphate buffer and urea were purchased from Fisher Scientific (Pittsburgh, PA). Acrylamide (AAm, 99%), N, N'-methylenebisacrylamide (Bis, 99%), ammonium persulfate (APS, 98%), polyethylene glycol (PEG 6000), N, N, N′, N′-Tetramethylethylenediamine (TEMED, 99%), dimethyl sulfoxide (DMSO), trifluoroacetic acid (TFA), α-Cyano-4-hydroxycinnamic acid (CHCA, 99%), N-acryloxysuccinimide (NAS) was purchased from Tokyo Chemical Industry (Tokyo, Japan). Rabbit anti-mouse polyclonal RFamide antibody was from Abcam Inc, MA. Fused-silica capillary with 200 μm i.d. and 360 μm o.d. was purchased from Polymicro Technologies (Phoenix, AZ). Millipore C18 Ziptip columns were used for sample cleaning, and all water used in this study was doubly distilled on a Millipore filtration system (Bedford, MA). The physiological saline consisted of 440 mM NaCl, 11mM KCl, 26 mM $MgCl_2$, 13 mM $CaCl_2$, 11 mM Trizma base, and 5 mM maleic acid in pH 7.45.

2.2. Synthesis of monolithic affinity column

Synthesis of affinity column was modified based on previous publications [18, 19]. Briefly, a mixture containing 20mg acrylamide, 30mg N, N'-methylenebisacrylamide and 30mg PEG in 1 mL of 0.2 M sodium bicarbonate/0.5 M sodium chloride buffer was heated at 55-60 °C for 15min. Then, 4 μL of 20% (v/v) TEMED was added to the above-mentioned solution and followed by nitrogen de-gassing. 5 μL N-Acryloxysuccinimide (NAS) (140 mg/mL dissolved in DMSO) was then added on top of the solution, and after 1min, 2 μL of 20% (w/v) ammonium persulfate (APS) was added to initiate polymerization. After 30s, 18 μL aliquot of this solution was quickly mixed with 2 μL of ligand solution and pumped through the pre-treated capillary. Ligand solution consisted of 1ug/uL anti-RFamide antibody, anti-Arginine Vasopressin antibody

and anti-amyloid beta antibody. The entire reaction can be completed within 30 min at room temperature. After reaction, the column was washed with 25 mM ammonium bicarbonate before sample loading.

2.3. Tissue dissection and extraction

Blue crabs (*Callinectes sapidus*) were purchased from a local grocery store. The crabs were kept in an artificial seawater tank at 10-12 °C without food. Prior to dissection, the crabs were anesthetized for 30 min by packing in ice [20, 21]. Brains were dissected in cold physiological saline. Pituitary gland was dissected from a mouse model. Animal experiments were conducted following institutional guidelines (UW-Madison IACUC). The neuropeptides were extracted using acidified methanol which contained methanol, water and acetic acid in the ratio of 90:9:1 and was kept in ice during extraction. Two brains were homogenized in 50 μL acidified methanol and centrifuged at 16,000 rcf to harvest the supernatants [22, 23]. The extraction procedure was repeated for three times and the supernatants were combined and dried using a SpeedVac concentrator. The residue was reconstituted with 10 μL of 0.1% TFA and desalted by Ziptip C18 column before injection onto the instrument.

2.4. MALDI-MS/MS acquisition

A MALDI-LTQ-Orbitrap XL (Thermo Scientific, Bremen, Germany) was used for MALDI MS analysis. 10 mg/mL CHCA was applied as matrix. For MALDI MS experiments, survey crystal positioning system (CPS) was used as the plate motion mode and 2 microscans were summed per step. Mass spectrum of each spot was averaged by 20 steps of MS acquisition. FTMS mode was used for full MS scans with a laser energy of 5 μJ. Automatic gain control (AGC) was set at a target value of $1e^6$ for full MS and $1e^4$ for HCD fragmented ions. Database searching and *de*

novo sequencing were performed by PEAKS 7 (Bioinformatics Solution Inc., ON, Canada) and verified manually.

2.5. LC-MS/MS acquisition

Digested protein fractions were separated by a self-packed C_{18} column before loading to Q Exactive Orbitrap mass spectrometer from Thermo Scientific (San Jose, CA). Mobile phase A consisted of water with 0.1% FA, and mobile phase B was composed of ACN with 0.1% FA. Peptides were separated using a solvent gradient of 0 – 10% B over 0.5 min and then 10 – 30% B over 70 min at a flow rate of 350 nL/min. Data-dependent acquisition (DDA) parameters recorded MS scans in profile mode from *m*/*z* 250 – 3000 at a resolution of 35,000. Automatic gain control (AGC) targets of 1×10^6 and maximum injection times (IT) of 100 ms were selected. The 10 most intense precursor ions were selected for MS/MS higher-energy collisional dissociation (HCD) fragmentation with an isolation width of 2.0 *m*/*z* and placed on an exclusion list for 40 s. Tandem mass spectra were acquired at a resolution of 17,500 in profile mode with an AGC target of 1×10^5, a maximum IT of 150 ms, a normalized collision energy (NCE) of 27, and a fixed lower mass at *m*/*z* 110.

3. Results and discussion

3.1. Affinity separation of neuropeptides

Neuropeptides are an important class of signaling molecules that are present and released in the nervous system. A variety of neuropeptide families have been discovered with physiological functions ranging from regulating feeding behavior to modulating pain sensing [24, 25]. The FMRFamide-related peptides are a family of neuropeptides that are characterized by the possession of an Arg-Phe-NH_2 motif at their C-termini [26]. FMRFamide-like peptides are among the largest families of neuropeptides found in crustacean organism [27]. The pleiotropic

physiological functions of RFamide family neuropeptides have been extensively studied in numerous species of crustacean. Their diverse neuromodulatory roles include but not limited to muscular modulation [28], digestive system modulation [29], cardiac excitatory modulator [30] and pyloric circuit modulation [31], etc. However, the study of neuropeptides has always been challenging due to their extremely low quantities and wide dynamic range in highly salty body fluids. Furthermore, the current lack of DNA sequences for many organisms and the post-translational modifications (PTMs) commonly observed in most identified neuropeptides make it difficult to predict the final products from the genomic information. For functional studies with improved mass spectrometric signal, it will be beneficial to extract and enrich an individual neuropeptide family from other neuropeptides and biological matrix; however, very few studies have looked into this issue due to the difficulties in extraction and separation of these minute quantities of neuropeptides from complex mixtures. Our group previously employed immuno-dot-blot and immunoprecipitation techniques to extract RFamide family neuropeptides, but these methods require multiple steps and large sample amount (up to 100 μL tissue extraction) [32].

By employing monolithic affinity column for sample purification in this work, much lower loading amount was used for MS detection. Peptide extracts from crab brains were loaded to the affinity column and incubated at room temperature for 30 min. Phosphate buffer of pH 8 was used as washing buffer to remove unspecific binding peptides. After washing for 10 min, elution buffer of 50% ACN containing 0.5% formic acid was applied to elute and collect target neuropeptides. Fractions of washing and eluting steps were both collected and analyzed by MALDI Orbitrap with a resolution of 70,000 at *m/z* 400. Mass spectra of washing fraction and elution fraction had different detected peaks, indicating good affinity separation was achieved. In elution, most of the major mass spectral peaks were from FMRFamide family and were marked

with yellow stars in Figure 2B. As shown in Table 1 and 2, in the washing fraction, a total of 15 neuropeptides were identified based on mass fingerprint matching using a home-built crustacean database in Mascot. Neuropeptides were detected from the RYamide, allatostatin (AST) and orcokinin (Ork) families but none was FMRFamide-like neuropeptides, supporting the selectivity and specificity of our isolation technique. In the eluting fraction, the same database search was performed and a total of 15 neuropeptides were detected with most of the mass spectral peaks being assigned to the RFamide family neuropeptides or the C-terminal truncated forms. After affinity enrichment, MS/MS fragmentation was performed to confirm neuropeptide sequences. Representative tandem mass spectra were shown in Figure 3. These results demonstrated the high specificity and efficiency when monolithic affinity extraction was employed for purification and enrichment of targeted neuropeptides.

3.2. Single peptide extraction from mouse pituitary gland

After successful separation of neuropeptide family from other peptide families in complex tissue extract, we move on to investigate whether the same type of affinity column can be used to isolate and enrich a single peptide of interest in tissue matrices. Arginine vasopressin (AVP) or antidiuretic hormone, is a hypothalamo-neurohypophysial peptide which is involved in homeostasis by regulating water absorption in the renal tubules and by vasoconstriction [33, 34]. AVP plays a major role in the homeostasis of fluid balance, vascular tonus, and the regulation of the endocrine stress response. The measurement of AVP levels is difficult due to its short half-life and laborious method of detection [35]. Therefore, a highly efficient method is needed to capture AVP from complex biological matrix. As illustrated in Figure 1, mouse pituitary gland was dissected and extracted using acidified methanol to remove tissue debris. Washing and eluting fractions were collected for 10 min each and were analyzed using both MALDI and LC-

ESI MS. For MALDI MS acquisition shown in Figure 4, comparison was made in the peptide range from 900 to 2800 Da. AVP displayed in lower abundance compared than other peptides in original mouse pituitary gland extraction shown in Figure 4A. After affinity purification, AVP at *m/z* 1084.44 was only detected in elution (Figure 4C) and showed in higher intensity level, whereas other peptides from pituitary gland were removed and only found in washing fraction. In LC-MS/MS acquisitions, washing and elution fractions were analyzed by the same data-dependent acquisition (DDA) method. Resulting data were both searched through PEAKS software for identification. As shown in Figure 5, LC chromatogram of elution was clean compared to washing fraction. By monolithic affinity purification, AVP was enriched and pulled out from tissue extract. Figure 5C showed doubly charged AVP signal in the extracted ion chromatogram eluting at 32~33 min in LC gradient. These results indicate that monolithic affinity column efficiently enriched a single target peptide from complicated matrices.

4. Conclusions

In this work, cryogel type monolithic column was fabricated and immobilized with antibodies for affinity chromatography coupled to MALDI and ESI MS. Preparation of monolithic column takes about 30 min. The affinity purification process can be completed within 1 hr. For each affinity column, 2 ug antibody is sufficient for ligand immobilization. Compared to previous immunoprecipitation method published in our group, this approach significantly reduced sample consumption from 100 uL to 5 uL and doesn't require multiple fractionation steps. It is highly suitable for enrichment of low abundance and labile target analytes. With micro-scale sample consumption for column loading, the limit of detection was significantly improved. As summarized in Figure 6, the same type of monolithic column was synthesized followed by binding of enzyme or antibodies. It is successfully applied in separation of neuropeptides in

specific family and enrichment of a single target peptide from tissue extracts. With the ability to incorporate with diverse ligands and subsequent analytical platforms, this strategy offers great potential for peptidomics and proteomics studies.

References

1. Solmaz Hajizadeh, B.M., *Cryogels with affinity ligands as tools in protein purification.*, in *Affinity chromatography*. 2015. p. 183-199.
2. Pfaunmiller, E.L., Paulemond, Marie Laura Dupper, Courtney M., Hage, David S., *Affinity monolith chromatography: a review of principles and recent analytical applications.* Analytical and Bioanalytical Chemistry, 2012. **405**(7): p. 2133-2145.
3. Zheng, X., Yoo, Michelle J., Hage, David S., *Analysis of free fractions for chiral drugs using ultrafast extraction and multi-dimensional high-performance affinity chromatography.* The Analyst, 2013. **138**(21): p. 6262.
4. Dedecker, M., Leene V. Jelle, Jaeger D. Geert, *Unravelling plant molecular machineries through affinity purification coupled to mass spectrometry.* Current Opinion in Plant Biology, 2015. **24**: p. 1-9.
5. Li, X., Wang, Wenqi, Chen, Junjie, *From pathways to networks: Connecting dots by establishing protein-protein interaction networks in signaling pathways using affinity purification and mass spectrometry.* Proteomics, 2015. **15**(2-3): p. 188-202.
6. Meyer, K., Selbach, Matthias, *Quantitative affinity purification mass spectrometry: a versatile technology to study protein–protein interactions.* Frontiers in Genetics, 2015. **6**.
7. Nakayama, N., Bando, Yasuhiko, Fukuda, Tetsuya, Kawamura, Takeshi, Nakamura, Haruhiko, Marko-Varga, György, Nishimura, Toshihide, *Developments of mass spectrometry-based technologies for effective drug development linked with clinical proteomes.* Drug Metabolism and Pharmacokinetics, 2016. **31**(1): p. 3-11.
8. Dogan, A., Ozkara, S., Sari, M. M., Uzun, L., Denizli, A., *Evaluation of human interferon adsorption performance of Cibacron Blue F3GA attached cryogels and*

interferon purification by using FPLC system. J Chromatogr B Analyt Technol Biomed Life Sci, 2012. **893-894**: p. 69-76.

9. Dainiak, M.B., Galaev, I. Y., Mattiasson, B., *Affinity cryogel monoliths for screening for optimal separation conditions and chromatographic separation of cells.* J Chromatogr A, 2006. **1123**(2): p. 145-50.
10. Andac, M.G., I. Denizli, A., *Dye attached poly(hydroxyethyl methacrylate) cryogel for albumin depletion from human serum.* J Sep Sci, 2012. **35**(9): p. 1173-82.
11. Par Arvidsson , F.M.P., Irina N. Savina , Vladimir I. Lozinsky ,Sara Fexby , Leif Bulow , Igor Yu. Galaev , Bo Mattiasson, *C hromatography of microbial cells using continuous supermacroporous affinity and ion-exchange columns.* Journal of Chromatography A, 2002. **977**: p. 27-38.
12. Per Erik Gustavsson, P.L., *Continuous superporous agarose beds for chromatography and electrophoresis.* Journal of Chromatography A, 1999. **832**: p. 29-39.
13. Sorensen, S., Myrhoj, V., Nguyen, T. H. Aaslo, P., Hansen, Y. B., *Affinity purification of native glycodelin from amniotic fluids for biological investigations and development of a glycodelin ELISA for clinical studies.* Protein Expr Purif, 2016.
14. Mali, S., Moree, W. J., Mitchell, M., Widger, W., Bark, S. J., *Observations on different resin strategies for affinity purification mass spectrometry of a tagged protein.* Anal Biochem, 2016. **515**: p. 26-32.
15. Yu, H., Reiser, J., Besenfelder, U., Razzazi-Fazeli, E., Bergquist, J., Brem, G., Artemenko, K., Mayrhofer, C., *Exploring the oviductal fluid proteome by a lectin-based affinity approach.* Proteomics, 2016.

16. Thomas P.E., H., Gary Siuzdak, Robert Balckledge, *Electrospray and MALDI Mass Spectrometry in the identification of Spermicides in Criminal Investigations.* Journal of Forensic Sciences, 1999. **44**: p. 783-788.

17. Schubert, K.O., Weiland, F., Baune, B. T., Hoffmann, P., *The use of MALDI-MSI in the investigation of psychiatric and neurodegenerative disorders: A review.* Proteomics, 2016. **16**(11-12): p. 1747-58.

18. Jiang, S., Zhang, Z., Li, L., *A one-step preparation method of monolithic enzyme reactor for highly efficient sample preparation coupled to mass spectrometry-based proteomics studies.* J Chromatogr A, 2015. **1412**: p. 75-81.

19. Palm, A.K., Novotny, M. V., *Analytical characterization of a facile porous polymer monolithic trypsin microreactor enabling peptide mass mapping using mass spectrometry.* Rapid Commun Mass Spectrom, 2004. **18**(12): p. 1374-82.

20. Hui, L.D.A., B. T. Jia, C. Liang, Z. Christie, A. E. Li, L., *Mass spectrometric characterization of the neuropeptidome of the ghost crab Ocypode ceratophthalma (Brachyura, Ocypodidae).* Gen Comp Endocrinol, 2013. **184**: p. 22-34.

21. Hui, L., Xiang, F., Zhang, Y., Li, L., *Mass spectrometric elucidation of the neuropeptidome of a crustacean neuroendocrine organ.* Peptides, 2012. **36**(2): p. 230-9.

22. Hui, L., Cunningham, R., Zhang, Z., Cao, W., Jia, C., Li, L., *Discovery and characterization of the Crustacean hyperglycemic hormone precursor related peptides (CPRP) and orcokinin neuropeptides in the sinus glands of the blue crab Callinectes sapidus using multiple tandem mass spectrometry techniques.* J Proteome Res, 2011. **10**(9): p. 4219-29.

23. Ma, M., Wang, J., Chen, R., Li, L., *Expanding the Crustacean neuropeptidome using a multifaceted mass spectrometric approach.* J Proteome Res, 2009. **8**(5): p. 2426-37.

24. Fu, Q., Kutz, Kimberly K., Schmidt, Joshua J., Hsu, Yun-Wei A., Messinger, Daniel I., Cain, Shaun D., de la Iglesia, Horacio O., Christie, Andrew E., Li, Lingjun, *Hormone complement of theCancer productus sinus gland and pericardial organ: An anatomical and mass spectrometric investigation.* The Journal of Comparative Neurology, 2005. **493**(4): p. 607-626.

25. Andrew E. Christie, E.S., Patsy S. Dickinson, *Crustacean neuropeptides.* Cell. Mol. Life Sci, 2010. **67**: p. 4135-4169.

26. Findeisen, M., Rathmann, Daniel, Beck-Sickinger, Annette G., *RFamide Peptides: Structure, Function, Mechanisms and Pharmaceutical Potential.* Pharmaceuticals, 2011. **4**(9): p. 1248-1280.

27. OuYang, C., Liang, Zhidan, Li, Lingjun, *Mass spectrometric analysis of spatio-temporal dynamics of crustacean neuropeptides.* Biochimica et Biophysica Acta (BBA) - Proteins and Proteomics, 2015. **1854**(7): p. 798-811.

28. A.J. Mercier, J.L., *Differential effects of neuropeptides on circular and longitudinal muscles of the crayfish hindgut.* Peptides, 2002. **23**: p. 1751-1757.

29. J. C. Jorge-Rivera, E.M., *TNRNFkRFamide and SDRNFLRFamide modulate muscles of the stomatogastric system of the crab Cancer borealis.* J Comp Physiol A, 1996. **179**: p. 741-751.

30. Wilkens, J.L., *Sites and modes of action of proctolin and the FLP F2 on lobster cardiac muscle.* Journal of Experimental Biology, 2005. **208**(4): p. 737-747.

31. Andrew M. Swensen, E.M., *Multiple Peptides Converge to Activate the Same VoltageDependent Current in a Central Pattern-Generating Circuit.* The Journal of Neuroscience, 2000. **20**: p. 6752-6759.

32. Ma, M., Sturm, Robert M., Kutz-Naber, Kimberly K., Fu, Qiang, Li, Lingjun, *Immunoaffinity-based mass spectrometric characterization of the FMRFamide-related peptide family in the pericardial organ of Cancer borealis.* Biochemical and Biophysical Research Communications, 2009. **390**(2): p. 325-330.

33. Rotondo, F., Butz, Henriett, Syro, Luis V., Yousef, George M., Di Ieva, Antonio, Restrepo, Lina M., Quintanar-Stephano, *Arginine vasopressin (AVP): a review of its historical perspectives, current research and multifunctional role in the hypothalamo-hypophysial system.* Pituitary, 2016. **19**(4): p. 345-355.

34. YK, O., *Vasopressin and vasopressin receptor antagonists.* Electrolyte Blood Press, 2008. **6**: p. 51-55.

35. Evers, K.S., Wellmann, Sven, *Arginine Vasopressin and Copeptin in Perinatology.* Frontiers in Pediatrics, 2016. **4**: p. 1-10.

Table 1. Crustacean neuropeptides in other families from brain detected in washing fraction.

Family	***m/z***	**Sequence**
Rya	1027.53	SRFVGGSRY+ Amidated (C-term)
AST	754.39	GQYAFGLa
AST	934.43	SDM(O)YSFGLa
AST	948.52	LMFAPLAW
AST	956.48	WPKGGARW+ Amidated (C-term)
AST	1027.53	AWPKGGARW+ Amidated (C-term)
AST	1044.56	LMFAPLAWP + Amidated (C-term)
AST	1513.81	LMFAPLAWPKGGAR+ Amidated (C-term)
Ork	1048.51	IDRTGFGFH+ Amidated (C-term)
Ork	1027.53	DIERSGFGF
Ork	1270.58	DEIDRTGFGFH+ Amidated (C-term)
Ork	1256.49	NFDEIDRSGFG
Ork	1292.56	DEIDRTGFGFH+ Amidated (C-term)
Ork	1474.56	NFDEIDRSGFGFA
Ork	1302.6	FDEIDRTGFGF + Amidated (C-term)

Table 2. MALDI detection of FMRFamide neuropeptides in crustacean brain isolated by monolithic affinity chromatography.

Observed *m/z*	**Sequence**
695.4	NFLRF+Amidated (C-term)
710.34	YGSDRN+Amidated (C-tem)
851.5	RNFLRF+ Amidated (C-tem)
965.5	NRNFLRFa
970.5	YGSDRNFL+Amidated (C-tem)
1022.51	GNRNFLRFa
1073.55	TNYGGFLRFa
1079.62	LDRNFLRF+ Amidated (C-term)
1104.55	GAHKNYLRFa
1124.60	GLSRNYLRRa
1126.6	YGSDRNFLR+ Amidated (C-term)
1147.58	APQRNFLRFa
1150.6	ALDRNFLRF + Amidated (C-term)
1158.55	YGNRSFLRFa
1274.67	YGSDRNFLRF

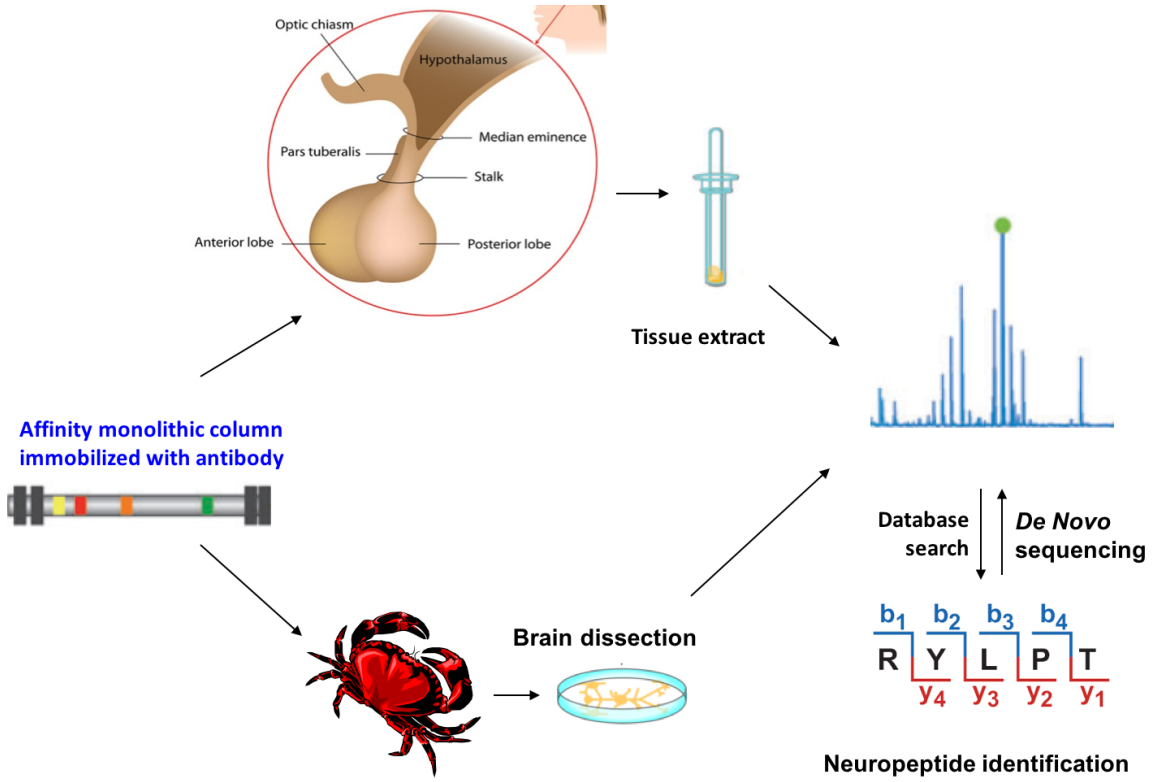

Figure 1. Schematic illustration of monolithic affinity purification in different tissue types.

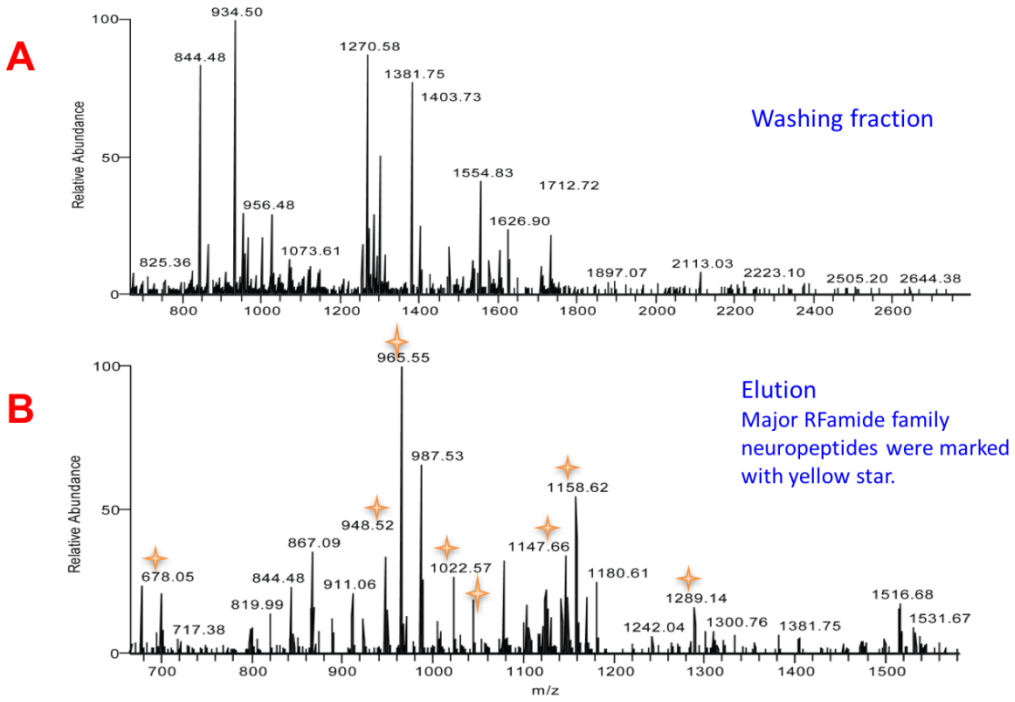

Figure 2. Mass spectral comparison between washing and eluting fraction of monolith affinity column separation.

A. MALDI mass spectrum of washing fraction in crustacean brain extraction. B. MALDI mass spectrum of eluting fraction in crustacean brain extraction. Major targeted neuropeptides after enrichment were marked by yellow stars.

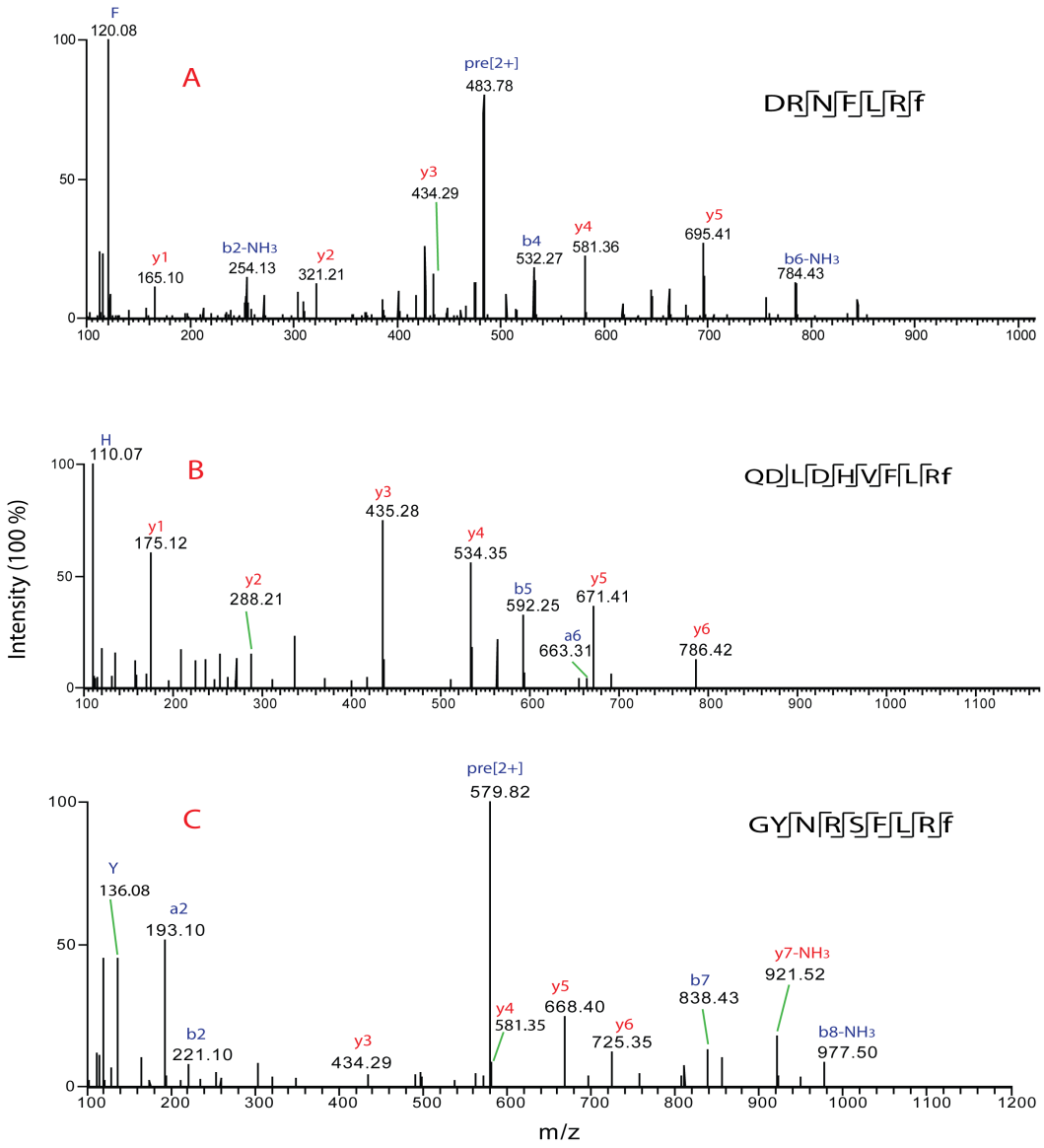

Figure 3. Representative tandem MS spectra of enriched neuropeptides in RFamide family.

A. MS/MS fragmentation of DFNFLRf. B. MS/MS fragmentation of QDLDHVFLRf. C. MS/MS fragmentation of GYRSFLRf. (lower case means C-terminal amidated residue)

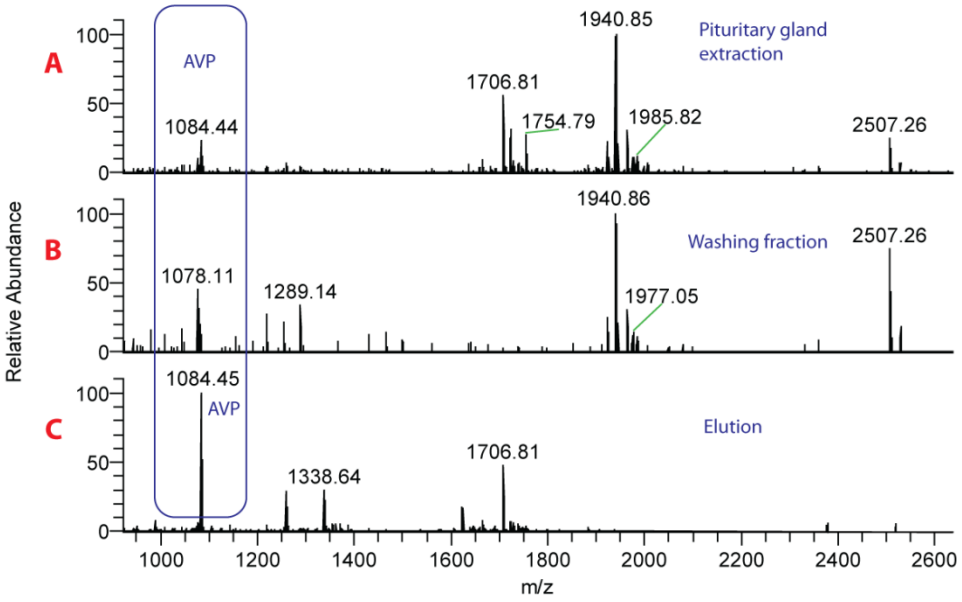

Figure 4. MALDI mass spectra of washing and eluting collection in mouse pituitary gland extraction.

A. Mass spectrum of mouse pituitary gland extraction before affinity purification. B. Mass spectrum of washing fraction of pituitary gland after affinity purification. C. Affinity enriched AVP in extraction sample. AVP peak was highlighted by blue rectangle, which had significantly enhanced signal intensity.

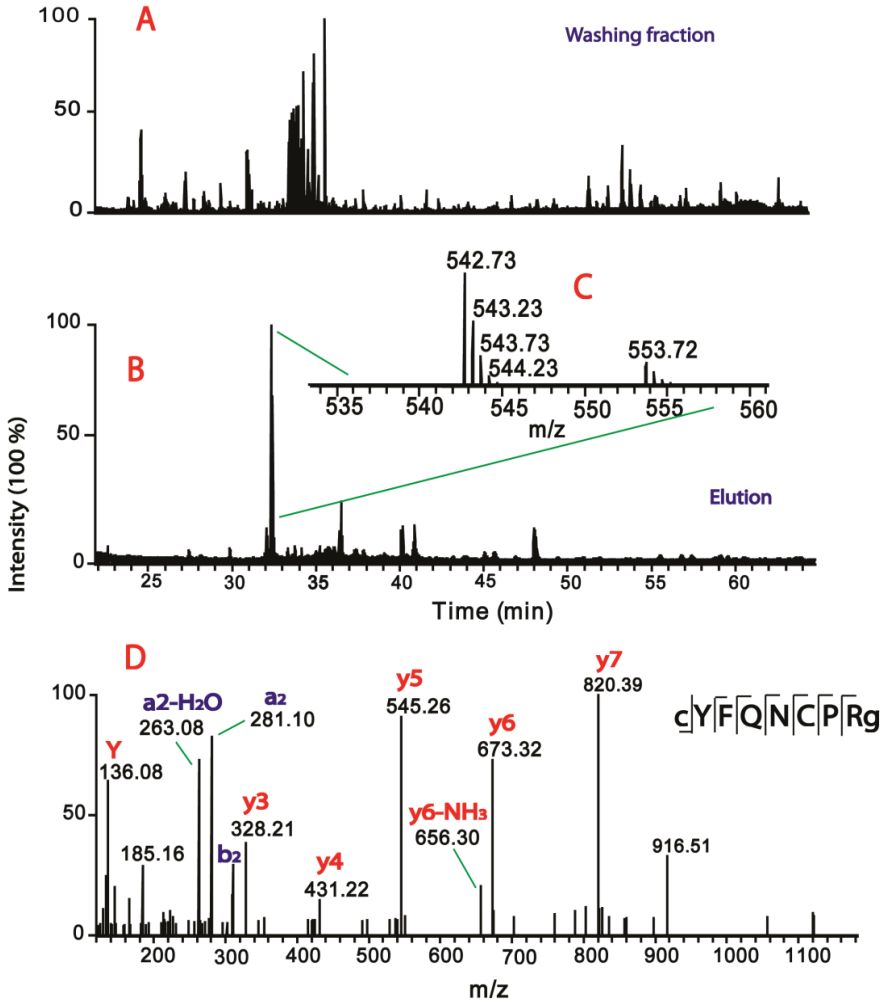

Figure 5. LC-MS/MS comparison of washing and eluting collection in mouse pituitary gland extraction.

A. LC chromatogram of washing fraction. B. LC chromatogram of elution fraction. C. Doubly charged AVP showed in the extracted ion chromatogram eluted at 32~33 min in elution. D. MS/MS spectrum of AVP.

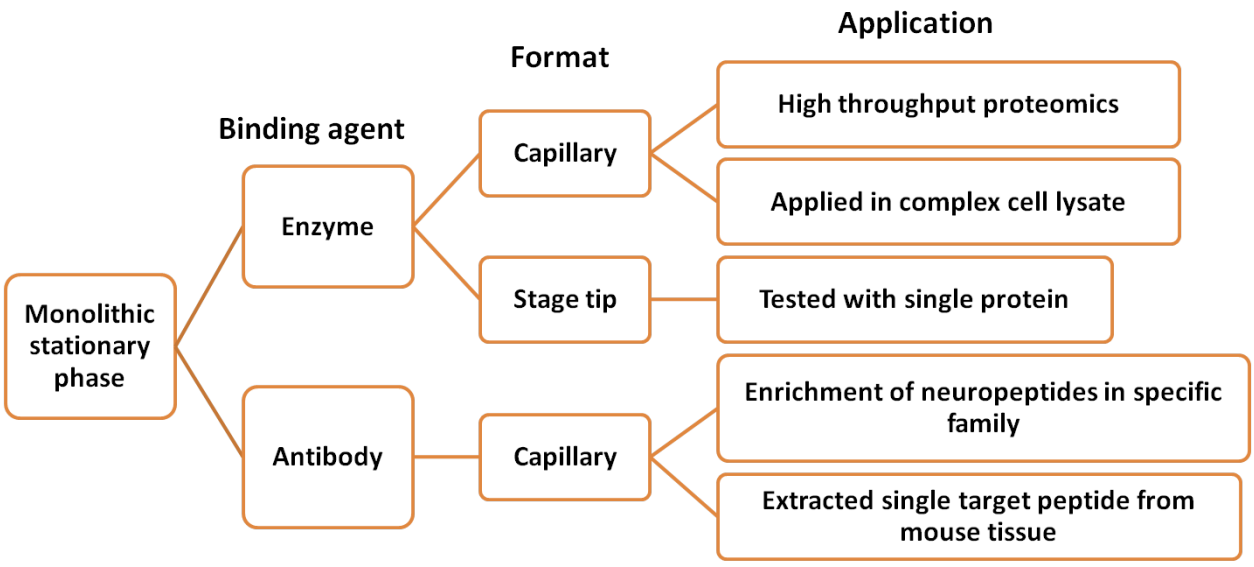

Figure 6. Development and application of monolithic stationary phase.

Chapter 5

Instrumentation and application of MALDI mass spectrometric imaging platform

Adapted from:

1. Zhang Z., **Jiang S.**, Li L., Semi-automated liquid chromatography-mass spectrometric imaging platform for enhanced detection and improved data analysis of complex peptides. *J Chromatogr A*, 2013 (1293): 44-50.
2. Liang Z., **Jiang S.**, Li L., Enzymatic degradation of neuropeptides probed by *in vivo* microdialysis coupled with MALDI-MS. *Analyst,* to be submitted.

Abstract

Matrix-assisted laser desorption/ionization (MALDI) is a soft ionization technique used in mass spectrometry, allowing the analysis of biomolecules (such as DNA, proteins, peptides and sugars) and large organic molecules (such as polymer, dendrimers and other macromolecules). It provides an attractive alternative to electrospray ionization (ESI) and produced mostly protonated ions. MALDI mass spectrometric imaging (MSI) provides additional distribution maps of selected compounds. But MSI is usually considered lack of separations compared to LC-ESI analysis. Thus, in this chapter, a new analytical platform combining separation and MSI will be introduced. By interfacing LC separation to MSI, analysis and characterization of complex neuropeptide (NP) extracts from tissues was achieved. Furthermore, MSI platform was integrated to *in vivo* microdialysis sampling for real time monitoring of signaling molecules in live animal model. Considering the high salt concentration *in vivo*, MALDI detection is proven to be the method of choice due to its higher tolerance to impurities and salts compared to ESI. Thus, less sample preparation is needed reducing sample loss from clean-up steps. Furthermore, by implementing microdialysis with MSI detection, *in vivo* NP degradation was monitored and quantified, offering great potential for dynamic neurochemical studies.

1. Introduction

Since the introduction of MALDI techniques in 1997, mass spectrometric imaging (MS imaging) has been widely adopted to create molecular ion images without the use of radioactive or fluorescent labeling tags [1, 2]. Numerous MS imaging studies have shown capabilities to create distribution maps for compounds from small molecules to large proteins with a variety of MS platforms [3-6]. Although separations, most commonly including liquid chromatography (LC) and capillary electrophoresis (CE), have been widely employed and coupled to a variety of MS instruments to achieve highly efficient separation and enhanced MS signal for the analysis of complex samples such as trace-level peptide mixtures, few separation tools have ever been coupled to MS imaging since separation tends to cause loss of spatial distribution information [7-11]. On the other hand, MS imaging (MSI) offers unique advantages when it is coupled with separation tools such as LC and CE. The separation dimensions are able to provide highly efficient fractionation to reduce the inherent complexity and to enable more accurate quantification for MSI. Furthermore, by converting discrete mass spectra to a continuous ion trace with enhanced MS imaging signals, analytes can be studied from a new perspective as individual colored regions with MSI, offering enriched information for complex sample analysis.

In recent years, our group has designed an interface that coupled separation to MS imaging analysis [12-14]. The possibility of employing MALDI MS imaging for LC-MALDI and CE-MALDI coupling has been explored [15]. In order to add separation dimensions to MS imaging, a well-designed interface is the key to enable smooth sample collection and to form homogeneous trace on the sampling plate. MALDI MSI has almost been exclusively used for tissue imaging of various compounds [16-18], but the inherent characteristics of MSI also make it a great choice for coupling to a micro-scale separation method. In contrast to the regular

offline LC/CE–MALDI coupling schemes as mentioned above, continuous collection of LC or CE flow can be easily achieved with MSI detection, which preserves the temporal resolution from separation dimension. In addition, the imaging software enables convenient data analysis based on either mass-to-charge (*m*/*z*) or retention time, indicating the potential which could be comparable to current LC–ESI-MS software. Compared with CE, LC features a different separation mechanism (e.g., reversed phase LC is based on hydrophobicity) and is much more widely adopted; however, LC separation is impacted by Eddy diffusion and mass transfer kinetics within a column which requires additional consideration when coupled to MALDI MSI [19]. We have reported an improved LC–MSI device for quantitative analysis of complex peptides [15]. Lauryl methacrylate-co-ethylene dimethacrylate (LMA-EDMA) monolithic column is fabricated for RPLC separation. The LC flow and matrix flow are independently controlled and mixed on a commercially available ground stainless steel MALDI plate. With MALDI plate moving along *x*-axis, a straight, continuous and homogenous LC trace is formed on the surface of the MALDI plate directly. Combined with the micro-meter scale spatial resolution from MSI acquisitions, this novel interface design retains temporal resolution for the separation down to sub-second time scale, resulting in enhanced mass profiling and accurate quantitation. This system is highly robust and is semi-automated highlighting its great potential as an attractive alternative to the widespread use of LC–ESI-MS for comparative proteomics and peptidomics studies due to its complementary feature and unique capabilities.

In addition to the development of CE-MSI and LC-MSI, in this chapter we will also discuss how to apply this platform to online monitoring of secreted neuropeptide in live animal models. To investigate NP degradation and determine the length of action in extracellular space, we employ MSI platform coupled with *in vivo* microdialysis to trace the *in vivo* degradation profile

of selected NPs. A MS-based detection platform using MALDI-MS was developed to enable semi-quantitative measurements of changes in peptide abundance during degradation at multiple time points. This platform allows for high-throughput analysis of samples with μL or sub-μL volume. MALDI MSI is coupled with microdialysis collection to study body fluid samples, which offers the capability to trace the dynamic degradation process in an off-line, 'real-time' manner. As a prime *in vivo* sampling technique, microdialysis has long been used in neuroscience studies to sample a wide range of molecules, including NPs and neurotransmitters, directly from extracellular space with minimal perturbation to the animal [20-23]. The coupling of MSI detection with microdialysis collection allows us to identify the degradation products and the imaging results enabled the visualization of relative abundance changing trends of target molecules. More importantly, we can take full advantage of microdialysis collection as the temporal resolution was maintained on the MALDI platform, thus allow us to monitor the 'real-time', *in vivo* changes. This novel platform promises great potential in correlating *in vivo* neurochemical dynamics with physiological processes in a highly time-resolved manner. In addition, this study presents one of the most in-depth studies on extracellular NP degradation in the crustacean nervous system.

2. Materials and methods

2.1. Chemicals and materials

Acetic acid, hydrochloric acid, sodium hydroxide, acetone, acetonitrile, urea and ammonium bicarbonate were obtained from Fisher Scientific (Pittsburgh, PA, USA). Lauryl methacrylate (LMA, 96%), ethylene dimethacrylate (EDMA, 98%), butandiol (99%), 1-propanol (99.5%), 3-(trimethoxysilyl) propyl ethacrylate (98%), 2,2′-Azobis(2-methylpropionitrile) (AIBN, 98%), trifluoroacetic acid (TFA), α-Cyano-4-hydroxycinnamic acid (CHCA, 99%), iodoacetamide

(IAA) and bovine serum albumin (BSA) were purchased from Sigma–Aldrich (St. Louis, MO, USA). D/L-dithiothreitol (DTT) and sequencing grade modified trypsin were from Promega (Madison, WI, USA). Ethanol (200 proof) was purchased from Decon Laboratories (King of Prussia, PA, USA). C18 Ziptip column from Millipore was used for sample cleaning, and all water used was doubly distilled on a Millipore filtration system (Bedford, MA, USA). The physiological saline consisted of 440 mM NaCl, 11 mM KCl, 26 mM $MgCl_2$, 13 mM $CaCl_2$, 11 mM Trizma base, and 5 mM maleic acid in pH 7.45.

2.2. Animals and *in vivo* microdialysis

CMA/20 Elite probes with 4 mm membranes of polyarylether sulfone (PEAS) were purchased from CMA Microdialysis (Harvard Apparatus, Holliston, MA, USA). A KD Harvard 22 (Harvard Apparatus, Holliston, MA, USA), and an 11 Elite Nanomite Syringe Pump (Harvard Apparatus, Holliston, MA, USA) were used to drive perfusion fluid through microdialysis probes and tubing. Additional FEP (CMA) and PEEK (Upchurch-Scientific, Index Health and Science, Oak Harbor, WA, USA) tubing was used to lengthen the tubing of the microdialysis probe as needed. Flanged connectors from CMA and BASi (West Lafayette, IN, USA) were used to connect the tubing. Probes were rinsed with crab saline prior to implantation.

The procedure for *in vivo* microdialysis surgery on Jonah crabs was adapted from previous publications [22, 24]. Briefly, after the microdialysis probe was surgically implanted into the crab, the animal was allowed to recover for at least 24 h with crab saline as perfusion fluid before dialysate was collected for MS analysis. For the peptide degradation study, different NP standards and the mammalian peptide, bradykinin, were added into the perfusion crab saline. The flow rate was set to 0.5 μL/min by a programmable syringe pump. The outlet microdialysate was deposited directly onto a MALDI plate pre-coated with matrix whose movement was

mechanically controlled by a syringe pump at a speed of 3.7 mm/min. Matrix pre-coating was performed by an automated TM-sprayer to improve extraction efficiency of target molecules from dialysate [25]. CHCA matrix (10 mg/mL in 0.1% FA and 50% ACN) was applied simultaneously as collection went on driven by syringe pump at a flow rate of 0.5 μL/min.

2.3. Sample preparation

Neuropeptides were extracted from the pericardial organ (PO) of blue crabs (*Callinectes sapidus*). The crabs were purchased from local grocery store and kept in an artificial seawater tank at 10–12 °C without food. During dissection, the crabs were first anesthetized for 15–30 min in ice, and POs were dissected in physiological saline. Three POs were combined, homogenized in 50 μL acidified methanol (1% acetic acid in 90% methanol) in ice and centrifuged at 16,100 rcf for 8 min before harvesting the supernatants. The extraction was repeated for 3 times and the supernatants were combined and dried. The residue was reconstituted in 10 μL of 0.1% TFA and desalted with Ziptip C18 column.

2.4. Integrated MSI platform

MS imaging was generated by depositing LC elution or microdialysate on a MALDI target plate. Matrix was applied either by a separate capillary or by an automated sprayer. MALDI plate was controlled by a syringe pump to move horizontally so that sample traces were collected continuously. This platform can be readily integrated with separation dimensions and animal models. For separation coupled to MSI interface, a LC column and a matrix delivery capillary was assembled together to apply LC elution on the MALDI plate. This platform also enables flexible combination with live animal for online analysis. In this work, *in vivo* microdialysis surgery was done on Jonah crabs as described in previous publications [21, 24]. After microdialysis probe was surgically implanted into the crab, the animal was allowed to recover

for at least 24 h with crab saline (440 mM NaCl; 11 mM KCl; 13 mM $CaCl_2$; 26 mM $MgCl_2$; 10 mM HEPES acid; pH 7.4, adjusted with NaOH) as perfusion fluid before dialysate was collected for MS analysis. For peptide degradation study, different NP standards and mammalian peptide, bradykinin were added into perfusion crab saline. The flow rate was set at 0.5 μL/min by a programmable syringe pump. The outlet microdialysate was deposited directly onto a matrix pre-coated MALDI plate (Thermo Scientific). Matrix pre-coating was performed by an automated TM-sprayer to improve extraction efficiency of target molecules from dialysate [20, 25]. CHCA matrix was applied simultaneously as collection went on driven by syringe pump at a flow rate of 0.5 μL/min.

2.5. Instrumentation and data processing

The MS images of collected sample traces were acquired on Autoflex III MALDI-TOF/TOF (Bruker Daltonics, Bremen, Germany) equipped with 200 Hz Smartbeam II laser and MALDI-LTQ-Orbitrap XL mass spectrometer (Thermo Scientific, Bremen, Germany) equipped with 60 Hz 337 nm N_2 laser in positive ion mode. For each pixel, the step size was set at 100 μm × 100 μm (on the x and y axis). MALDI TOF images was processed with FlexImaging 2.0 (Bruker Daltonics, Bremen, Germany) and Quantinetix (ImaBiotech, Loos, France). MALDI Orbitrap imaging data was further processed through MSiReader [26] and all images were normalized by internal standard.

3. Results and discussion

3.1. Application in neuropeptide characterization of tissue samples

Routinely, collecting LC fractions on a MALDI plate spot-by-spot and acquiring mass spectrum from each time point are extremely labor intensive. The data analysis requires a manual search of the mass spectra generated from each spot. In contrast, a distinctive feature of LC-MSI data

analysis is the ability to analyze data based on either mass-to-charge ratio or retention time from the constructed image. With the imaging software, a "mass filter" is able to be specified on the mass spectrum and the image for the selected mass range will be shown. Alternatively, because the position of image reflects retention time, by selecting a region or a pixel of interest (ROI) on the image of the LC trace, the mass spectrum can be retrieved and displayed for the selected retention time. We applied this platform in neuropeptide analysis extracted from the blue crab *Callinectes sapidus*. The analysis of neuropeptides is challenging because of their extremely low concentration and diverse physical and chemical properties in a complex biological matrix. As listed in Table 1, 262 putative neuropeptides were detected, including 65 previously identified from our home-built neuropeptide database.

3.2. Interfacing MSI with *in vivo* analysis of neuropeptide degradation

MSI platform offers the capability of maintaining sample temporal resolution, which could work in complementary with continuous microdialysis collection. To address the challenges of quantifying NP changes with MALDI technique, MSI was employed. Rather than providing quantitative information in the form of ratio change at different time points, the measurement was achieved by constructing MSI images of collected microdialysate with *m/z* distribution and signal intensity. An MSI image result contains information about the identities of targeted molecules, locations as well as signal intensities. In this platform, microdialysis collection and matrix application were carried out simultaneously and required no additional sample preparation step.

Herein, FMRFamide, FLP I, CabTRP Ia and AST-B_3 were delivered individually with and without bradykinin in each experiment *via* retro-dialysis. NPs were added into perfusion crab saline solution at different concentrations and infused at a flow rate of 0.5 μL/min before

switched back to crab saline perfusion. Collection of microdialysate was done continuously onto customized MALDI target plate. The overall workflow was illustrated in Figure 1. Infusion time and concentration were optimized by *in vitro* assay.

3.3. Degradation products observed by MSI

The acquired mass spectrometric imaging data was processed against MSiReader software to generate high quality images. It took about 1 hr to 1.5 hr from the start of delivered NPs reaching the probe implantation site to detect related MS signals from collected microdialysate trace. Figure 2 illustrated the full MS images of AST-B_3 peptide throughout microdialysate collection. As the administration of peptide being continued for 3 hrs, the signal intensity of the intact peptide increased to reach an equilibrium and maintain at that steady state over injection process. The perfusion solution was switched back to crab saline at 180 min, and the collection was continued for another two hours where the signal intensity was at similar level which may result from less degradation. The signal was a bit wobbly over the traces, which was most likely due to the inconsistency of trace collection and matrix application at such a low flow rate. The homogeneity of matrix crystallization would also possibly affect the detection.

To visualize neuropeptide degradation, the first trace was collected starting from 1 hr as shown in Figure 3. The length of each trace was around 20 min to 25 min with its scale bar indicating the signal intensity. The brighter color indicated higher intensity and the black image at the first half of the traces indicated no detectable signals of m/z of interest. One of the limiting factor is the MS instrument sensitivity thus requiring accumulation of generated *in vivo* degradation products to reach detection limit. As shown in the results, intact NPs along with various degradation products were detected simultaneously such as bradykinin and its degradation product PPGFSPFR at *m/z* 904.4676. RFamide at *m/z* 321.2034, a sequence shared

between FLP I and FMRFamide, whereas LRFamide, and FLRFamide belonging to FLP I were also detected around the similar time period. Such results confirmed our assumption of substance accumulation in the circulating system and diffusion across microdialysis probe. The detection of these degradation products from continuous administration of NPs also served as an evidence that physical concentration of these NPs were kept at steady level by various peptidases *in vivo*.

In addition to providing information about the timeline of degradation products generation, this platform also gave us the opportunity to observe dynamic changing patterns of NPs and their degradation products which would potentially provide interesting insights into their functional roles. Taken FLP I peptide as an example, as shown in Figure 4, after switching back to crab saline perfusion, the signal intact peptide gradually became undetectable over time as the image turned darker. Some of its degradation products, on the other hand, had very different changes. During the 25 min collection time, the intact peptide at *m/z* 1053.5588 disappeared in the last 10 min. Two of the degradation products, DRNFLRFamide and RNFLRFamide presented a bit longer in the trace. Signals of several shorter chain degradation products, including NFLRFamide, FLRFamide, and LRFamide, however became stronger towards the later of this trace when intact peptide got eliminated. This MSI results suggested that the shorter chain degradation products were generated from longer chain peptide degradation products or even the intact peptide. The difference in their production time might be resulted from the specific activities of multiple peptidases involved. The cleavage of peptide bonds at different residues required different enzymes, which may offer some interesting insights and perspectives into our fundamental understanding of how neuropeptides function.

4. Conclusions

MSI platform combines the advantage of MALDI detection which can be incorporated with upstream separation and downstream online monitoring. It is flexible to a variety of applications without loss of spatial and temporal resolution. Coupling with microdialysis collection, it offered a great opportunity to monitor the *in vivo* degradation processes of NPs in crustacean in an off-line 'real-time' manner. By maintaining the temporal resolution of microdialysis collection, the spatial information contained in MSI results allowed visualization of the dynamic changes throughout the degradation process. This platform offers a great potential in future application to the study of dynamic biological events.

Reference

1. Caprioli RM, F.T., Gile J., *Molecular Imaging of Biological Samples: Localization of Peptides and Proteins Using MALDI-TOF MS.* Anal. Chem, 1997. **69**: p. 4751-4760.
2. Kru¨ger, M.K.a.R., *Ion Formation in MALDI: The Cluster Ionization Mechanism.* Chem. Rev., 2003. **103**: p. 427-439.
3. Pierre Chaurand, S.A.S.a.R.M.C., *Imaging mass spectrometry: a new tool to investigate the spatial organization of peptides and proteins in mammalian tissue sections.* Curr Opin Chem Biol., 2002. **6**: p. 676–681.
4. McDonnell, L.A. and R.M. Heeren, *Imaging mass spectrometry.* Mass Spectrom Rev, 2007. **26**(4): p. 606-43.
5. Gemperline, E., B. Chen, and L. Li, *Challenges and recent advances in mass spectrometric imaging of neurotransmitters.* Bioanalysis, 2014. **6**(4): p. 525-540.
6. OuYang, C., Z. Liang, and L. Li, *Mass spectrometric analysis of spatio-temporal dynamics of crustacean neuropeptides.* Biochimica et Biophysica Acta (BBA) - Proteins and Proteomics, 2015. **1854**(7): p. 798-811.
7. Sandra, K., et al., *Highly efficient peptide separations in proteomics Part 1. Unidimensional high performance liquid chromatography.* J Chromatogr B Analyt Technol Biomed Life Sci, 2008. **866**(1-2): p. 48-63.
8. Sandra, K., et al., *Highly efficient peptide separations in proteomics. Part 2: bi- and multidimensional liquid-based separation techniques.* J Chromatogr B Analyt Technol Biomed Life Sci, 2009. **877**(11-12): p. 1019-39.

9. van den Broek, I., et al., *Quantitative bioanalysis of peptides by liquid chromatography coupled to (tandem) mass spectrometry.* J Chromatogr B Analyt Technol Biomed Life Sci, 2008. **872**(1-2): p. 1-22.

10. Kasicka, V., *Recent advances in CE and CEC of peptides (2007-2009).* Electrophoresis, 2010. **31**(1): p. 122-46.

11. Herrero, M., E. Ibanez, and A. Cifuentes, *Capillary electrophoresis-electrospray-mass spectrometry in peptide analysis and peptidomics.* Electrophoresis, 2008. **29**(10): p. 2148-60.

12. Junhua Wang, M.M., Ruibing Chen, and Lingjun Li, *Enhanced Neuropeptide Profiling via Capillary Electrophoresis Off-Line Coupled with MALDI FTMS.* Anal Chem, 2008. **80**: p. 6168-6177.

13. Wang, J., et al., *Advancing matrix-assisted laser desorption/ionization-mass spectrometric imaging for capillary electrophoresis analysis of peptides.* Anal Chem, 2011. **83**(9): p. 3462-9.

14. Zhang, Z., et al., *Pressure-assisted capillary electrophoresis coupling with matrix-assisted laser desorption/ionization-mass spectrometric imaging for quantitative analysis of complex peptide mixtures.* Anal Chem, 2012. **84**(18): p. 7684-91.

15. Zhang, Z., S. Jiang, and L. Li, *Semi-automated liquid chromatography-mass spectrometric imaging platform for enhanced detection and improved data analysis of complex peptides.* J Chromatogr A, 2013. **1293**: p. 44-50.

16. Fonslow, B.R. and J.R. Yates, 3rd, *Capillary electrophoresis applied to proteomic analysis.* J Sep Sci, 2009. **32**(8): p. 1175-88.

17. Greer, T., R. Sturm, and L. Li, *Mass spectrometry imaging for drugs and metabolites.* J Proteomics, 2011. **74**(12): p. 2617-31.

18. Amstalden van Hove, E.R., D.F. Smith, and R.M. Heeren, *A concise review of mass spectrometry imaging.* J Chromatogr A, 2010. **1217**(25): p. 3946-54.

19. Weidner, S.M. and J. Falkenhagen, *LC-MALDI-TOF imaging MS: a new approach in combining chromatography and mass spectrometry of copolymers.* Anal Chem, 2011. **83**(23): p. 9153-8.

20. Jiang, S., et al., *Investigation of signaling molecules and metabolites found in crustacean hemolymph via in vivo microdialysis using a multifaceted mass spectrometric platform.* Electrophoresis, 2016. **37**(7-8): p. 1031-8.

21. Liang, Z., C.M. Schmerberg, and L. Li, *Mass spectrometric measurement of neuropeptide secretion in the crab, Cancer borealis, by in vivo microdialysis.* Analyst, 2015. **140**(11): p. 3803-13.

22. Schmerberg, C.M. and L. Li, *Mass spectrometric detection of neuropeptides using affinity-enhanced microdialysis with antibody-coated magnetic nanoparticles.* Anal Chem, 2013. **85**(2): p. 915-22.

23. Schmerberg, C.M., Z. Liang, and L. Li, *Data-independent MS/MS quantification of neuropeptides for determination of putative feeding-related neurohormones in microdialysate.* ACS Chem Neurosci, 2015. **6**(1): p. 174-80.

24. Behrens, H.L., R. Chen, and L. Li, *Combining microdialysis, NanoLC-MS, and MALDI-TOF/TOF to detect neuropeptides secreted in the crab, Cancer borealis.* Anal Chem, 2008. **80**(18): p. 6949-58.

25. Zhang, Z., J. Kuang, and L. Li, *Liquid chromatography-matrix-assisted laser desorption/ionization mass spectrometric imaging with sprayed matrix for improved sensitivity, reproducibility and quantitation.* Analyst, 2013. **138**(21): p. 6600-6.

26. Robichaud, G., et al., *MSiReader: An Open-Source Interface to View and Analyze High Resolving Power MS Imaging Files on Matlab Platform.* Journal of The American Society for Mass Spectrometry, 2013. **24**(5): p. 718-721.

Table 1. Putative neuropeptides from the pericardial organs of *Callinectes sapidus* detected by separation coupled to MSI platform*.

m/z	Sequence	Family
676.23		
796.37	NPYSFGLa	AST-A
818.56		
834.50		
876.35		
909.35	ARPYSFGLa	AST-A
916.55	KIFEPLVA	OTHERS
932.45		
933.64		
937.55	PRVYSFGLa/ELNFLRFa	AST-A/RFa
946.56		
951.46		
956.45	PFCNAFTGCa	CCAP
962.46	APQPYAFGLa	AST-A
965.45	NRNFLRFa	RFa
976.58	SGFYANRYa	RYa
992.46	APSGFLGM(O)Ra	CabTRP
1004.46	FSGTYNFGLa	AST-A
1010.46		
1015.56		
1022.47	GNRNFLRFa	RFa
1030.60	pEGFYSQRYa	Rya
1042.57	YPSGFLGM(O)Ra	CabTRP
1046.47		
1052.47	SPRLTYFGLa	AST-A
1065.55	RDNFVLRFa	RFa
1076.49		
1079.47		
1094.49	ENRNFLRFa	RFa
1095.67		
1107.55	AGWSSMRGAWa	AST-B
1123.58	TGNRNFLRFa	RFa
1124.48	GLSRNYLRFa	RFa
1126.58		
1141.58		
1143.68		
1146.47	GYSKNYLRFa	RFa
1155.51		
1158.59	YGNRSFLRFa	RFa
1170.68		

1172.48	AYNRSFLRFa	RFa
1176.62		
1182.52	TSWGKFQGSWa	AST-B
1198.58	NFDEIDRSGFa	Ork
1199.48	NFDEIDRSGF	Ork
1201.47		
1208.66		
1209.56	TGWNKFQGSWa	AST-B
1212.69		
1213.59	DEIDRSGFGFA	Ork
1217.48		
1220.49	SGDWSSLRGAWa	AST-B
1222.59	GNWNKFQGSWa	AST-B
1226.79		
1230.69	SLKSDTVTPLLG	CPRP
1233.69		
1236.68		
1243.70		
1244.51	DLKSDTVTPLR	CPRP
1249.48		
1252.59	NNWSKFQGSWa	AST-B
1256.49	NFDEIDRSGFG	Ork
1257.69	DFDEIDRSGFG	Ork
1267.59		
1270.60	NFDEIDRSGFA	Ork
1271.79	pQDLDHVFLRFa	RFa
1274.62		
1286.50	NFDEIDRSSFG	Ork
1287.70	ASLKSDTVTPLR	CPRP
1288.60	QDLDHVFLRFa	RFa
1291.72		
1293.51	STNWSSLRSAWa	AST-B
1300.45	NFDEIDRSSFA	Ork
1302.59	RSAEGLGRMGRL	CPRP
1306.60		
1309.60		
1316.50		
1328.51		
1342.60		
1342.90	DVRTPALRLRFa	RFa
1348.60		
1353.61		
1358.66		
1360.60	FDEIDRSGFGFA	Ork
1361.74	RSAQGLGKM(O)ERL	CPRP
1370.78		

1372.61	KIFEPLRDKNL	OTHERS
1380.52	NNNWTKFQGSWa	AST-B
1381.60	GYRKPPFNGSIFa	SIFa
1386.88		
1401.60		
1403.67	NFDEIDRSGFGF	Ork
1410.71		
1414.82		
1415.70	RSAEGLGRMGRLL	CPRP
1429.79		
1431.71		
1433.64	NFDEIDRSSFGF	Ork
1438.62		
1443.71		
1445.71		
1455.72		
1456.61		
1456.91		
1463.68		
1470.72	VPNDWAHFRGSWa	AST-B
1473.72		
1473.80		
1474.69	NFDEIDRSGFGFA	Ork
1477.62		
1486.76		
1491.72		
1500.72		
1502.71	NFDEIDRSGFGFV	Ork
1504.62	NFDEIDRSSFGFA	Ork
1505.65	DFDEIDRSSFGFA	Ork
1508.90		
1512.71		
1513.62		
1521.72	RSTPGYGRMDRIL	CPRP
1522.92		
1523.83		
1530.72		
1532.68	NFDEIDRSSFGFV	Ork
1547.65	NFDEIDRSSFGFN	Ork
1553.82		
1555.63		
1563.73		
1576.74		
1584.73		
1586.83	MFAPLAWPKGGARWa	AST-B
1590.58		

1592.83		
1602.73		
1604.83		
1606.78		
1618.76		
1625.83		
1628.83		
1648.93		
1657.64		
1663.75	RSTPGYGRMDRILAA	CPRP
1671.74		
1685.67		
1687.65		
1701.74		
1702.94		
1705.94		
1712.84		
1719.88		
1729.79		
1739.84		
1740.89		
1744.79		
1746.75		
1753.86		
1754.85		
1758.75		
1760.95	RSAQGLGKM(O)EHLLASY	CPRP
1761.83		
1767.75		
1768.95		
1775.85		
1776.90		
1780.81		
1781.85		
1790.85		
1791.93		
1798.65		
1799.85		
1830.76		
1831.78		
1839.91		
1872.76		
1881.76		
1888.83		
1890.02		
1895.86		

1899.76	pQIRYHQCYFNPISCF	AST-C
1909.83		
1912.81		
1921.97		
1923.89		
1925.08		
1926.77		
1933.97		
1937.87		
1942.67		
1944.89		
1944.95		
1947.94		
1958.27		
1958.87		
1960.67		
1967.87		
1978.26		
1978.67		
1981.78		
1992.05		
1995.00		
2001.63		
2016.78		
2017.08		
2023.07		
2041.98		
2049.78		
2051.09		
2060.88		
2061.10		
2063.75		
2069.88		
2072.88		
2073.94	SPMEPSAALAVEHGTTHPLE	CPRP
2080.98		
2081.87		
2090.89		
2095.08		
2097.97		
2099.89		
2105.89		
2109.19		
2130.80		
2137.92		
2141.89		

2145.79	
2155.99	
2156.90	
2162.89	
2173.09	
2175.20	TSPMEPSAALAVEHGTTHPLE CPRP
2182.99	
2188.88	
2196.80	
2215.10	
2222.00	
2226.07	
2231.00	
2233.11	
2235.95	
2241.20	
2258.90	
2276.01	
2282.91	
2312.01	
2324.06	
2337.99	
2357.92	
2369.92	
2372.92	
2383.73	
2400.40	
2401.12	
2415.34	
2424.90	
2432.02	
2441.16	
2444.32	
2446.13	
2458.42	
2468.33	
2472.23	
2473.13	

* The sequence and family were marked to previously identified neuropeptides.

Table 2. Amino acid sequence and calculated monoisotopic masses of degradation products of neuropeptides using Protein Prospector (UCSF). a indicates C-terminal amidation.

Neuropeptide Sequence	Amino Acid Sequence of Degradation Product	Theoretical $[M+H]^+$	Measured $[M+H]^+$
FMRFamide	FMRFa	599.3122	599.3146
	FMR	435.2173	435.2198
	FM	279.1162	279.0864
	MRFa	452.2428	452.2455
	RFa	321.2034	321.2048
	RFa-NH_3	304.1768	304.1783
FLP I SDRNFLRFamide	SDRNFLRFa	1053.5588	1053.5625
	SDRNFLRFa-H_2O	1035.5483	1035.5539
	SDRNGLRFa-NH_3	1036.5323	1036.5380
	DRNFLRFa	966.5268	966.5302
	RNFLRFa	851.4999	851.5033
	NFLRFa	695.3988	695.4010
	FLRFa	581.3588	581.3581
	LRFa	434.2874	434.2894
	SDRNFLR	889.4639	889.4692
	SDRNFL	733.3682	733.3546
CabTRP APSGFLGMRamide	APSGFLGMRa	934.4927	934.4957
	PSGFLGMRa	863.4456	863.4586
	SGFLGMRa	766.4029	766.4057
	GFLGMRa	679.3708	679.3729
	FLGMRa	622.3494	622.3512
	FLGMRa-NH_3	605.3228	605.3257
	LGMRa	475.2809	475.2822
	LGMRa-NH_3	458.2544	458.2564
	GMRa	362.1969	362.1983
	GMRa-NH_3	345.1703	345.1720
	APSGFL	573.3031	573.2935
AST-B SGKWSNLRGAWamide	SGKWSNLRGAWa	1260.6569	1260.6650
	GKWSNLRGAWa	1173.6276	1173.6327
	KWSNLRGAWa	1116.6061	1116.6109
	WSNLRGAWa	988.5112	988.5150
	WSNLRGAWa-NH_3	971.4846	971.4877
	SNLRGAWa	802.4318	802.4346
	NLRGAWa	715.3998	715.4020
	LRGAWa	601.3569	601.3590
	RGAWa	488.2728	488.2744
	SGKWSNLRGA	1057.5538	1057.5360
	SGKWSNLRG	986.5166	986.4945
	SGKWSNLR	929.4952	929.4984
	SGKWSNL	773.3941	773.3964
	SGKWSN	660.3100	660.3082

	SGKWS	546.2671	546.2702
	SGKWS-H_2O	528.2565	528.2574
	SGKWS-NH_3	529.2405	529.2343
	SGKW	459.2350	459.2371
	SGK	273.1557	273.1564
Bradykinin RPPGFSPFR	RPPGFSPFR	1060.5687	1060.5736
	PPGFSPFR	904.4676	904.4697
	PPGFSPFR-NH_3	887.4410	887.4467
	PGFSPFR	807.4148	807.4177
	PGFSPFR-H_2O	790.3883	790.3968
	PGFSPFR-NH_3	789.4042	789.3913
	GFSPFR	710.3620	710.3631
	FSPFR	653.3402	653.3427
	SPFR	506.2722	506.2745
	PFR	419.2401	419.2423
	FR	322.1874	322.1890
	RPPGFSPF	886.4570	886.4586

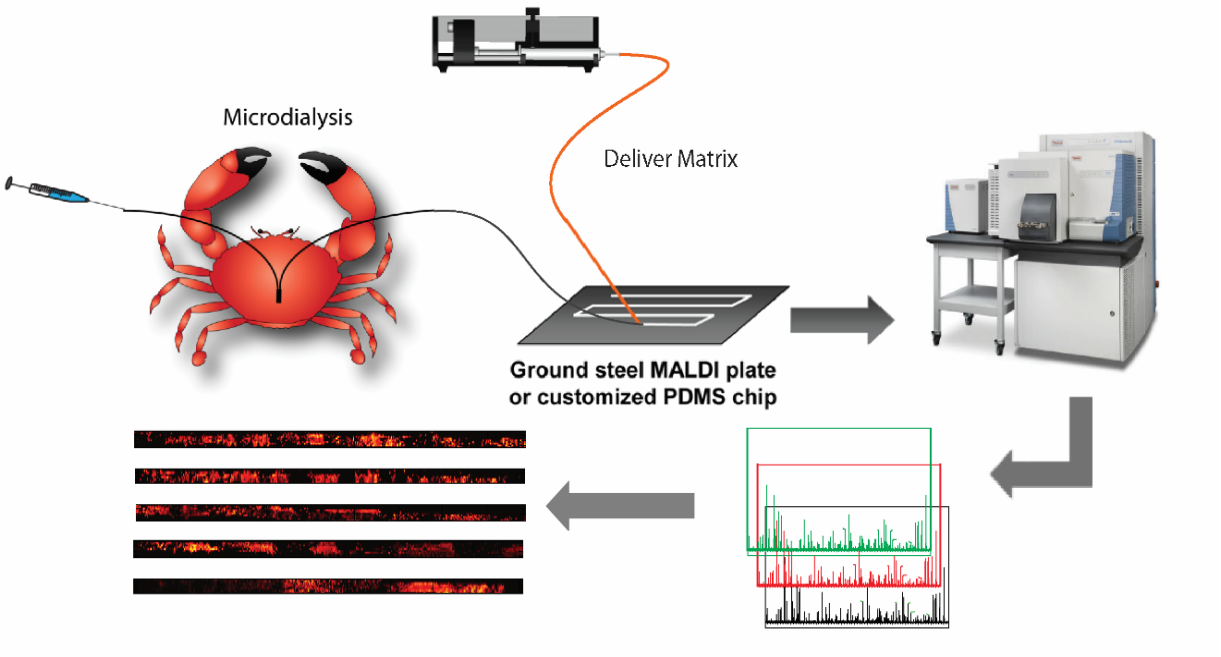

Figure 1. Graphic illustration of microdialysis-MALDI-MSI workflow. Microdialysate collection and matrix application were done simultaneously onto a customized MALDI target plate.

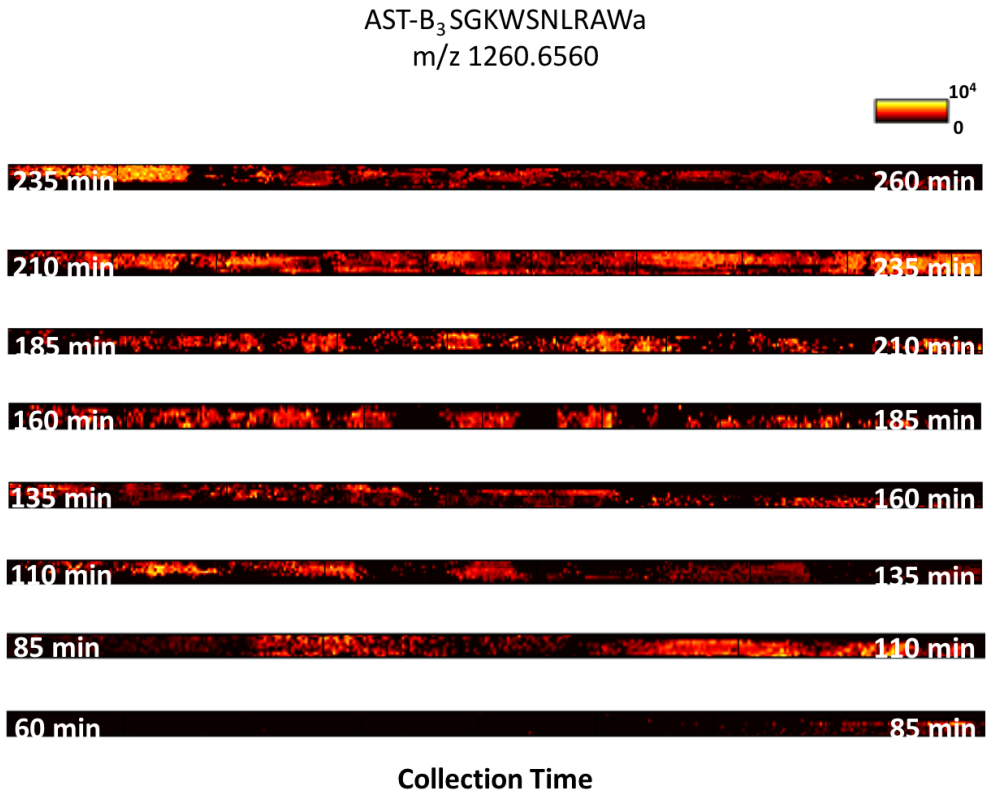

Figure 2. MSI results of AST-B_3 throughout microdialysate collection. As indicated by images, it became detectable after 80 min, and maintained at similar level until the end of collection.

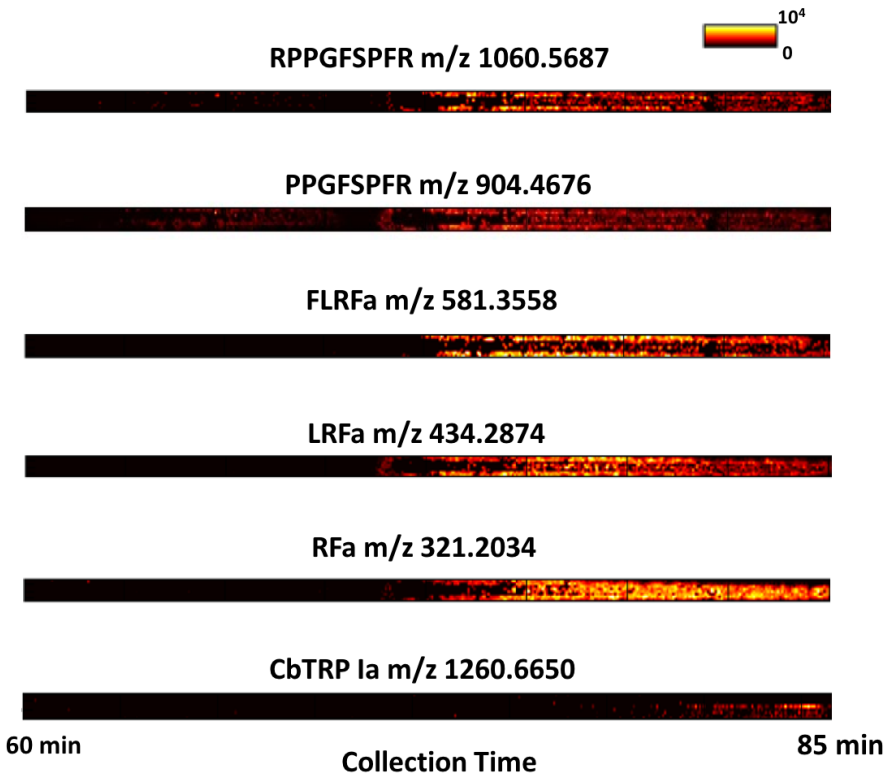

Figure 3. Examples of first microdialysate trace where NPs became detectable. Images of intact NPs, CbTRP Ia and bradykinin were extracted together with several degradation products.

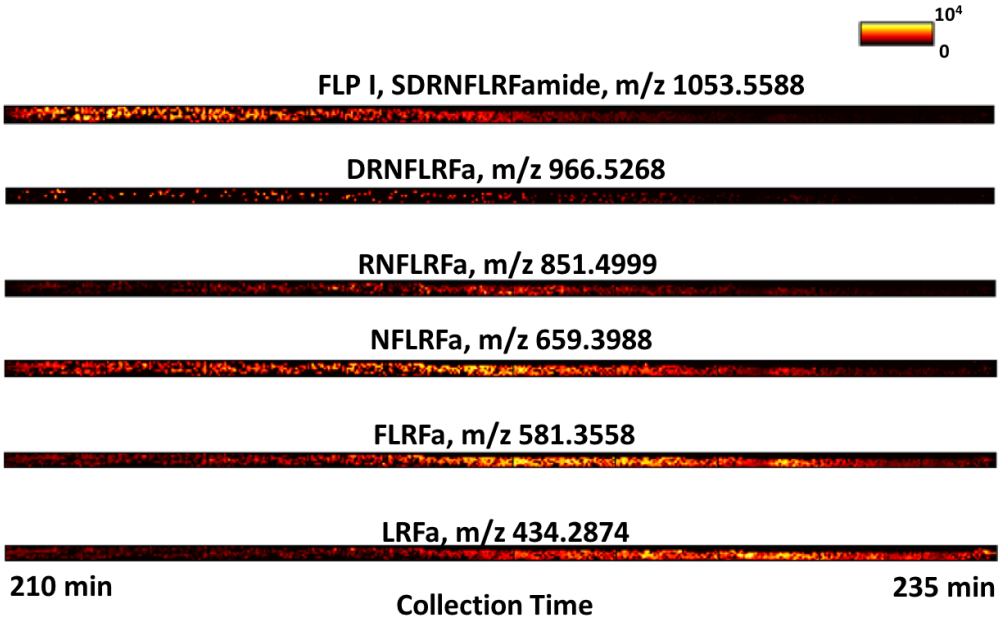

Figure 4. Extracted images of FLP I and several degradation products in trace collection from 210 min to 235 min.

Chapter 6

Investigation of signaling molecules and metabolites found in crustacean hemolymph via *in vivo* microdialysis using multi-faceted mass spectrometric platform

Adapted from:

1. **Jiang S.,** Liang Z., Hao L., Li L., Investigation of signaling molecules and metabolites found in crustacean hemolymph via in vivo microdialysis using multi-faceted mass spectrometric platform. *Electrophoresis.* 2016, 37(7-8); 1031-038.

Abstract

Neurotransmitters (NTs) are endogenous signaling molecules which play an important role in regulating various physiological processes in animals . Detection of these chemical messengers is often challenging due to their low concentration levels and fast degradation rate *in vitro*. In order to address these challenges, herein we employed *in vivo* microdialysis (MD) sampling to study neurotransmitters in the crustacean model *Cancer borealis*. Multi-faceted separation tools, such as capillary electrophoresis (CE) and ion mobility mass spectrometry were utilized in this work. Small molecules were separated by different mechanisms and detected by matrix-assisted laser desorption/ionization mass spectrometric imaging (MALDI-MSI). Performance of this separation-based MSI platform was also compared to liquid chromatography-electrospray ionization mass spectrometry (LC-ESI-MS). By utilizing both MALDI and ESI MS, a total of 208 small molecule neurotransmitters and metabolites were identified, of which 39 were identified as signaling molecules secreted *in vivo*. In addition, the inherent property of sub micro-scale sample consumption using CE enables shorter time of MD sample collection. Temporal resolution of *in vivo* MD was improved by approximately 10-fold compared to LC-ESI-MS, indicating the significant advantage of applying separation-assisted MALDI imaging platform.

1 Introduction

Monitoring signaling molecules in circulatory systems can provide important insight into functional behavior related to environmental change, drug effects, and disease states [1-3]. *In vivo* microdialysis (MD) is a powerful sampling technique that allows direct collection of signaling molecules from extracellular space with minimum disturbance to their physiological conditions [4, 5]. Usually, MD probes consist of two pieces of microporous tubings sheathed in a semi-permeable membrane that is plugged at one end. With a MD probe implanted into an area of interest within an animal, molecules that fall below the molecular-weight cutoff (MWCO) threshold of the probe will passively diffuse across the membrane according to their concentration gradients. Perfusion through the membrane, typically performed at 0.1-3.0 μL/min, generates a stream of dialysate that can be analyzed for compounds of interest [6, 7]. The MD sampling technique has been applied to a wide variety of tissues and organs in the body including liver, heart, skin, blood, placenta, stomach, and ear, with analytes of interest ranging from low molecular weight substances including amino acids and metabolites, to higher molecular substances such as neuropeptides [8, 9]. The advantages of MD benefits a variety of applications in neurochemical and clinical studies [10-12].

Tremendous challenges confront scientists attempting *in vivo* neurochemical measurements. For example, neurotransmitters may change in concentration rapidly requiring high temporal resolution detection capability. Additionally, low endogenous levels of many compounds present *in vivo*, typically at nM-pM range [13], can make the detection of these molecules difficult. Despite the unique advantage of *in vivo* sampling by MD, the low recovery rate of molecules also poses additional challenges for analysis. To address these problems, researchers have made great advancements in both MD sampling strategies and downstream analytical platforms.

Attempts to increase MD recovery have been made by various laboratories. One successful technique, affinity-enhanced MD, improves recovery by using affinity agents added to the perfusion fluid to capture analytes of interest thereby increased the amount of target analytes recovered [14-18]. High temporal resolution, defined as the shortest time duration over which a dynamic change event can be observed, is critical for the functional study of targeted compounds. To be able to accurately correlate the concentration of analytes with behavior or stimuli, the analysis time must be shorter than the duration of measured events. In MD experiments, temporal resolution is limited by the downstream analytical sensitivity of the instrument platform used to study the termporal events. Analytical techniques like capillary electrophoresis (CE) with laser-induced fluorescence detection have been successfully coupled with MD aiming to improve temporal resolution [19-23]. It often necessitates additional sample work-up in order to render the analytes fluorescent. The coupling of CE with mass spectrometry provides enhanced sensitivity without the need for sample derivatization to detect low abundance molecules [24]. Analysis of MD samples by CE can provide improved temporal resolution compared to LC, as smaller amount of sample is needed for CE separation due to its capability of handling sub-uL volume of samples. Dialysate can be either on-line or off-line loaded and separated by a CE system for analysis of NTs, amino acids, peptides, and biomarker detection [25-27]. Decoupling sampling from analytical measurement can be highly desirable. In the case of offline CE-MS, analytical separation can be coupled to dialysate collection to increase throughput and reduce sample losses from pipetting and non-specific adsorption to the wall of fraction collection vials. The CE eluate can then be analyzed on a mass spectrometry platform to facilitate the on-the-fly measurement of several neurotransmitter and metabolite compounds within a single MD time point.

In this work, we employed CE separation coupled to *in vivo* MD of Jonah crab (*Cancer borealis*) to study secreted neurotransmitters (NTs) and metabolites in crustacean hemolymph. Instead of analyzing CE fractions by ESI-MS, we incorporated MALDI mass spectrometric imaging (MSI) with CE separation for small molecule measurement. MALDI was selected because the technique has a higher tolerance to salts and impurities which is a benefit when interrogating dialysate samples. Therefore, CE separated dialysate from crab does not need to be further desalted and cleaned up, reducing sample loss associated with additional manipulation. Neurotransmitters have lower molecular masses than peptides or proteins that often makes identifying isobaric molecules by accurate mass matching alone challenging especially when it is possible to have multiple metabolic features of similar or same *m/z* within one scan even after CE separation. To address this challenge, a second dimension of separation was applied to the gas-phase with ion mobility mass spectrometry (IMS). With IMS, molecular features within MD-CE fractions of crustacean hemolymph can be further separated based on their gas-phase drift times. With the flexibility of integrating multi-faceted MS platforms, metabolic coverage of crustacean hemolymph was significantly improved compared to using a single platform. Sensitivity and feature identification performance of this MD-CE-MSI platform was evaluated by comparing to a LC-MS approach utilizing a high-mass accuracy and high-resolution orbitrap mass analyzer (Q Exactive) [28-30].

2 Materials and methods

2.1 Chemicals and materials

Acetic acid, ammonium hydroxide, acetone, acetonitrile (ACN), methanol (MeOH), ammonium bicarbonate, and urea were purchased from Fisher Scientific (Pittsburgh, PA). α-Cyano-4-hydroxycinnamic acid (CHCA) and formic acid (FA) were from Sigma Aldrich (St. Louis, MO).

Fused-silica capillary with 75 μm i.d. and 365 μm o.d. was purchased from Polymicro Technologies (Phoenix, AZ). A TM-Sprayer from HTX Technologies (Carrboro, NC) was used to spray MALDI matrix (10 mg/mL CHCA in 50% ACN). Millipore C_{18} Ziptip column was used for sample cleaning, and all water used in this study was doubly distilled on a Millipore filtration system (Bedford, MA).

2.2 *In vivo* Microdialysis

CMA/20 Elite probes with 4 mm membranes of polyarylethersulfone (PAES) were purchased from CMA Microdialysis (Harvard Apparatus, Holliston, MA, USA). A KD Harvard 22 (Harvard Apparatus, Holliston, MA, USA), and a Pump 11 Elite Nanomite Syringe Pump (Harvard Apparatus, Holliston, MA,USA) were used to drive perfusate through MD probes and tubing. Probes consisted of a 6,000 Da MWCO tip were rinsed with crab saline prior to implantation.

Jonah crabs, *Cancer borealis*, were purchased from Ocean Resources, Inc. (Sedgwick, ME, USA) and The Fresh Lobster Company (Gloucester, MA, USA). Crabs were maintained in an artificial seawater tank at 10~13 °C and were allowed to adjust to the tanks for at least one week after shipment before performing microdialysis. Details of animal housing procedures were described elsewhere [17]. Animals were housed, treated and sacrificed following the animal care protocol in accordance with the University of Wisconsin-Madison's animal care guidelines. The surgery of microdialysis was adapted from previous publications [31]. After the probe was surgically implanted in the crab, the animal was allowed to recover for at least 24 h before dialysate was collected for MS analysis. Physiological crab saline (440 mM NaCl; 11 mM KCl; 13 mM $CaCl_2$; 26 mM $MgCl_2$; 10 mM HEPES acid; pH 7.4, adjusted with NaOH) was used as perfusion solution. The flow rate was set to be 0.5 μL/min by a programmable syringe pump.

Dialysate samples were collected with a refrigerated fraction collector (BASi HoneyComb, Bioanalytical Systems, Inc. Indianapolis, IN, USA). The dialysate fractions were concentrated ~10 fold in a SpeedVac (Thermo Fisher Scientific, Waltham, MA, USA) prior to downstream analysis.

2.3 CE-MSI

The interface for coupling CE to mass spectrometric imaging instrumentation was modified from previous work in our group [32, 33]. Briefly, a 60 cm long with 75 μm i.d./365 μm o.d. fused-silica capillary was pretreated and used for CE separation. A fracture was made near the outlet of the capillary and coated with cellulose acetate membrane to form an ion permeable channel. The inlet end of CE column was placed 15 cm higher than outlet to maintain siphoning flow after retraction by pressure.

CE eluate was deposited directly onto a customized MALDI plate (Thermo Scientific, San Jose, CA, USA) whose movement was mechanically controlled by a syringe pump at a speed of 3.7 mm/min. After the CE trace dried, CHCA matrix (10 mg/mL) was applied to the plate using a TM- sprayer to generate a homogenous trace on the plate. The parameters were carefully adjusted and set as follows: matrix flow rate: 200 mL/min; nozzle velocity: 1200 mm/min; temperature: 85 °C; gas pressure: 13 psi; line spacing: 3mm; number of layers: 2; dry time: 1 min. The matrix covered CE trace was then analyzed using a MALDI LTQ Orbitrap XL (Thermo Scientific, San Jose, CA, USA) with imaging experimental set up. In order to improve multiplexing and throughput the instrument method consisted of a full MS scan from *m/z* 100-900 followed by three tandem mass scans set up in parallel. By setting up raster and spiral movements of MALDI laser beam, orbitrap full scans were acquired every 100 μm with 11 μJ MALDI laser energy, followed by three parallel targeted tandem mass scans at 50 um with HCD

collision energy ranging from 35 to 55. The imaging data was then processed using ImageQuest software (Thermo Scientific).

2.4 MALDI-ion mobility mass spectrometry

Data was acquired on a MALDI-IM-MS enabled instrument (Synapt G2 Q-TOF, Waters, Milford, MA, USA) with a Nd: YAG laser at a repetition rate of 200 Hz. External calibration was performed using Glu-1-Fibrinopeptide B (Glu-Fib) standard of 1.0 μM before each experiment. The MD-CE fractions of crustacean hemolymph were deposited on a MALDI-Synapt target plate every 30s under the same CE experimental condition. Mass spectra were acquired in sensitivity mode and over a mass range of *m/z* 100 to 900. Laser energy attenuation was 300 (arbitrary units). Ion mobility separation was performed at a drift gas pressure of 2.30 Torr using nitrogen gas, a wave velocity of 650 m/s, and a wave height of 40.0 V.

2.5 LC-MS analysis

A LC-MS experiment was also performed in order to compare the performance of separation-assisted MALDI platform. In the LC-MS experiment, an automated combination of positive and negative ionization polarities was utilized to achieve comprehensive identification of small molecule metabolites. This extended feature of fast polarity switching on the mass analyzer enables unbiased detection of metabolites in complex biological samples [28]. For LC-MS experiments, microdialysate was collected for five hours, desalted by C_{18} Ziptip, and concentrated into 30 μL H_2O containing 0.1% FA. A Dionex UltiMate 3000 LC system was coupled with a Q Exactive Orbitrap mass spectrometer (Thermo Scientific). With 5μL injection of the desalted sample, metabolite separation was achieved with a Phenomenex biphenyl column (75.1 μm × 150 mm, 1.7 μm, 100 Å) heated to 30 ℃at a flow rate of 0.3 mL/min. Mobile phase A (MPA) was 0.1% FA in H_2O and mobile phase B (MPB) was 0.1% FA in MeOH. The 12 min

binary gradient was set as follows: 0-5 min, 0-2% MPB; 5-10 min, 2%-50% MPB; 10-12min, 90% MPB. Full MS scans were acquired from *m/z* 70 to 1000 for both positive and negative ESI modes. Orbitrap resolution was 70 K (m/z 400), automatic gain control (AGC) target was 1×10^6, and maximum injection time (IT) was 100 ms. Raw data files were processed by SIEVE™ software for peak alignment and framing to generate a list of detected mass features.

3 Results and discussion

3.1 *In vivo* MD sampling coupled offline to CE-MSI technique (MD-CE-MSI) for untargeted metabolomics study

Previously, our group has employed the MD sampling technique on crabs to study neuropeptide content in the circulating hemolymph [17, 31, 34]. However, the study of NT in the model crustacean system, which is an essential component of neuromodulators in the nervous system, has been lacking. One of the advantages of MD sampling is that it yields simpler samples due to the size-defined MWCO dialysis membrane which excludes large molecules such as proteinsand large neuropeptides. In the MD-CE-MSI experiments, dialysate was collected for two hours. The resulting dialysate was concentrated ten folds before CE-MSI analysis. Loading amount of the sample was 0.2~0.4 μL, indicating shorter time intervals can be achieved to meet the requirement of monitoring physiological changes. By coupling CE with MALDI-MS, an increased flexibility for the independent optimization of CE and MS experiments was realized. In addition, CE fractions are available for reanalysis and further biochemical characterization on the same spots or places if required. In MD-CE-MSI experiments, a syringe pump was used to drive crab saline through MD probes at a flow rate of 0.5 uL/min. In order to fully preserve the resolution from the CE separation, we have introduced trace level MSI incorporated with CE [32, 33]. CE eluent was continuously deposited onto a horizontally moving MALDI target plate. To create a uniform

and homogenous matrix layer on the acquired CE trace, CHCA (10 mg/mL) was applied to the CE trace using a TM sprayer. With higher tolerance to contaminations and impurities using MALDI, desalting steps prior to MALDI Orbitrap analysis were omitted thereby increasing the recovery rate of target analytes. Schematic illustration of MD-CE-MSI was shown in Figure 1.

3.2 Multiplex imaging set up of MD-CE-MSI

MD-CE-MSI data was acquired in the small molecule range *m/z* 100-900 Da on a MALDI Orbitrap analyzer and processed using ImageQuest software. In a MD-CE-MSI data, each analyte appears as a colored image extracted away from background ions. Fig. 2D shows the total ion count (TIC) of the imaging data for the CE separation from 2 min to 20 min. The signals in the TIC trace represent both analytes of interest and matrix background peaks. Unlike matrix ions, target analytes featured specific migration times, indicated by the colored region in the CE trace displayed in Fig. 2 (A, B and C). Fig. 2A displays the extracted region of interest (ROI) for 5-hydroxyindoleacetic acid (5-HIAA) migrated at 11 min, the main metabolite of serotonin through enzymatic conversion by monoamine oxidase-A [35]. Levels of 5-HIAA have been associated with aggressive behavior and autistic spectrum disorders [36]. Fig. 2B displays the CE migration time (14 min) for aminobenzoic acid, one of the most abundant molecules found in crustaean hemolymph. It is a substrate of enzyme anthranilate hydroxylase in benzoate degradation via hydroxylation pathway, also known as a component of tryptophan metabolism [37]. In Fig. 2C shows ROI of dopamine observed at 12.5 min in CE-MD trace, which plays a number of important roles in brain, body as well as elsewhere in biology [38]. The MALDI mass spectra of each representative metabolite and their corresponding structures are displayed in Fig. 2E, 2F, 2G, respectively.

The HMDB database searching was performed with 5 ppm error tolerance. From the suggested compounds, each one of the identities was manually examined so as to keep only endogenous metabolites in the results. Metabolites from plants or drugs, exogenous metabolites and food additives were filtered out. Furthermore, experiments of tandem mass fragmentation were carried out to determine the structure of the high abundant metabolites displayed in the CE-MSI trace. Fig. 3 displays how MS/MS confirmation data for dopamine was acquired during a MD-CE-MSI acquisition. In order to collect MS and MS/MS mass spectra for a given image, raster and spiral movements for the MALDI laser beam were used. This acquisition method is displayed graphically in Fig. 3C. Fig. 3A shows the MS/MS ROI for dopamine at CE migration time of 12.5 min. Fig. 3B displays the ROI data in a three-dimensional format which includes image width information and signal intensity. Fig. 3D and 3E show that the experimental precursor and fragment ions observed for dopamine matched well with those resulting from the dopamine standard. With the ability of collecting MS/MS data on MD-CE prepared samples, analytes were identified with higher confidence and revealed the potential of studying neurotransmitters in a more targeted way. However, ambiguity still existed when assigning the identities of some neurotransmitters, as many small molecules share the exact same *m/z* even with mass accuracy less than 3 ppm. For one *m/*z at a particular CE migration time, it was possible that multiple metabolic features were present. In order to address this problem, we employed a second dimension for separation, ion mobility, combined with MALDI MS (MALDI-IMS).

3.3 MALDI-IMS for separation of isobaric molecules

Ion mobility (IM) brings an additional dimension to MALDI-MS experiments by adding the capability of separating different compound families from one another. The ion mobility cell,

positioned between quadrupole and time-of-flight (TOF) analyzer in Synapt G2 instrument, allows the separation of isobaric compounds with similar *m/z* based on their collisional cross section, gas phase conformation and charge, which cannot be differentiated by single mass criterion [39-41]. Different ion conformations have different ion cross sections and result in different drift times. This particular property makes MS comparable to LC separation and allows for separation and identification of chemical families such as matrix, lipids, and small molecules by their drift time inside the ion mobility cell. Here MD-CE fractions of crustacean hemolymph were further separated by ion mobility mass spectrometry. As observed in the averaged mass spectrum of one fraction migrated at 11 min measured with MALDI-IMS in Fig. 4A, many compounds had the same *m/z*, but it is possible to discriminate between them according to their drift time. Fig. 4B showed the driftscope image corresponding to the 3D visualization of detected signals. The mass scale was the y-axis, the drift time was x-axis, and the color scale represents signal intensity constituting the third dimension of the driftscope image. Target analytes were filtered from background at a minimum intensity threshold of 1,000 counts visualized in this 3D mapping Fig. 4C. As shown in Fig. 4, isobaric ions were successfully separated by their different conformations in the mobility cell.

The zoomed image in driftscope Fig. 5 illustrated how the added drift time differentiated isobaric small molecules from diverse classes. Taking the metabolite of *m/z* 191.0468 as an example, four different small molecules showed on driftsope in the mass range of 1 Da, indicated by red dots in the white circle in the enlarged driftscope image visualization Fig. 5A and 5B. Three of them shared the same *m/z* of 191.0468, and were successfully separated by their mobility in gas phase. Although only one peak was observed in the mass spectrum, it actually contained three different compounds. Through HMDB MS search with maximum 10 ppm mass

error for MALDI-TOF analyzer, these ions were 2,3-diaminosalizylic acid found in blood, sodiated adduct of pyrroloylglycine which is the biomarker of hyperlipidemia, and 1-(2-Furanyl)-1-pentanone which appears to be an additive found in animal food. The other metabolite co-migrated in this MD-CE fraction was a protonated ion *m/z* 191.1280, which was matched as beta-damascenone belonging to lipid class. Therefore, food additive should be excluded from dicovery results, while the other three remained. This example illustrated how ion mobility differentiates a large number of isobaric molecules by their IM drift time and helps to refine the dicovery data. Approximately 20% more peaks have been detected with the addition of ion mobility separation and they were marked by solid dots in supplementary data Table 1.

3.4 LC-MS approach for comprehensive investigation and comparison to MALDI platform

Finally, the performance of multi-staged MALDI platform was further evaluated by comparing it to a LC-MS approach (Figure 6). We utilized the automated combination of positive and negative ionization mode mass spectra derived from fast polarity switching that has been widely used in lipidomics and drug metabolomics area [42, 43]. This extension enables detection of metabolites in complex biological samples and provided complementary identification of untargeted metabolomics [44, 45]. Owing to fast polarity switching approach, two total ion chromatograms as well as averaged mass spectrum clearly revealed its benefit of complementary recognition gained from the integration of two ionization modes as shown in Fig. 7 (A, B and C). Resultant data was aligned by SIEVE^{TM} for peak detection and processed through HMDB, yielding 137 metabolites identified in total. Among them, 83 were detected exclusively by the LC-ESI approach. For MALDI-MS platform integrated with CE imaging and ion mobility, 71 were uniquely found as summerized in Fig. 7D. A list of the identified signaling molecules and metabolites was provided in supporting information Table 1. In CE analysis, molecules migrated

through capillary based on their mass and charge. Metabolites that are predominantly polar and highly charged were better detected in CE. In LC analysis, the amount of sample loaded onto the LC column was substantially higher than in CE, thus lower abundant molecules were better identified in LC technique. These findings demonstrated the significantly increased metabolic coverage by the combination of CE/IM-MALDI-MSI and LC-MS platform.

4 Concluding remarks

In summary, we applied micro-separation approaches, CE and ion mobility, coupled with multiplexed MALDI imaging platform for NT and metabolites identification. LC-MS was also used for evaluation and comprehensive investigation, yielding 208 small molecule metabolites identified in total. In addition, these molecules were classified to 11 biochemical families detailed in Table 1. Among them, the ones belonging to nucleosides, amino acids, peptides and analogues, amines and their metabolites are considered highly significant for further studies. More importantly, the improved temporal resolution with CE-MSI platform, 5 min dialysate loaded into the CE column, comparing to 1h dialysate loaded into the LC-MS system, enables more accurate monitoring of NT release and dynamic changes, providing a more powerful tool for functional studies.

Acknowledgements

We thank Dr. Robert Sturm for critical reading an early draft of this manuscript. This work is supported by the National Institutes of Health grants (1R01DK071801 and S10RR029531). SJ gratefully thanks a former Li Research Group member Dr. Zichuan Zhang for scientific discussions and making helpful suggestions. LL acknowledges an H. I. Romnes Faculty Research Fellowship and a Vilas Distinguished Achievement Professorship with funding provided by the Wisconsin Alumni Research Foundation and University of Wisconsin-Madison School of Pharmacy.

References

[1] Kennedy, R. T., *Curr. Opin. Chem. Biol.* 2013, *17*, 860-867.

[2] Sebolt-Leopold, J. S., English, J. M., *Nature* 2006, *441*, 457-462.

[3] Maceyka, M., Spiegel, S., *Nature* 2014, *510*, 58-67.

[4] Sundström, I., Arts, J., Westerlund, D., Andrén, P. E., *The Analyst* 2010, *135*, 405-413.

[5] Lee, G. J., Park, J. H., Park, H. K., *Neurol. Res.* 2008, *30*, 661-668.

[6] Watson, C. J., Venton, B. J., Kennedy, R. T., *Anal. Chem.* 2006, *78*, 1391-1399.

[7] OuYang, C., Liang, Z., Li, L., *Biochimica et Biophysica Acta (BBA) - Proteins and Proteomics* 2015, *1854*, 798-811.

[8] Nandi, P., Lunte, S. M., *Anal. Chim. Acta* 2009, *651*, 1-14.

[9] Cebada, J., Alvarado-Álvarez, R., Becerra, E., Neri-Bazán, L., Rocha, L., García, U., *J. Neurosci. Methods* 2006, *153*, 1-7.

[10] Timofeev, I., Carpenter, K. L. H., Nortje, J., Al-Rawi, P. G., O'Connell, M. T., Czosnyka, M., Smielewski, P., Pickard, J. D., Menon, D. K., Kirkpatrick, P. J., Gupta, A. K., Hutchinson, P. J., *Brain* 2011, *134*, 484-494.

[11] Bossers, S. M., de Boer, R. D. H., Boer, C., Peerdeman, S. M., *Acta Neurochir. (Wien).* 2012, *155*, 345-353.

[12] Darvesh, A. S., Carroll, R. T., Geldenhuys, W. J., Gudelsky, G. A., Klein, J., Meshul, C. K., Van der Schyf, C. J., *Expert Opinion on Drug Discovery* 2011, *6*, 109-127.

[13] Li, Q., Zubieta, J.-K., Kennedy, R. T., *Anal. Chem.* 2009, *81*, 2242-2250.

[14] Duo, J., Stenken, J. A., *Anal. Bioanal. Chem.* 2010, *399*, 773-782.

[15] Duo, J., Stenken, J. A., *Anal. Bioanal. Chem.* 2010, *399*, 783-793.

[16] Pettersson, A., Amirkhani, A., Arvidsson, B., Markides, K., Bergquist, J., *Anal. Chem.* 2004, *76*, 1678-1682.

[17] Schmerberg, C. M., Li, L., *Anal. Chem.* 2013, *85*, 915-922.

[18] Zhang, H., Ou, J., Wei, Y., Wang, H., Liu, Z., Chen, L., Zou, H., *Anal. Chim. Acta* 2015, *883*, 90-98.

[19] Lada, M. W., Vickroy, T. W., Kennedy, R. T., *Anal. Chem.* 1997, *69*, 4560-4565.

[20] Hogan, B. L., Lunte, S. M., Stobaugh, J. F., Lunte, C. E., *Anal. Chem.* 1994, *66*, 596-602.

[21] Zhou, Y., Mabrouk, O. S., Kennedy, R. T., *J. Am. Soc. Mass Spectrom.* 2013, *24*, 1700-1709.

[22] Wang, M., Hershey, N. D., Mabrouk, O. S., Kennedy, R. T., *Anal. Bioanal. Chem.* 2011, *400*, 2013-2023.

[23] Hao, L., Zhong, X., Greer, T., Ye, H., Li, L., *Analyst* 2015, *140*, 467-475.

[24] Isbell, T. A., Strickland, E. C., Hitchcock, J., McIntire, G., Colyer, C. L., *J. Chromatogr. B* 2015, *980*, 65-71.

[25] Guihen, E., O'Connor, W. T., *Electrophoresis* 2010, *31*, 55-64.

[26] Schiavone, N. M., Sarver, S. A., Sun, L., Wojcik, R., Dovichi, N. J., *J. Chromatogr. B* 2015, *991*, 53-58.

[27] Yang, C., Liu, H., Yang, Q., Zhang, L., Zhang, W., Zhang, Y., *Anal. Chem.* 2003, *75*, 215-218.

[28] Kluger, B., Bueschl, C., Neumann, N., Stückler, R., Doppler, M., Chassy, A. W., Waterhouse, A. L., Rechthaler, J., Kampleitner, N., Thallinger, G. G., Adam, G., Krska, R., Schuhmacher, R., *Anal. Chem.* 2014, *86*, 11533-11537.

[29] Yamada, M., Kita, Y., Kohira, T., Yoshida, K., Hamano, F., Tokuoka, S. M., Shimizu, T., *J. Chromatogr. B* 2015, *995-996*, 74-84.

[30] Oh, H.-A., Kim, D., Lee, S. H., Jung, B. H., *J. Pharm. Biomed. Anal.* 2015, *107*, 32-39.

[31] Liang, Z., Schmerberg, C. M., Li, L., *The Analyst* 2015, *140*, 3803-3813.

[32] Wang, J., Ye, H., Zhang, Z., Xiang, F., Girdaukas, G., Li, L., *Anal. Chem.* 2011, *83*, 3462-3469.

[33] Zhang, Z., Ye, H., Wang, J., Hui, L., Li, L., *Anal. Chem.* 2012, *84*, 7684-7691.

[34] Behrens, H. L., Chen, R., Li, L., *Anal. Chem.* 2008, *80*, 6949-6958.

[35] Carpenter, L. L., Anderson, G. M., Siniscalchi, J. M., Chappell, P. B., Price, L. H., *Neuropsychopharmacology* 2003, *28*, 339-347.

[36] Burgess, N. K., Sweeten, T. L., McMahon, W. M., Fujinami, R. S., *J. Autism Dev. Disord.* 2006, *36*, 697-704.

[37] Arvadia, P., Narwaley, M., Whittal, R. M., Siraki, A. G., *Arch. Biochem. Biophys.* 2011, *515*, 120-126.

[38] Rice, M. E., Patel, J. C., Cragg, S. J., *Neuroscience* 2011, *198*, 112-137.

[39] Stauber, J., MacAleese, L., Franck, J., Claude, E., Snel, M., Kaletas, B. K., Wiel, I. M. V. D., Wisztorski, M., Fournier, I., Heeren, R. M. A., *J. Am. Soc. Mass Spectrom.* 2010, *21*, 338-347.

[40] Xu, L., Kliman, M., Forsythe, J. G., Korade, Z., Hmelo, A. B., Porter, N. A., McLean, J. A., *J. Am. Soc. Mass Spectrom.* 2015, *26*, 924-933.

[41] Cole, L. M., Mahmoud, K., Haywood-Small, S., Tozer, G. M., Smith, D. P., Clench, M. R., *Rapid Commun. Mass Spectrom.* 2013, *27*, 2355-2362.

[42] Gallart-Ayala, H., Courant, F., Severe, S., Antignac, J. P., Morio, F., Abadie, J., Le Bizec, B., *Anal. Chim. Acta* 2013, *796*, 75-83.

[43] Shin, M., Ji, D., Kang, S., Yang, W., Choi, H., Lee, S., *Arch. Pharmacal Res.* 2013, *37*, 760-772.

[44] Guo, B., Wang, M., Liu, Y., Zhou, J., Dai, H., Huang, Z., Shen, L., Zhang, Q., Chen, B., *J. Agric. Food Chem.* 2015, *63*, 6954-6967.

[45] Braña-Magdalena, A., Leão-Martins, J. M., Glauner, T., Gago-Martínez, A., *J. AOAC Int.* 2014, *97*, 285-292.

Table 1. Complementary identification of signaling molecules and metabolites by MALDI-MSI and ESI-MS [#].

CompMW	Composition	Δppm	HMDB	MALDI	ESI	Class
92.0478	$C_3H_9O_3$	4.95	Glycerol		x	1
99.1052	$C_6H_{14}N$	4.29	Methylpiperidine		x	2
101.1208	$C_6H_{16}N$	3.71	Hexylamine		x	3
103.0633	$C_4H_9NO_2$	0.05	Dimethylglycine**		x	6
103.0633	$C_4H_9NO_2$	0.05	N-Ethylglycine		x	6
103.0637	$C_4H_{10}O_2N$	3.83	Aminoisobutyric acid*		x	5
104.059	$C_3H_9O_2N_2$	4.29	2,3-Diaminopropionic acid		x	5
105.0793	$C_4H_{12}O_2N$	3.28	Diethanolamine	x	x	3
115.0636	$C_5H_{10}O_2N$	2.56	Proline*	x	x	6
116.084	$C_6H_{13}O_2$	2.53	Methylpropyl acetate	x		5
117.0792	$C_5H_{12}O_2N$	2.09	Valine*	x	x	6
117.0792	$C_5H_{12}O_2N$	2.09	Norvaline	x		6
119.0583	$C_4H_{10}O_3N$	0.68	Threonine	x		6
122.0482	$C_6H_7ON_2$	1.73	Niacinamide	x		7
127.0634	$C_6H_{10}O_2N$	0.75	1-Piperideine-2-carboxylic acid	x	x	7
127.0998	$C_7H_{14}ON$	0.87	1-(1-Pyrrolidinyl)-2-propanone		x	10
131.0947	$C_6H_{14}O_2N$	0.72	Leucine	x		6
132.0419	$C_6H_3N_4$	2.54	Dodecanedioic acid		x	5
134.0943	$C_6H_{15}O_3$	0.22	Polypropylene glycol		x	4
136.0385	$C_5H_5ON_4$	0.1	Threonic acid	x		5
137.0477	$C_7H_8O_2N$	0.34	Aminobenzoic acid*	x	x	5
137.0841	$C_8H_{12}ON$	0.44	Hydroxyphenethylamine		x	3
137.0841	$C_8H_{12}ON$	0.44	Tyramine●	x		3
139.0996	$C_8H_{14}ON$	0.65	4,5-Dimethyl-2-propyloxazole		x	10
141.1153	$C_8H_{16}ON$	0.28	Conhydrinone	x		4
143.0735	$C_{10}H_{10}N$	0.17	Quinaldine		x	8

143.0945	$C_7H_{14}O_2N$	0.73	Proline betaine	x		5
144.1262	$C_7H_{17}ON_2$	0.27	Acetylcadaverine		x	4
145.0738	$C_6H_{12}O_3N$	0.48	Isobutyrylglycine	x		6
146.0576	$C_7H_5N_4$	1.95	Trimethoprim		x	4
147.0684	$C_9H_{10}ON$	0.07	3-(2-Furanylmethyl)-1H-pyrrole		x	10
148.0524	$C_9H_9O_2$	0.04	Cinnamic acid	x		5
152.0949	$C_8H_{13}ON_2$	0.26	Isopropyl-methoxypyrazine	x		4
153.0173	$C_5H_9NO_2$	0.41	Acetamidopropanal	x		4
153.0789	$C_8H_{11}NO_2$	0.36	Dopamine*	x		3
157.1102	$C_8H_{16}O_2N$	0.35	Homostachydrine		x	5
158.0577	$C_8H_5N_4$	1.17	Pantothenic acid		x	5
159.1259	$C_8H_{18}O_2N$	0.03	Aminooctanoic acid	x	x	5
160.0887	$C_{11}H_{13}O$	0.57	3-Phenyl-4-pentenal	x		10
161.1051	$C_7H_{16}O_3N$	0.43	Carnitine*		x	9
162.1255	$C_8H_{19}O_3$	0.43	Octanetriol		x	2
165.0789	$C_9H_{12}O_2N$	0.33	Phenylalanine*	x	x	6
170.1305	$C_{10}H_{19}O_2$	0.92	Citronellic acid		x	5
173.0686	$C_8H_6N_5$	1.06	Methylglutaric acid		x	5
176.0472	$C_{10}H_9O_3$	0.68	Methylumbelliferone	x	x	4
177.9974	$C_2H_3O_6N_4$	4.06	Arsenobetaine	x		5
179.1673	$C_{12}H_{22}N$	0.42	Memantine		x	3
187.0844	$C_9H_8N_5$	0.18	Phthalic acid		x	5
187.1196	$C_9H_{16}O_3N$	1.17	Hydroxydecanoic acid		x	5
187.1207	$C_9H_{18}O_3N$	0.64	Polyethylene glycol		x	9
187.1207	$C_9H_{18}O_3N$	0.64	N-Heptanoylglycine**		x	6
188.1035	$C_9H_{15}O_4$	1.78	Histidinyl-Arginine	x	x	6
188.1399	$C_{10}H_{19}O_3$	1.71	N-Acetyldopamine	x		4
188.1524	$C_9H_{21}O_2N_2$	0.29	N6,N6,N6-Trimethyl-L-lysine*●	x	x	5
190.0395	$C_7H_8N_2O_3$	0.46	2,3-Diaminosalicylic acid*	x		5
190.0395	$C_7H_8N_2O_3$	0.46	Pyrroloylglycine●	x		6

190.1355	$C_{13}H_{19}O$	1.27	beta-Damascenone●	x	x	10
191.0436	$C_6H_{10}O_6N$	3.33	gamma-Carboxyglutamic acid	x	x	5
191.0582	$C_{10}H_9NO_3$	0.1	5HIAA	x		4
194.093	$C_{11}H_{13}O_3$	0.71	Oxododecanoic acid	x		5
195.0882	$C_{10}H_{12}O_3N$	0.46	13E-tetranor-16-carboxy-LTE4		x	4
197.0674	$C_5H_8O_2N_7$	3.67	Dopa/N-Hydroxy-L-tyrosine		x	6
198.1618	$C_{12}H_{23}O_2$	0.79	Dodec-2-enoic acid		x	5
202.0452	$C_4H_7O_4N_6$	0.52	Glucose●	x		1
203.1145	$C_9H_{16}O_4N$	1.15	Octenedioic acid●	x		5
203.1156	$C_9H_{18}O_4N$	0.66	Acetylcarnitine*●	x	x	9
204.051	$C_6H_5ON_8$	2.71	Cyromazine	x		10
204.0899	$C_{11}H_{13}O_2N_2$	0.23	Tryptophan*	x	x	6
204.1148	$C_{13}H_{17}O_2$	1.01	Hydroxyethyl-2,2-dimethyl-2H-1-benzopyran		x	10
207.0387	$C_7H_6O_3N_5$	2.49	Amino-4-hydroxy-6-pteridinecarboxylic acid	x		5
207.0884	$C_{11}H_{12}O_3N$	0.57	Inosine		x	11
207.0894	$C_{11}H_{14}O_3N$	0.57	Phenylpropionylglycine**●	x	x	4
210.1618	$C_{13}H_{23}O_2$	0.74	Citral propylene glycol acetal		x	4
211.0834	$C_{10}H_{12}O_4N$	4.9	Octenedioic acid	x		5
212.0947	$C_{13}H_{13}ON_2$	1.13	Harmine		x	10
212.1142	$C_6H_{13}ON_8$	4.09	prolyl-proline		x	6
213.0256	$C_4H_4O_4N_7$	3.26	Carboxyglutamic acid	x	x	5
213.0999	$C_{10}H_{16}O_4N$	2.14	Phenazopyridine	x	x	10
214.1558	$C_{12}H_{21}O_3$	5	Olmesartan		x	10
215.1511	$C_{11}H_{20}O_3N$	4.74	3,4-Methylenesebacic acid	x		5
215.152	$C_{11}H_{22}O_3N$	0.56	Nonanoylglycine	x		6
216.135	$C_{11}H_{19}O_4$	0.62	Ribose-1-arsenate		x	4
217.1313	$C_{10}H_{20}O_4N$	0.39	Propionylcarnitine*	x	x	9
218.1881	$C_{12}H_{27}O_3$	0.33	8,8-Dimethoxy-2,6-dimethyl-2-octanol	x		4
219.1096	$C_9H_{16}O_5N$	4.79	Succinylacetone●	x		3
220.1098	$C_{13}H_{17}O_3$	0.55	Ethyl 2-benzylacetoacetate		x	10

222.089	$C_{12}H_{15}O_4$	0.83	Monoisobutyl phthalic acid		x	5
224.1886	$C_{13}H_{25}ON_2$	1.07	Cuscohygrine	x	x	10
225.0764	$C_9H_{12}O_4N_3$	0.65	Polyethylene glycol	x	x	9
225.944	H_3O_{14}	2.24	2,5-Dichloro-4-oxohex-2-enedioate	x	x	10
226.014	$C_{15}HON_2$	1.93	Phenyl vinyl sulfide		x	10
226.1064	$C_9H_{15}O_3N_4$	0.73	Histidinyl-Alanine	x	x	6
226.1195	$C_{12}H_{17}O_4$	4.36	Kynurenic acid	x	x	5
226.1203	$C_{12}H_{19}O_4$	0.82	3,4-Methylenesebacic acid	x		5
226.168	$C_{12}H_{23}O_2N_2$	3.18	Gamma-Cadinene		x	10
226.193	$C_{14}H_{27}O_2$	1.13	Tsuzuic acid	x		5
229.0206	$C_4H_4O_5N_7$	2.43	2-Amino-4-hydroxy-6-pteridinecarboxylic acid	x	x	5
229.1668	$C_{12}H_{22}O_3N$	4.23	Tyrosyl-Lysine	x	x	6
230.1508	$C_{12}H_{21}O_4$	4.28	N-Decanoylglycine		x	6
231.1469	$C_{11}H_{22}O_4N$	0.58	Isobutyryl-carnitine		x	9
233.1261	$C_{10}H_{20}O_5N$	0.85	Hydroxypropionylcarnitine	x		9
234.085	$C_8H_{15}O_6N_2$	0.69	Threoninyl-Aspartate	x		6
237.1338	$C_9H_{16}ON_7$	1.1	N-Nonanoylglycine**		x	6
238.1178	$C_9H_{15}O_2N_6$	1.16	Undecanedioic acid		x	5
238.1203	$C_{13}H_{19}O_4$	0.78	Hexenoylcholine		x	9
238.156	$C_{14}H_{21}O_3$	3.66	Estriol-3 or 16 or 17-glucuronide		x	4
238.1567	$C_{14}H_{23}O_3$	0.72	Hydroxydodecanoic acid	x		5
240.1353	$C_{13}H_{19}O_4$	1.09	Imiquimod		x	4
242.0801	$C_{11}H_{15}O_6$	4.49	Elenaic acid	x	x	5
242.1509	$C_{13}H_{21}O_4$	3.65	3,3'-Dithiobis[2-methylfuran]	x	x	10
243.0853	$C_9H_{14}O_5N_3$	0.81	Cytidine	x		11
243.1826	$C_{13}H_{24}O_3N$	3.37	Halobetasol propionate	x		9
243.1833	$C_{13}H_{26}O_3N$	0.49	N-Undecanoylglycine	x		6
245.1626	$C_{12}H_{24}O_4N$	0.34	Valerylcarnitine	x		9
250.1317	$C_{13}H_{19}O_3N_2$	0.07	Isoleucyl-Proline	x	x	6
251.1495	$C_{10}H_{18}ON_7$	0.84	N-Decanoylglycine		x	6

252.1948	$C_{13}H_{25}ON_4$	3.48	Capryloylcholine	x	x	9
253.0948	$C_8H_{12}O_3N_7$	0.79	N-Acetylvanilalanine	x		3
254.0553	$C_{11}H_7O_2N_6$	0.7	Glutamyl-taurine		x	6
254.1514	$C_{10}H_{19}O_2N_6$	3.19	Heptanoylcholine		x	9
254.1879	$C_{11}H_{23}ON_6$	2.54	Kessyl glycol		x	9
256.0497	$C_2H_9O_7N_8$	1.38	Hydroxyprolyl-Cysteine	x	x	6
257.1989	$C_{10}H_{24}ON_7$	0.66	N-Lauroylglycine		x	6
258.0808	$C_5H_{15}O_8N_4$	4.51	Cysteinyl-Histidine	x	x	9
259.1782	$C_9H_{22}O_2N_7$	0.52	Hexanoylcarnitine	x		9
260.1022	$C_{10}H_{17}O_6N_2$	0.87	alpha-glutamyl-hydroxyproline		x	6
265.1312	$C_{10}H_{16}O_2N_7$	4.62	Tiglylcarnitine	x	x	9
265.1651	$C_{11}H_{20}ON_7$	0.99	N-Undecanoylglycine		x	6
266.1644	$C_{14}H_{23}O_3N_2$	0.88	Myristic acid	x		5
267.0965	$C_{10}H_{14}O_4N_5$	4.14	Glutamyl-Valine●	x	x	6
267.1445	$C_9H_{22}O_6N_3$	0.47	Pivaloylcarnitine		x	9
268.0801	$C_{10}H_{11}O_5N_4$	2.41	Carbinoxamine	x		4
268.0805	$C_{10}H_{13}O_5N_4$	0.92	Inosine	x	x	11
271.2144	$C_{11}H_{26}ON_7$	1.18	Tridecanoylglycine	x		6
272.0246	$C_4H_9O_{10}N_4$	4.83	Cysteinyl-Hydroxyproline	x		4
273.9657	$C_2HO_{12}N_4$	4.62	Sebacic acid or 2-Ethylsuberic acid		x	5
274.0951	$C_{10}H_{11}O_2N_8$	0.85	Serinyl-Phenylalanine	x	x	6
274.1391	$C_9H_{19}O_4N_6$	4.28	Glutamyl-Lysine	x		6
276.1294	$C_7H_{17}O_4N_8$	6.2	Saccharopine●	x		6
278.1264	$C_{10}H_{15}O_2N_8$	0.84	Prolyl-Tyrosine	x		6
278.1992	$C_{12}H_{23}N_8$	3.5	Palmitaldehyde	x		4
279.1808	$C_{11}H_{26}O_5N_3$	0.76	N-Lauroylglycine		x	6
280.0208	$C_9HO_2N_{10}$	2.97	5-phosphonooxy-L-lysine		x	6
282.1828	$C_{12}H_{23}O_2N_6$	1.01	N1-Acetylspermine	x		3
283.0914	$C_9H_{18}O_9N$	0.87	Guanosine		x	11
285.1937	$C_{11}H_{24}O_2N_7$	1	Octenoylcarnitine	x		9

288.1546	$C_{10}H_{21}O_4N_6$	0.07	Arginyl-Asparagine	x		6
290.0623	$C_8H_7O_3N_{10}$	1.34	Arabinosylhypoxanthine	x		11
290.1182	$C_6H_{13}O_4N_{10}$	1.06	LPA		x	9
291.1829	$C_{17}H_{26}O_3N$	1.79	Norcapsaicin	x	x	10
292.0904	$C_{10}H_{17}O_8N_2$	1.68	Edetic Acid	x	x	5
294.1441	$C_{11}H_{23}O_7N_2$	5.44	Tocopheronic acid●	x	x	5
294.1827	$C_{13}H_{23}O_2N_6$	1.31	Decenoylcholine	x		9
298.1162	$C_9H_{15}O_4N_8$	3.62	Methylguanosine	x	x	11
299.173	$C_{11}H_{22}O_3N_7$	3.66	Diphthine		x	6
301.225	$C_{12}H_{28}O_2N_7$	0.94	2,6-Dimethylheptanoyl carnitine		x	9
304.0919	$C_{11}H_{17}O_8N_2$	4.14	N-Acetylaspartylglutamic acid	x	x	5
306.1805	$C_{13}H_{27}O_6N_2$	5.18	Carboxy-gamma-chromanol●	x	x	10
306.1939	$C_{13}H_{23}ON_8$	3.88	Retinal	x	x	9
309.1683	$C_{15}H_{22}O_4N_3$	1.72	Diethyl glutarate	x		9
310.139	$C_{11}H_{23}O_8N_2$	4.77	Arginyl-Asparagine	x		6
310.1777	$C_{13}H_{23}O_3N_6$	0.97	Valdiate		x	9
311.1701	$C_{12}H_{20}O_3N_7$	1.49	N-Undecanoylglycine		x	6
312.1061	$C_8H_{13}O_4N_{10}$	4.96	N2-(3-Hydroxysuccinoyl)arginine	x		6
313.225	$C_{13}H_{28}O_2N_7$	0.91	Decenoylcarnitine		x	9
314.1154	$C_{18}H_{18}O_5$	0	Hydroxyenterolactone	x		10
315.2406	$C_{17}H_{34}O_4N$	1.06	Decanoylcarnitine		x	9
316.0485	$C_2H_9O_9N_{10}$	2.03	(o-carboxybenzamido) Glutaramic acid	x		5
318.1474	$C_7H_{23}O_8N_6$	2.2	Hydroxyenterodiol	x		10
320.098	$C_{11}H_{13}O_4N_8$	2.93	7-Methylguanosine		x	11
321.1547	$C_{12}H_{24}O_7N_3$	2.65	Diphthine	x		6
321.1785	$C_{10}H_{24}O_5N_7$	4.88	Phenylalanyl-Arginine	x	x	6
326.1338	$C_{11}H_{23}O_9N_2$	2.49	Sakacin A		x	6
326.1939	$C_{14}H_{31}O_8$	0.44	Dodecylbenzenesulfonic Acid	x		5
327.1501	$C_8H_{22}O_7N_7$	6.32	6-Acetylmorphine●	x	x	4
332.1807	$C_{12}H_{25}O_5N_6$	5.36	Betulalbuside A●	x	x	9

334.0881	$C_8H_{19}O_{12}N_2$	1.89	Rofecoxib-threo-3,4-dihydrohydroxy acid	x		5
334.2144	$C_{20}H_{30}O_4$	0.04	Dehydropinifolic acid		x	5
336.0543	$C_8H_{15}O_{14}$	3.73	Thyrotropin releasing hormone	x		6
336.2271	$C_{15}H_{33}O_6N_2$	1.57	Leukotriene B4	x	x	9
340.1419	$C_{19}H_{21}O_4N_2$	3.39	19-Oxotestosterone	x		9
340.2064	$C_{11}H_{27}O_6N_6$	4.64	3-O-Methylrosmarinic acid		x	5
341.1658	$C_9H_{24}O_7N_7$	3.97	Peroxysimulenoline●	x	x	10
341.2563	$C_{19}H_{36}O_4N$	0.84	Dodecenoylcarnitine		x	9
345.0018	$H_8O_{15}N_7$	4.54	Clopidogrel carboxylic acid derivative		x	4
358.2328	$C_{15}H_{31}O_4N_6$	0.08	Kinetensin 1-3		x	6
362.1698	$C_{16}H_{21}O_4N_6$	1.18	Ethyl 4-ethoxybenzoate	x		4
365.2692	$C_{20}H_{36}O_3N_3$	1.06	Stearoylethanolamide	x		3
374.1003	$C_8H_{17}O_{11}N_6$	0.42	Acetolactate●	x	x	9
376.1889	$C_{10}H_{29}O_9N_6$	0.89	18-Oxocortisol	x	x	9
381.0798	$C_{11}H_{12}O_7N_9$	4.25	N-(1-Deoxy-1-fructosyl)tyrosine●	x	x	6
381.2512	$C_{21}H_{36}O_5N$	2.91	2-Hydroxylauroylcarnitine●	x	x	9
390.2225	$C_{15}H_{31}O_6N_6$	1.9	Lubiprostone		x	9
398.1703	$C_{18}H_{27}O_8N_2$	0.52	21-hydroxysteroid	x	x	9
400.1518	$C_{11}H_{25}O_{10}N_6$	0.95	Hydroxyleptocarpin	x	x	9
400.2568	$C_{16}H_{33}O_4N_8$	2.82	Arachidonylglycerol	x	x	9
406.1878	$C_8H_{28}O_9N_{10}$	2.02	Indolebutyric acid	x		5
413.1477	$C_6H_{22}O_{12}N_9$	0.66	Undecanedioic acid	x		5
414.2038	$C_{21}H_{23}N_{10}$	1	Eplerenone		x	9
416.1977	$C_{11}H_{29}O_9N_8$	2.93	Bixin		x	9
418.1624	$C_{11}H_{27}O_{11}N_6$	4.94	(R)-Byakangelicinn 2'-(3-methylbutanoate)		x	9
434.2433	$C_{21}H_{39}O_7P$	0.04	LPA(18:2(9Z, 12Z)/0:0)		x	9
434.2441	$C_{12}H_{33}O_9N_8$	1.81	Phenylpropionylglycine	x		6
445.2166	$C_{13}H_{32}O_{10}N_7$	6.53	LysoPE(0:0/14:1(9Z))●	x		9
446.2078	$C_{24}H_{25}O_3N_6$	2.03	PA(20:4(5Z,8Z,11Z,14Z)e/2:0)		x	9
446.2082	$C_{24}H_{27}O_3N_6$	2.93	Heliocide B2		x	9

464.2038	$C_{13}H_{31}O_{12}N_6$	1.74	N-Heptanoylglycine●	x	x	6
475.2992	$C_{21}H_{42}O_7N_5$	2.89	Netilmicin		x	10

[#] Metabolites were checked by x if found by MALDI or ESI platform.

* Matched with in-house constructed metabolite library consisting of m/z, RT and MS/MS information.

** Confirmed with MS/MS information.

● Metabolites additionally detected by CE-MALDI-IMS.

Classification: 1) Carbohydrates. 2) Not classified. 3) Amines and their metabolites. 4) Intermediates and derivatives. 5) Organic acids. 6) Amino acids, peptides and analogues. 7) Pyridines. 8) Quinolines. 9) Lipids. 10) Endogenous compounds/metabolites found in animals. 11) Nucleosides.

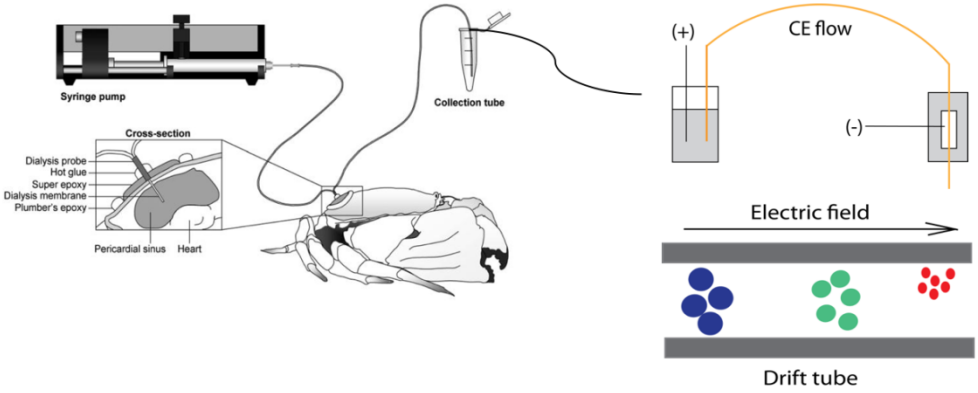

Figure 1. Multi-faceted MALDI imaging platform coupled to in vivo microdialysis.

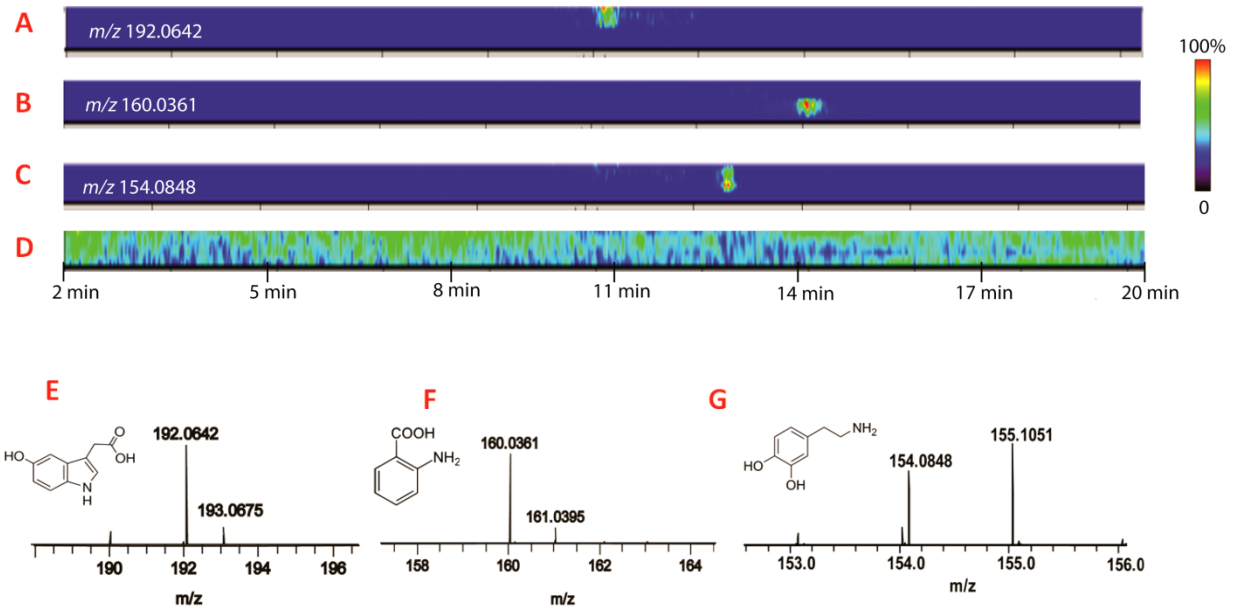

Figure 2. MALDI Orbitrap imaging of small molecule metabolites separated by CE.

(A, B, C) 2D images of 5-HIAA, aminobenzoic acid and dopamine, respectively. (D) Image of total ion count (TIC) of the acquired MD-CE trace. (E, F, G) Mass spectra and structures of 5-HIAA, aminobenzoic acid dopamine, respectively.

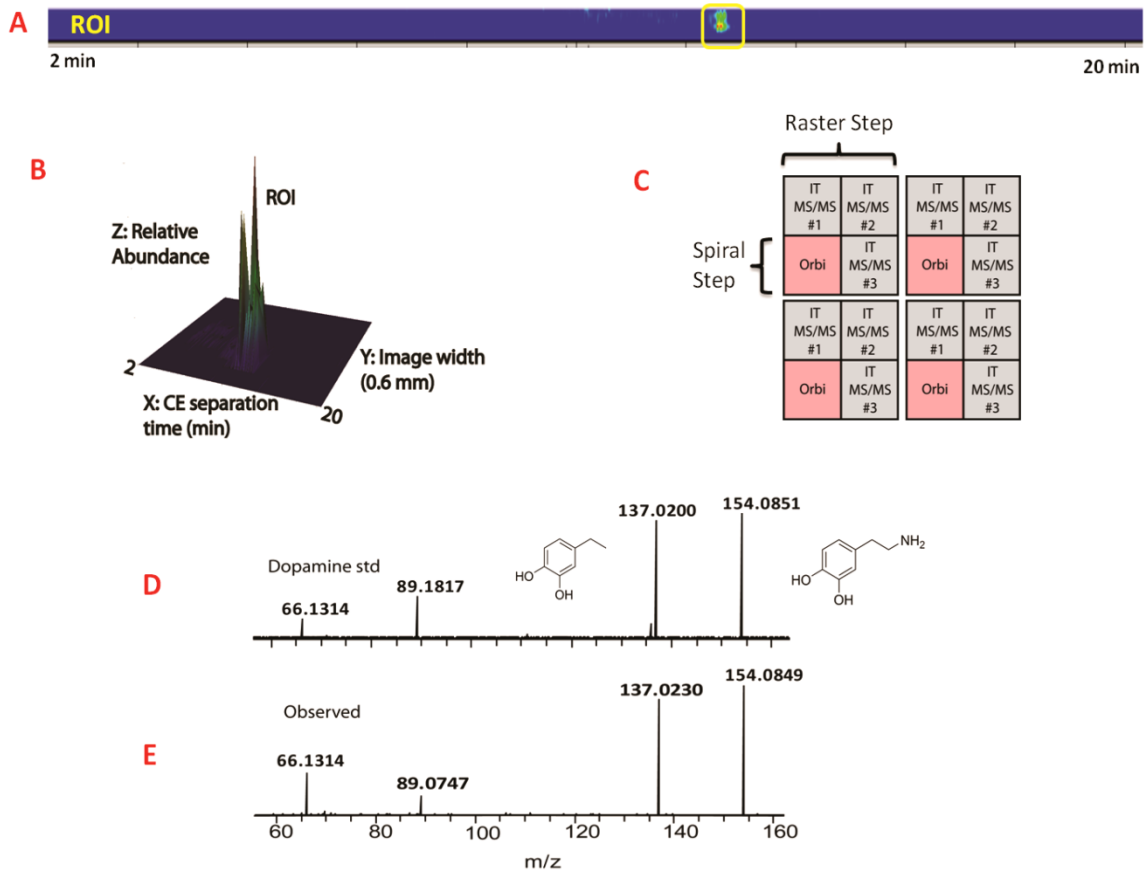

Figure 3. Illustration of multiplexed MD-CE-MSI on MALDI Orbitrap instrument.

(A) 2D imaging of dopamine identified in MD-CE-MSI. (B) 3D imaging of dopamine identified in MD-CE-MSI. The x axis in the 3D image represents CE separation time from 2 to 20 min. Y axis is the width of the CE image that is 0.6 mm. Z axis showed relative abundance of the extracted ion from TIC. (C) Illustration of laser movement in the multiplexed method. Orbitrap full scan was acquired every 100 µm shown in pink color, followed by three tandem mass fragmentation at 50 µm. (D) MS/MS fragmentation of dopamine standard acquired under the same instrumental condition acquired on MALDI Orbitrap. (E) MS/MS spectrum of observed dopamine in MD-CE-MSI.

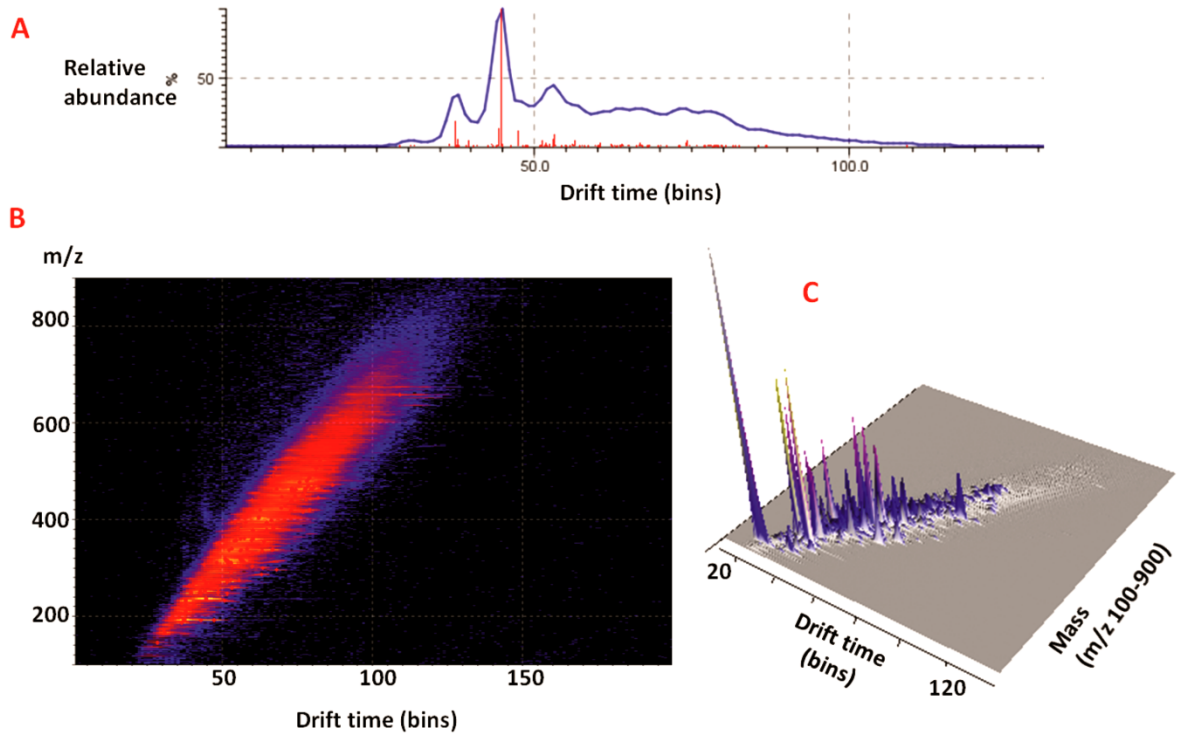

Figure 4. Ion mobility separation of MD-CE fractions.

(A) Total ion chromatogram of MD-CE fraction migrated at 11 min which is further separated by ion mobility mass spectrometry. (B) Image from driftscope showed drift times of small molecules from *m/z* 100 to 900. (C) As shown in 3D driftscope image, isobaric molecules in one MD-CE fraction were successfully separated by their drift times.

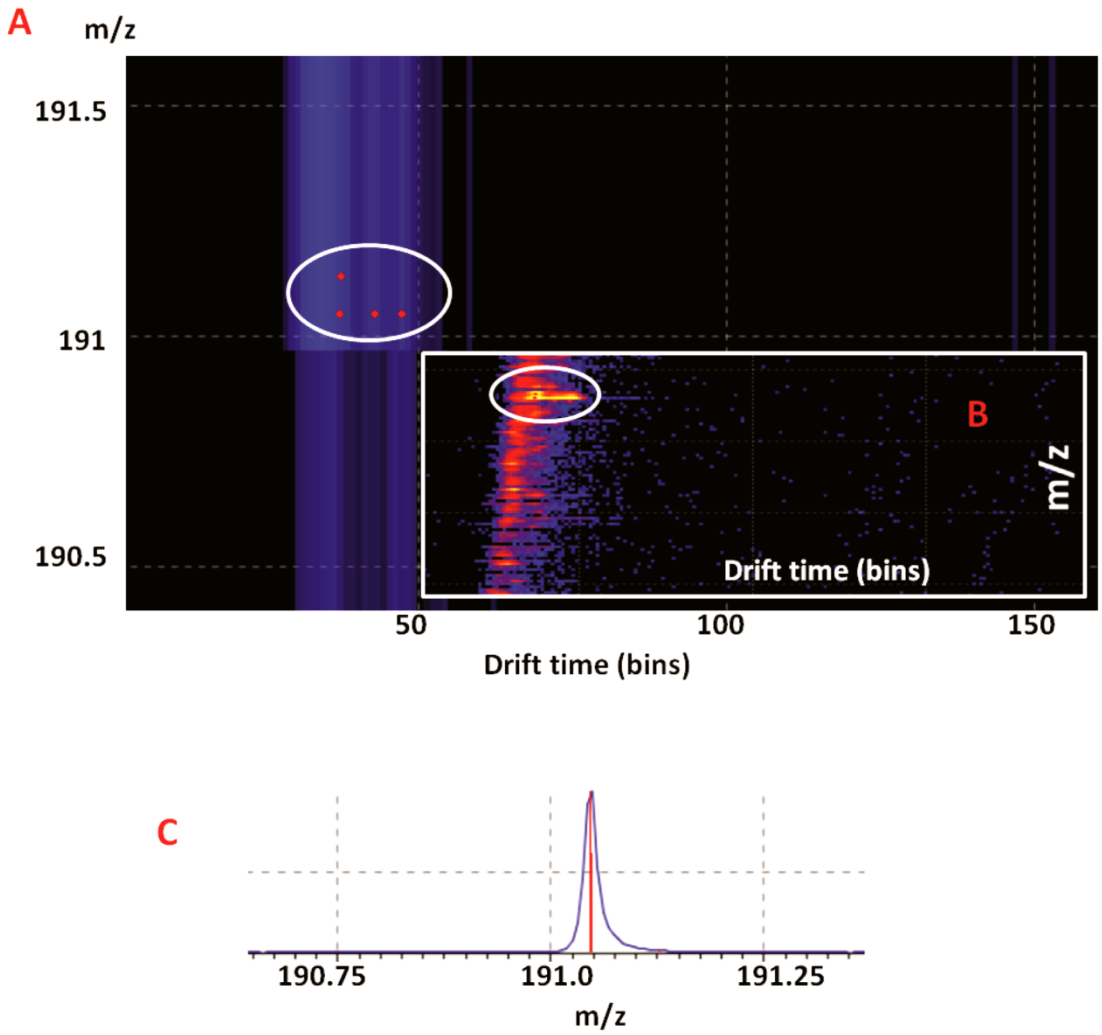

Figure 5. Ion mobility separation of small molecules in different classes with identical mass. (A) Zoom in figure of four different compounds eluted in one chromatographic peak. (B) Heat map of isobaric compounds filtered from background. (C) Chromatographic peak shared by four different molecules.

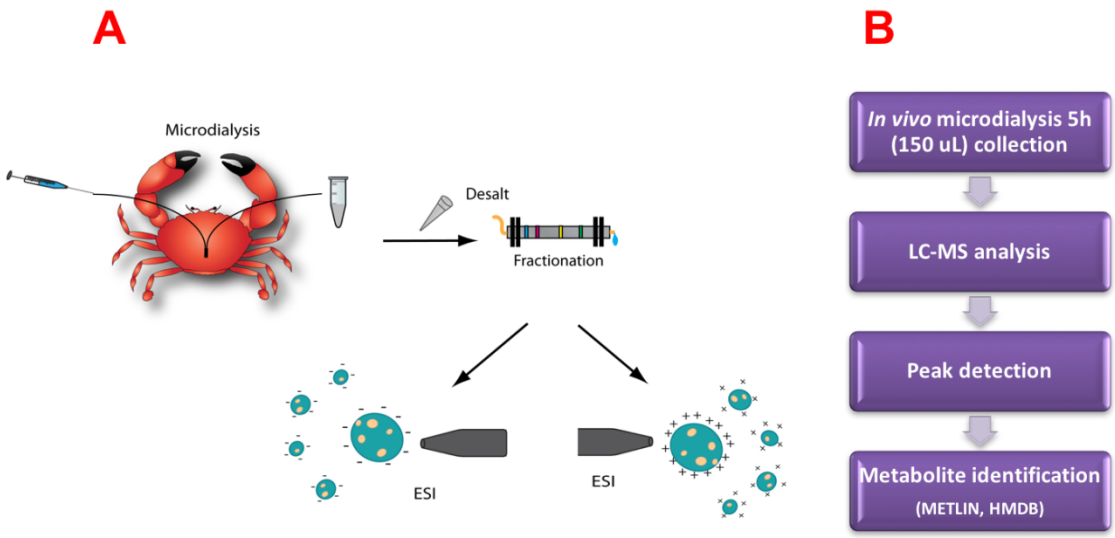

Figure 6. LC-MS acquisition for neurotransmitter identification via *in vivo* microdialysis. (A) 2 hrs microdialyate was collected, concentrated and desalted before LC-MS analysis. Fast polarity switching was utilized for complementary detection by acquiring of positive ESI and negative ESI in parallel. (B) LC-MS data of detected small molecules are searched against MELIN and HMDB for metabolite identification.

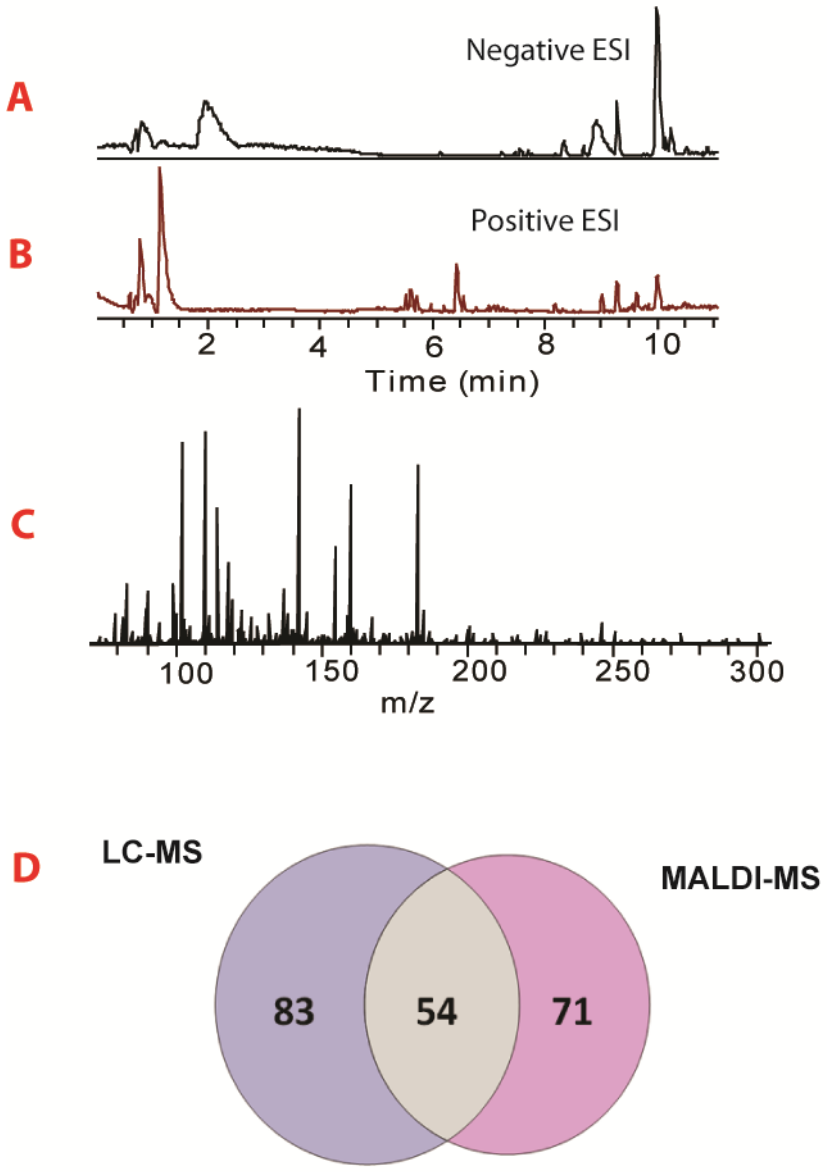

Figure 7. Untargeted LC-MS analysis of hemolymph metabolites.

(A) Base peak ion chromatogram acquired in negative ion mode. (B) Base peak chromatogram acquired in positive ion mode. (C) Averaged mass spectrum of detected mass features. (D) Venn diagram showed comparison of metabolomics identification of MALDI-MSI and LC-MS platform. 83 metabolites were uniquely identified by LC-MS, while 71 metabolites were exclusively found by the MALDI-MSI platform.

Chapter 7

Quantitative proteomics and peptidomics of human pancreatic carcinoid BON cell secretion

Abstract

Regulated exocytosis is a biological process for cells to secrete proteins and small molecules in a controlled manner. The process is mediated by a membrane-enclosed vesicle fusion with the plasma membrane and is usually triggered by high concentrations of calcium. The most extensively studied example is synaptic vesicle fusion with the plasma membrane for neuron communication. Dense core vesicle (DCV) is another type of vesicle that also undergoes regulated exocytosis. A common feature of DCV exocytosis in various cell types with synaptic vesicle exocytosis is that it is highly regulated. However, regulated exocytosis can possibly happen without external stimulation by absolute calcium. To further confirm the signaling mechanisms of this phenomenon, we applied quantitative proteomics approach to analyze the composition of DCV secretions at stimulated and resting conditions. By comparing the component and quantities of vesicle secretion, secretion pathway of DCV at resting state is further deducted.

1. Introduction

Synaptic vesicles are 40nm diameter vesicles that contain high concentrations of neurotransmitters and they are accumulated at the pre-synapse at resting conditions. When neurons receive an action potential, intracellular calcium concentration is significantly increased due to calcium influx. Within milliseconds of calcium rise, synaptic vesicles undergo fast fusion with the plasma membrane and release neurotransmitters to the cell exterior. The calcium-triggered process is generally conserved for regulated exocytosis in different cell types.

Dense core vesicle (DCV) exocytosis plays various and vital roles in different parts of the body depending on the contents that they secrete. For example, endocrine cells in the pituitary cells secrete multiple hormones to regulate growth, food intake, blood pressure and other processes; endocrine cells in the pancreas secrete insulin to regulate plasma glucose level; neuroendocrine chromaffin cells in the adrenal gland secrete catecholamine to control stress response. Cells in the immune system also have vesicles that are similar to DCVs and they secrete immunoreactive materials for immune response. In this section of the study, we focus on regulated exocytosis in neuroendocrine cells.

At resting conditions, DCVs accumulate and wait near the plasma membrane but will not undergo fusion. This is in direct contrast to constitutive exocytosis, the other type of exocytosis that exists in all types of cells, which occurs spontaneously and immediately after constitutive vesicles are generated. Regulated exocytosis happens within sub-seconds upon intracellular calcium rise. In neuroendocrine cells such as PC12 cells, regulated exocytosis can be induced by treating cells with depolarization reagent, acetylcholine receptor agonist or direct delivery of calcium into permeable cells.

Despite of the absolute requirement for calcium, regulated exocytosis can happen without external stimulation. We term this process as spontaneous exocytosis. Spontaneous exocytosis of synaptic vesicles have been observed for decades. Electrophysiological recording at the neuromuscular junction recorded not only large scale neurotransmitter release upon action potential stimulation, but also small peaks of neurotransmitter release at resting condition [1]. The mini-release of neurotransmitters corresponds to spontaneous exocytosis of single synaptic vesicles. Although occurring at resting condition, spontaneous exocytosis also require calcium [2] and may come from the same pool of synaptic vesicles that undergo stimulated exocytosis [3].

Similar to synaptic vesicles, DCVs may also undergo spontaneous exocytosis. Spontaneous DCV exocytosis has been proposed for basal release of DCV cargo including human growth hormone (hGH), NPY-pHluorin, processed ACTH and mature insulin in AtT-20, PC12 cells and primary chromaffin cells [4-8]. Studies in neuroendocrine BON cells found that an over-expressed DCV fluorescent cargo, NPY-Venus, are spontaneous secreted into culture medium. Spontaneous release of NPY-Venus can be mediated through mis-sorting to the constitutive vesicles at the TGN or, alternatively, spontaneous DCV exocytosis. To differentiate those two pathways, we propose to utilize proteomic analysis to determine whether endogenous DCV cargo also undergoes spontaneous release. If so, spontaneously secreted proteins at resting condition will share a similar protein composition to acutely stimulated proteins, both of which reflecting DCV luminal content.

Liquid chromatography coupled to tandem mass spectrometry (LC–MS/MS) has emerged as a core tool for proteomics, particularly for the identification and characterization of large and complex sets of proteins extracted from biological samples [9, 10]. Bottom-up proteomics is currently at the basis for much of the protein research undertaken in biology. One of its main

applications is protein quantification that is said absolute when it aims at estimating intracellular protein concentrations, and relative when it aims at comparing protein abundances between different samples [11]. Peptide identification is performed by inferring amino-acid sequences from the fragmentation patterns of precursor ions on MS/MS spectra either by sequence database searching, spectral library searching or *de novo* sequencing [12, 13]. Quantification by mass spectrometry is achieved by label-free method, isotopic labeling or isobaric labeling method. In label-free bottom-up proteomics, proteins are identified in their peptide forms and relative quantitation is achieved by comparing their area under curve. In order to detect, quantify and match chromatographic peaks in MS1 or MS2 extracted ion chromatograph, several tools have been developed to interpret quantitative MS data, such as MassChroQ, MaxQuant, Skyline and Progenesis [14-16].

To support the hypothesis of spontaneous release from regulatory pathway, we aim to identify proteome secreted from BON cells under acute stimulation or resting conditions. We utilized MS-based quantitative proteomics and peptidomics for BON cell secretion analysis. By comparing the protein and peptide changes under different conditions, strong evidence was provided in support of proposed hypothesis.

2. Materials and methods

2.1. Chemicals and reagents

Acetic acid, ammonium hydroxide, acetone, acetonitrile (ACN), methanol (MeOH), sodium chloride (99.5%) and ammonium bicarbonate were purchased from Fisher Scientific (Pittsburgh, PA). For tryptic digestion, iodoacetamide (IAA), urea, formic acid and dithiothreitol (DTT) were from Sigma-Aldrich. Sequencing grade modified trypsin was obtained from Promega (Madison, WI). Amicon Ultra 0.5 mL 10,000 MWCO centrifugal filters were purchased from Millipore

(Billerica, MA). Millipore C_{18} Ziptip column was used for sample cleaning, and all water used in this study was doubly distilled on a Millipore filtration system (Bedford, MA).

2.2. Cell culture

BON cells were maintained in DMEM/F12 (1:1) supplemented with 10% fetal bovine serum (Phenix Research, Candler, NC, US) and incubated at 37°C with 5% CO2. Cells were passaged every three days.

2.3. Sample collection

BON cells were seeded to 6-well plates and incubated with normal culture medium (2ml each well). After an overnight incubation, the culture medium was moved from two wells and replaced with fresh culture medium (phenol red-free, HEPES-free, FBS-free, 2ml each) after extensive wash (3 times) with HANKs buffer three times. After 18hrs, collect culture medium from those 2 wells as spontaneous stimulation group. For the other four wells, wash with PSS-Na three times, 1ml each time. Then two wells of cells were stimulated with 1mL PSS-Na/2.5uM ionomycin at 37 °C for 5 min known as the acute stimulation group. DMSO was used as unstimulated control. After three groups of treatment, cell samples were centrifuged at 14,000 rpm for 2min to remove cell debris, followed by snap freeze in liquid nitrogen. Fluorescence of NPY-Venus was determined by a plate reader and confirmed robust secretion under ionomycin stimulation.

2.4. Molecular weight cut-off (MWCO) fractionation

To separate protein and fraction from cell secretion, MWCO was performed and modified based on previous publication in our group [17, 18]. Briefly, three washing steps were first performed to remove contaminates from the filter, which were 500 μL of 50:50 H_2O:MeOH followed by 500 μL H_2O, and 400 μL of the solution used for MWCO separation. Three groups of cell

secretion were dried down in SpeedVac and re-dissolved in 70/30 aqueous 1M NaCl/MeOH solution prior to loading into the filters. The 10 kDa MWCO filters were then centrifuged at 14,000 rpm for 8 min at room temperature in an Eppendorf microcentrifuge (Brinkmann Instruments Inc., Westbury, NY). The flow through peptide fractions were concentrated and desalted using C_{18} Ziptips by washing the Ziptip with three times ACN, three washes of H_2O containing 0.1% FA, peptide binding and eluting from Ziptip column using 15 uL of 50% ACN in 0.1% FA. The retained protein fractions above 10 kDa were collected in other tubes for tryptic digestion and proteomic analysis.

2.5. Protein digestion

Protein fractions were dissolved in 8 M urea (0.96 g urea in 2.0 mL of 25 mM ammonium bicarbonate solution). DTT (1M in 25 mM ammonium bicarbonate) was added to the tube followed by gentle vortex for reduction of disulfide bonds. After reduction in 37 °C for 1 h, 200 mM IAA was added to the tube for alkylation for 1 h at room temperature in dark with shaking. In solution digestion was performed overnight at 37 °C after adding trypsin at an enzyme/substrate ratio of 1/30. In the next morning, formic acid was added to quench the reaction at a final concentration of 10%. The digested proteins were reconstituted and desalted with Ziptip C_{18} column.

2.6. LC-MS/MS acquisition

Digested protein fractions were separated by a self-packed C_{18} column before loading to Q Exactive Orbitrap mass spectrometer from Thermo Scientific (San Jose, CA). Samples were divided into three groups according to their stimulation conditions, which are spontaneous stimulation group #1, acute stimulation group #2 and control group #3. Each group has three bio-replicates for LC-MS/MS analysis. Mobile phase A consisted of water with 0.1% FA, and

mobile phase B was composed of ACN with 0.1% FA. Peptides were separated using a solvent gradient of 0 – 10% B over 0.5 min and then 10 – 30% B over 70 min at a flow rate of 350 nL/min. Data-dependent acquisition (DDA) parameters recorded MS scans in profile mode from *m*/*z* 250 – 3000 at a resolution of 35,000. Automatic gain control (AGC) targets of 1 x 10^6 and maximum injection times (IT) of 100 ms were selected. The 10 most intense precursor ions were selected for MS/MS higher-energy collisional dissociation (HCD) fragmentation with an isolation width of 2.0 *m*/*z* and placed on an exclusion list for 40 s. Tandem mass spectra were acquired at a resolution of 17,500 in profile mode with an AGC target of 1 x 10^5, a maximum IT of 150 ms, a normalized collision energy (NCE) of 27, and a fixed lower mass at *m*/*z* 110.

An inclusion list for signature peptides was built based on results from data dependent results. Proteomic identification for all three groups was also combined to construct a tandem mass spectra library for targeted quantitation. For targeted analysis in parallel reaction monitoring (PRM) mode, only included peptides were isolated and introduced to tandem mass fragmentation at a scheduled retention time windows of 3 to 5 min. Targeted PRM quantification was carried out using Skyline Software from the MacCoss group.

2.7. Large-scale proteomic quantification by MaxQuant

Secreted proteome among different groups were quantified by label-free quantification (LFQ) approach in MaxQuant [17, 18]. All raw files were searched against Uniprot human proteome database. Mass tolerance for full MS spectra was 20 ppm and 0.05 Da for fragment ions. "Unique plus razor peptides" were chosen to quantify a protein which offers a good compromise of using only peptides that undoubtedly belong to a protein and using as many peptide signals as possible [15]. MaxQuant results were further uploaded to Perseus software (Laboratory of Mass Spectrometry, LNBio, CNPEM) for subsequent proteome data analysis and bio-statistical

interpretation. Contaminants were removed from the identification data sets and scatter plots were used to check correlations between biological replicates. Student t-test was done with a threshold value of 0.05. A heat map is generated for visual representation of the relative expression levels of the proteins across different groups.

2.8. Parallel reaction monitoring for targeted analysis

The high resolving power of Orbitrap mass analyzer enables selective and sensitive high-resolution/accurate-mass (HR/AM) quantitative assays for precise targeted protein quantification in complex matrices. Parallel reaction monitoring (PRM) method that employed on a Q Exactive mass spectrometer, enhances selectivity of quantification significantly by targeting product ions [19-21]. Peptides from proteins of interest, Chromogranin A (CMGA), Secretogranin 1 (SCG1) and Secretogranin 2 (SCG2) were included for time scheduled PRM acquisition. Data was analyzed by Skyline software for targeted MS/MS quantification. Five most abundant product ions from selected peptides were used for relative comparison in Skyline. Tandem mass spectral library for this study was built on un-biased identification of BON secretion with a confidence cut-off score of 0.95.

3. Results and discussion

3.1. DCV cargo NPY-Venus undergoes spontaneous release in neuroendocrine BON cells

NPY-Venus is a soluble cargo protein targeted to DCVs. When expressed in BON cells, NPY-Venus was mainly localized to DCVs and undergo robust exocytosis upon stimulation with ionomycin/calcium. However, NPY-Venus was also secreted at resting condition over a long collection time. How NPY-Venus is secreted when cells are not stimulated? There are two possible pathways, 1) NPY-Venus is mis-sorted to the constitutive secretory pathway and/or 2) spontaneous DCV exocytosis at resting conditions. To test those two possibilities, we decide to

use endogenous DCV cargo proteins, which should not enter constitutive vesicles. If they are also spontaneously secreted, it will support the second possibility.

Endogenous DCV cargo PC1 was spontaneously secreted. Prohormone convertase 1 (PC1) processes hormones into their mature forms within DCVs. As illustrated in Figure 1, acute stimulation with ionomycin triggered robust PC1 secretion, confirming its localization to DCVs. Similar to NPY-Venus, endogenous PC1 was also detected in conditioned culture medium after incubating cells for 48 hours. This suggested that DCVs indeed undergo exocytosis. Quantification of NPY-Venus and PC1 showed that the ratio of externalized PC1 to internal PC1 was similar to that of NPY-Venus, suggesting that spontaneous DCV exocytosis was the major pathway for NPY-Venus release at resting condition.

To further confirm that BON cells undergo spontaneous exocytosis with an unbiased approach, we collected 3 samples for proteomic studies. The first sample was conditioned culture medium, which contained proteins that were spontaneously (ProSpon) secreted within 18 hours. The second and third sample were collected from an acute stimulation experiment. After washing cells extensively, we stimulated cells with ionomycin or DMSO as control for 10 minutes. During the short stimulation period, spontaneous DCV exocytosis contributed minimally to protein secretion. Proteins secreted by acute (Sample 2, ProAcute) ionomycin stimulation reflected DCV content, while proteins secreted in the presence of DMSO (ProDMSO) were possibly random sticky proteins to cell surface and should be at low amount. We set to determine whether the composition of ProSpon was similar to ProAcute.

3.2. Proteomic quantification across stimulation conditions

Raw data were processed with MaxQuant and its built-in Andromeda search engine for feature extraction, peptide identification, and protein inference [15, 22]. Peptide and protein FDRs were

both set at 1%. In proteome wide analysis, label free quantification was performed for nine samples. Heatmap in Figure 2B. was generated from Perseus for relative quantitation of secreted proteins. Good reproducibility was shown between biological replicates. DMSO treated group #3 was used as negative control to be subtracted from stimulated group #1 and #2. As shown in Figure 2B, proteins secreted by ionomycin stimulation was included in 18 hrs spontaneous stimulation from BON cells. Relative abundance for each protein was consistent within group #1 and #2, indicating those protein were possibly secreted by the same type of vesicles.

In MaxQuant protein profiles, proteins were sorted across groups. CMGA, the most dominant marker for carcinoid tumor BON cells, was selected as profile reference. As illustrated in Figure 3A, CMGA is shown at high intensity in culture medium and stimulated secretion, but low intensity in negative control. Thus, proteins that have similar profile trend are considered as BON secretion from particular vesicles while other proteins are contaminants or non-specific secretome. Principal component analysis (PCA) was utilized to verify biological differences between groups. As shown in Figure 3B, three groups of samples were distinguished as three components and bio-replicates were successfully grouped together. Student t-test was applied for selecting dominant secretome from DCVs. A volcano plot was used to quickly identify proteomic changes in large data sets composed of replicate data [2]. Shown in Figure 4, significance versus fold change for acute stimulation versus control was plotted on the y and x axis, respectively. Proteins highlighted in red were considered as dominant secretome as they had a fold change larger than 2.

3.3. Gene Ontology (GO) analysis of proteome composition

We identified 88 proteins from ProSpon and 212 proteins from ProAcute, while only 1 protein in ProDMSO. 57 proteins were shared by ProSpon and ProAcute (Figure 5). We grouped proteins

in ProSpon and ProAcute based on their molecular function. GO analysis shows that the distribution of proteins to each category was very similar for ProSpon or ProAcute, indicating that extra proteins in ProAcute followed a similar distribution pattern and they were possibly low abundant proteins in each category. The most enriched classes were catalytic activity, structural molecule activity and binding activity. This is consistent with the anticipated composition of DCVs. For example, DCV contains many enzymes for hormone processing, such as PCs, PAMs, and carboxypeptidases; various granins and other precursors of neuropeptides were present in the "binding activity" group. In summary, the similar distribution pattern in GO analysis suggested that ProSpon and ProAcute were from the same origin - DCV exocytosis.

3.4. PRM analysis for dominant proteins in secretion

Transferring from large-scale proteomics study, we further applied PRM quantification for targeted protein with enhanced sensitivity and selectivity. Signature peptides from dominant proteins were chosen for PRM acquisition on Q Exactive Orbitrap mass spectrometer. Tryptic peptide ADEPQWSLYPSDSQVSEEVKTR from SCG1 was shown in Figure 6 as an example. Fragmented y ions were used for relative comparison between spontaneous (Figure 6A, B) and acute stimulation (Figure 6C, D). Column bar in Figure 7B illustrated quantitation between cultured medium and acute stimulation for SCG1 achieved by PRM. As for SCG2, tryptic peptide TSYFPNPYNQEK was selected as signature peptide (Figure 8). As illustrated in bar gragh in Figure 9B, SCG2 was presented at similar level in cultured medium and acute stimulation. Compared to SCG2, SCG1 was secreted at a higher abundance after ionomycin treatment than 18 hrs spontaneous stimulation.

3.5. Identification of endogenous peptides

Peptide fractions of each group was analyzed by a high-res Orbitrap mass spectrometer. The resulting data was processed through PEAKS studio 7 software (Bioinformatics Solutions Inc.) for database search and peptide identification. Mass error was set to be 20 ppm for MS1 and 0.05 Da for MS2. Protein-derived peptides were found both in spontaneous stimulation and acute stimulation group. No peptides were detected in the control group. The most abundant peptides were derived from CMGA which is also the most dominant secretion in protein portion. 81 CMGA-derived peptides were identified in acute stimulation while 59 from basal secretion in cultured medium. Among the endogenous peptides, 6 of them have been reported to have bio-functions in signaling transportation. As listed in Table 1, SS-18 resides between the C-terminal single lysyl residue 303 processing site of pancreastatin, and the typical -KR-, N-terminal processing site of peptide WE-14. This peptide was also present in an extract of mid-gut carcinoid tumor [23]. Immunoreactivity of peptide WE-14 has been reported to present in subpopulations of CMGA expressing cells, notably in discrete clusters of chromaffin cells, cells of the anterior pituitary and in endocrine cells throughout the gastrointestinal tract [24]. GV-19 is contained within the structure of the exogenous protease generated peptide of porcine CMGA, named parastatin, due to its inhibitory effects on parathyroid cell secretion [25]. AL-11 is a major processed product in the insulinoma, mid-gut and lung carcinoids and phaeochromocytoma. It contains the domain of the protein encoding the exogenous protease-derived peptide, catestatin [19, 21, 26]. AL-11 represents the C-terminal undecapeptide of catestatin. In addition to its inhibition of nicotine stimulated catecholamine release from isolated chromaffin cells, catestatin also produces systemic pressor effects in mammals, possibly by means of histamine release [20]. Since AL-11 has been identified as a major endogenous product in four different human neuroendocrine tumors, it may represent a likely contender for the

bioactive entity residing within this domain of CMGA. In addition to CMGA, 19 SCG1-derived peptides and 4 neurotensin (NEUT)-derived peptides were found only in ionomycin treated group. 39 SCG2-derived peptides were detected in acute secretion and 12 in spontaneous secretion.

In the dominant peptides derived from Granin-family proteins, 137 endogenous peptides were identified for the first time. Relative quantification was done for each peptide on PEAKS after identification. As shown in Figure 10, intensities of representative peptides were compared for acute stimulated group and spontaneous stimulation group. Different peptides were presented at different levels in two groups. Detected peptides were mainly from human CMGA, SCG1, SCG2 and NEUT, which ranks in accordance with protein abundance. This finding further demonstrated basal exocytosis undergoes regulated secretory pathway.

4. Conclusion

To demonstrate signaling pathways, we characterized secretome from DCVs at both protein and peptide level. Label free quantification was performed for control group, acute stimulation and proposed spontaneous stimulation group. ProSpon and ProAcute and similar proteomic coverage and same relative abundance. Functional analysis indicated they fall in analogical groups. Additionally, endogenous peptides were identified and analyzed to be derived from the same dominant proteins. These results provided strong evidence to support the hypothesis of spontaneous exocytosis from DCVs undergoing regulated secretory pathways.

References

1. KATZ, P.F.A.B., *SPONTANEOUS SUBTHRESHOLD ACTIVITY AT MOTOR NERVE ENDINGS.* J. Physio., 1952. **117**: p. 109-128.
2. I. Llano1, J.G., C. Caputo2, F. A. Lai3, L. M. Blayney3, Y. P. Tan4 and A. Marty, *Presynaptic calcium stores underlie large-amplitude miniature IPSCs and spontaneous calcium transients* Nature neuroscience, 2000. **3**: p. 1256-1265.
3. Wilhelm, B.G., T.W. Groemer, and S.O. Rizzoli, *The same synaptic vesicles drive active and spontaneous release.* Nature neuroscience, 2010. **13**(12): p. 1454-1456.
4. Sambanis, A., G. Stephanopoulos, and H.F. Lodish, *Multiple episodes of induced secretion of human growth hormone from recombinant AtT-20 cells.* Cytotechnology, 1990. **4**(2): p. 111-9.
5. Zhang, X., et al., *Ca2+-dependent synaptotagmin binding to SNAP-25 is essential for Ca2+-triggered exocytosis.* Neuron, 2002. **34**(4): p. 599-611.
6. Matsuuchi, L. and R.B. Kelly, *Constitutive and basal secretion from the endocrine cell line, AtT-20.* J Cell Biol, 1991. **112**(5): p. 843-52.
7. Mains, R.E. and B.A. Eipper, *Secretion and regulation of two biosynthetic enzyme activities, peptidyl-glycine alpha-amidating monooxygenase and a carboxypeptidase, by mouse pituitary corticotropic tumor cells.* Endocrinology, 1984. **115**(5): p. 1683-90.
8. Sirkis, D.W., R.H. Edwards, and C.S. Asensio, *Widespread dysregulation of peptide hormone release in mice lacking adaptor protein AP-3.* PLoS Genet, 2013. **9**(9): p. e1003812.
9. Domon, B. and R. Aebersold, *Options and considerations when selecting a quantitative proteomics strategy.* Nature Biotechnology, 2010. **28**(7): p. 710-721.

10. Blein-Nicolas, M. and M. Zivy, *Thousand and one ways to quantify and compare protein abundances in label-free bottom-up proteomics.* Biochimica et Biophysica Acta (BBA) - Proteins and Proteomics, 2016. **1864**(8): p. 883-895.

11. Zhang, Y., et al., *Protein Analysis by Shotgun/Bottom-up Proteomics.* Chemical Reviews, 2013. **113**(4): p. 2343-2394.

12. Nesvizhskii, A.I., *A survey of computational methods and error rate estimation procedures for peptide and protein identification in shotgun proteomics.* Journal of Proteomics, 2010. **73**(11): p. 2092-2123.

13. Feng, J., D.Q. Naiman, and B. Cooper, *Probability-based pattern recognition and statistical framework for randomization: modeling tandem mass spectrum/peptide sequence false match frequencies.* Bioinformatics, 2007. **23**(17): p. 2210-2217.

14. Valot, B., et al., *MassChroQ: A versatile tool for mass spectrometry quantification.* Proteomics, 2011. **11**(17): p. 3572-3577.

15. Cox, J. and M. Mann, *MaxQuant enables high peptide identification rates, individualized p.p.b.-range mass accuracies and proteome-wide protein quantification.* Nature Biotechnology, 2008. **26**(12): p. 1367-1372.

16. MacLean, R.C., *Predicting epistasis: an experimental test of metabolic control theory with bacterial transcription and translation.* Journal of Evolutionary Biology, 2010. **23**(3): p. 488-493.

17. Cunningham, R., et al., *Investigation and reduction of sub-microgram peptide loss using molecular weight cut-off fractionation prior to mass spectrometric analysis.* J Mass Spectrom, 2012. **47**(10): p. 1327-32.

18. Chen, R., et al., *Measurement of neuropeptides in crustacean hemolymph via MALDI mass spectrometry.* J Am Soc Mass Spectrom, 2009. **20**(4): p. 708-18.

19. Mahata, S.K., et al., *Novel autocrine feedback control of catecholamine release. A discrete chromogranin a fragment is a noncompetitive nicotinic cholinergic antagonist.* J Clin Invest, 1997. **100**(6): p. 1623-33.

20. BRIAN P. KENNEDY, S.K.M., DANIEL T. O'CONNOR AND MICHAEL G. ZIEGLER, *Mechanism of Cardiovascular Actions of the Chromogranin A Fragment Catestatin In Vivo.* Peptides, 1998. **19**: p. 1241-1248.

21. Taylor, C.V., et al., *Formation of the catecholamine release-inhibitory peptide catestatin from chromogranin A. Determination of proteolytic cleavage sites in hormone storage granules.* J Biol Chem, 2000. **275**(30): p. 22905-15.

22. Cox, J., et al., *Andromeda: a peptide search engine integrated into the MaxQuant environment.* J Proteome Res, 2011. **10**(4): p. 1794-805.

23. Orr D.F., C.T., Johnsen A.H., Chalk R., Buchanan K.D., Sloan J.M., Rao P., Shaw C., *The spectrum of endogenous human chromogranin A-derived peptides identified using a modified proteomic strategy.* Proteomics, 2002. **2**: p. 1586-1600.

24. Gleeson CM1, C.W., Johnston CF, Buchanan KD., *Occurrence of WE-14 and chromogranin A-derived peptides in tissues of the human and bovine gastro-entero-pancreatic system and in human neuroendocrine neoplasia.* J Endocrinol., 1996. **151**: p. 409-420.

25. Fasciotto BH1, T.C., Greeley GH, Cohn DV., *Parastatin (porcine chromogranin A347-419), a novel chromogranin A-derived peptide, inhibits parathyroid cell secretion.* Endocrinology, 1993. **133**: p. 461-466.

26. Carl Miller, R.K., Josef Troger, Alois Saria,, R.F.-C. Wolfgang W. Fleischhacker, and a.H.W. Arnulf Benzer, *CSF of Neuroleptic-Naive First-Episode Schizophrenic. Patients: Levels of Biogenic Amines, Substance P, and Peptides Derived from Chromogranin A (GE-25) and Secretogranin II (Secretoneurin)* Biol Psychiatry, 1996. **39**: p. 911-918.

Table 1. Endogenous peptides derived from CMGA*.

CMGA-derived peptides	
SS-18	SGELEQEEERLSKEWEDS
WE-14	WSKMDQLAKELTAE
WA-8	WSKMDQLA
LF-19	LEGQEEEEDNRDSSMKLSF
AL-11	AYGFRGPGPQL
GV-19	GWRPSSREDSLEAGLPLQV

* The table listed endogenous peptides that has been reported to function in bioactivity. In addition to that, 16 CMGA-derived peptides were also detected that potentially affect exocytosis pathways.

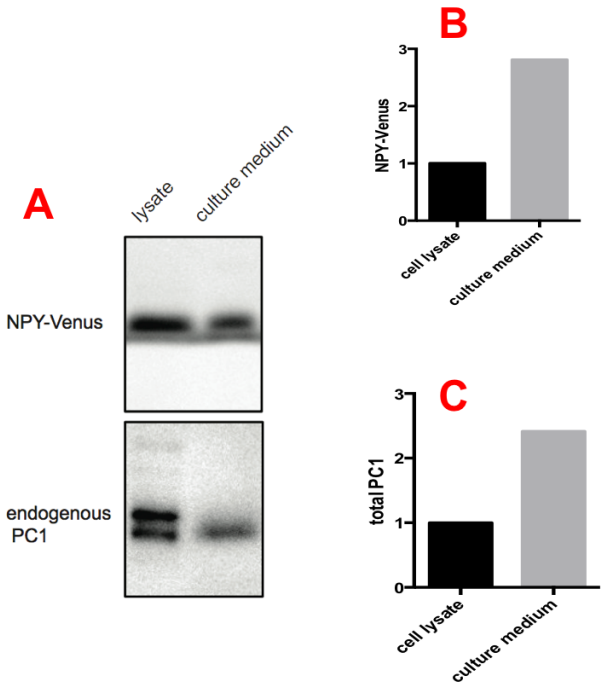

Figure 1. Endogenous DCV cargo PC1 was spontaneously secreted.

A. Western plot of NPY-Venus and endogenous PC1. B. Quantification of NPY-Venus in cell lysate and culture medium. C. Quantification of PC1 in cell lysate and culture medium.

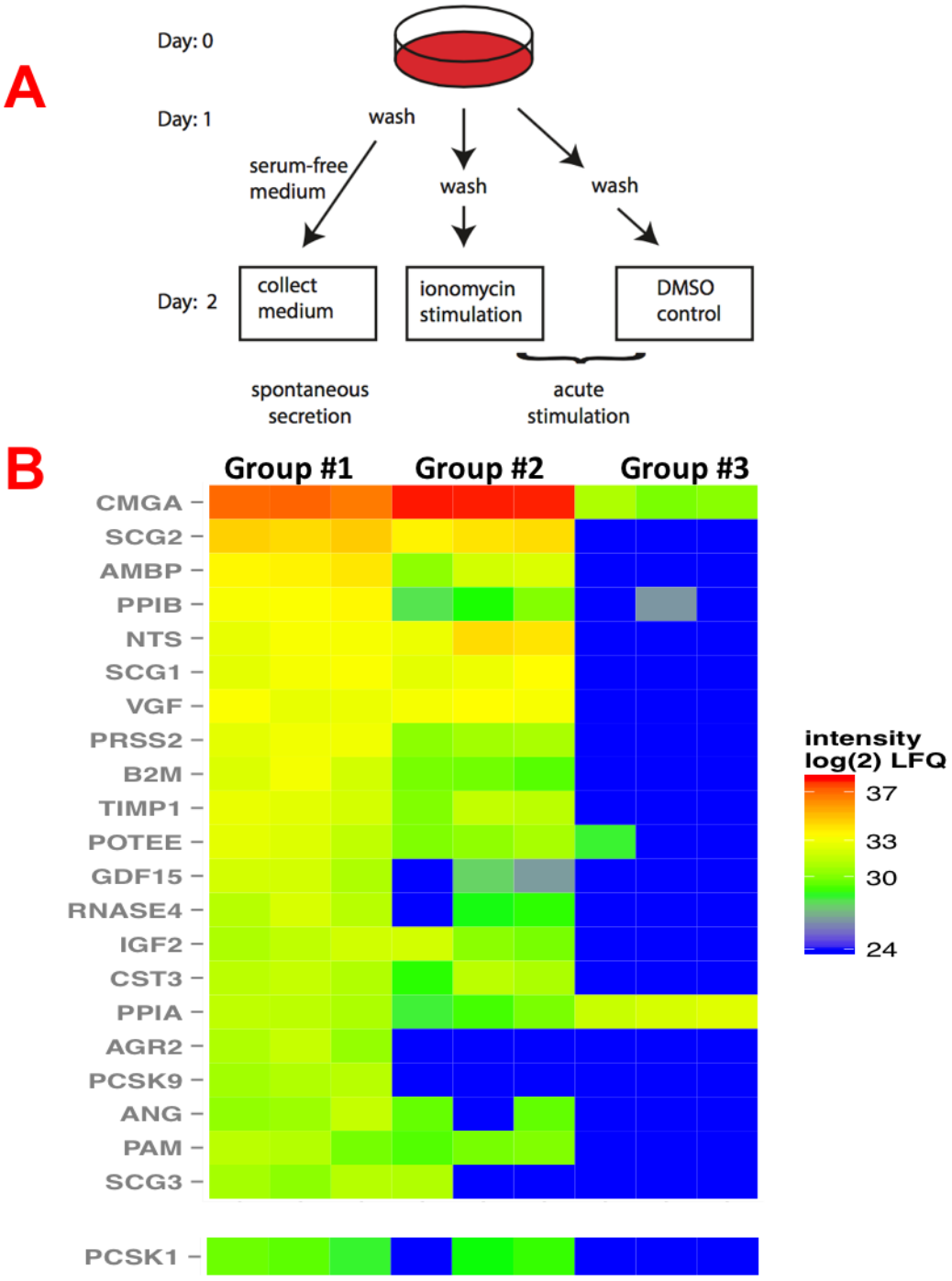

Figure 2. Unbiased MS Analysis of Spontaneously Secreted Materials.

A. Three treated for BON cells. B. Quantification of dominant proteins secreted from three conditions visualized in heatmap.

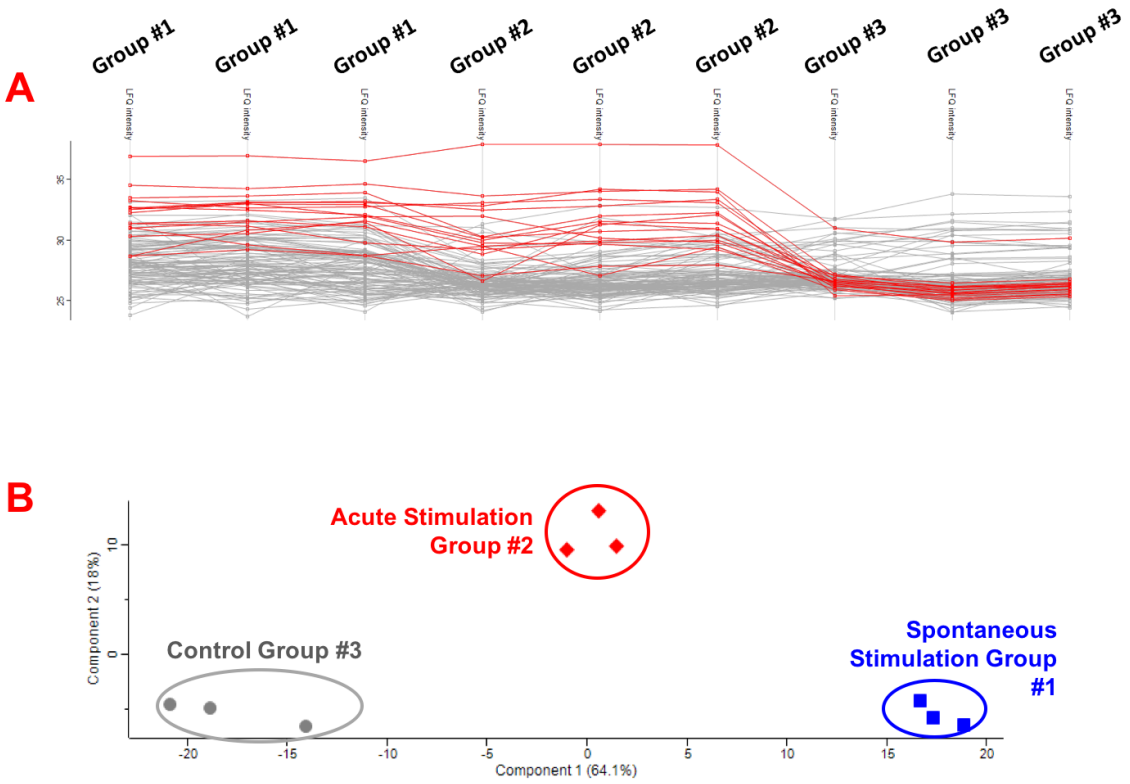

Figure 3. Label free quantification and statistical analysis.

A. Quantitative profiles of each bio-replicate. B. Principal component analysis of three groups.

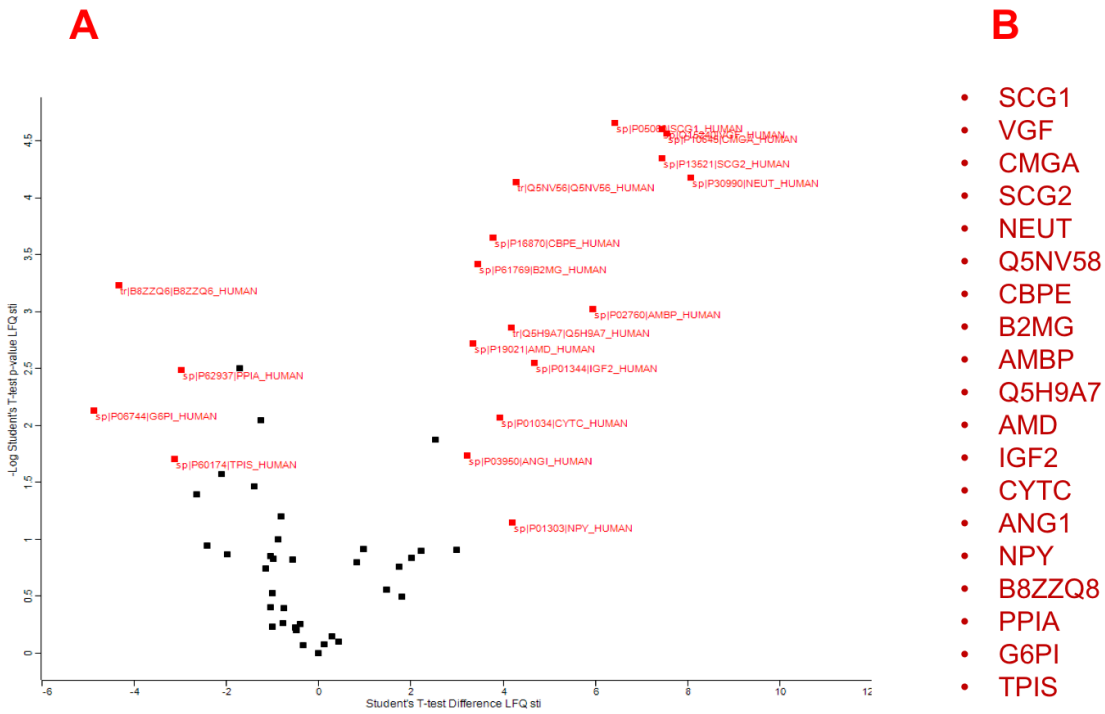

Figure 4. Volcano plot showed truly stimulated secretions from negative control.

A. Student t-test is used to determine if stimulation group and control group are significantly different from each other. B. Filtered gene name of protein secretion of fold change larger than 2.

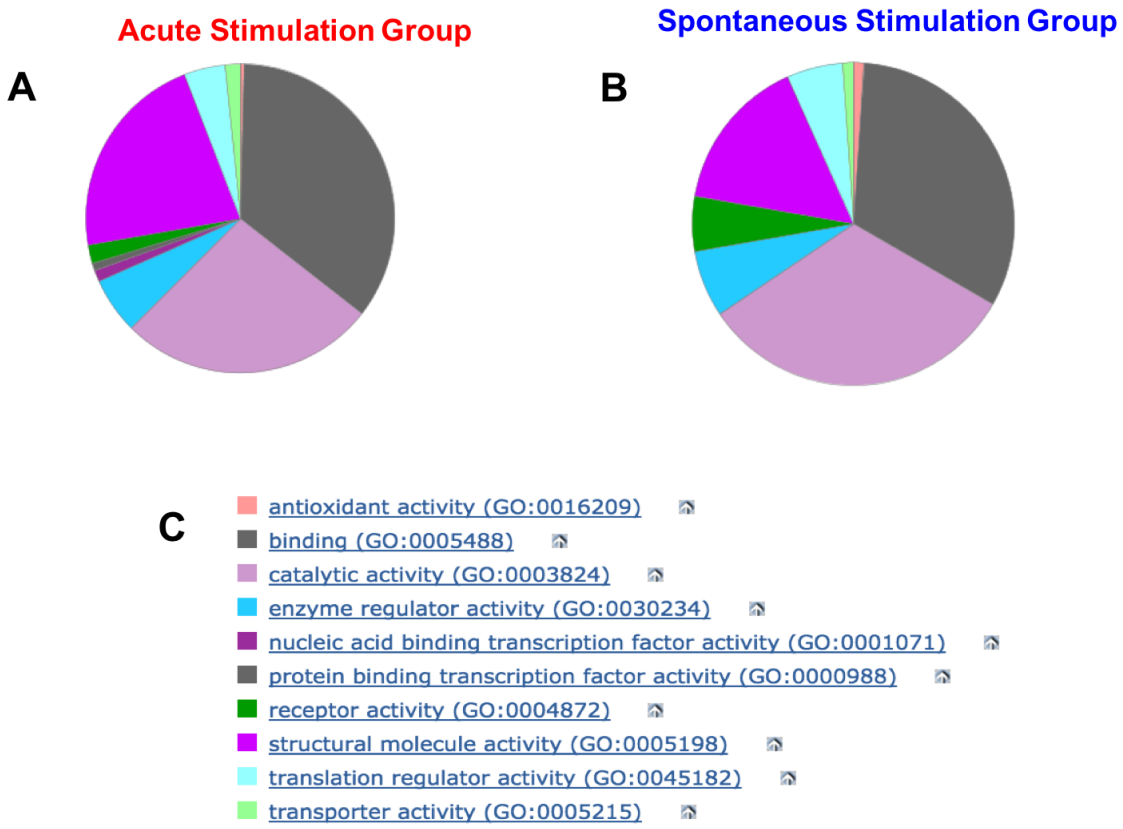

Figure 5. Gene Ontology analysis of protein secreted by different exocytosis.

A. Functional distribution of proteome in acute stimulation group. B. Functional distribution of proteome in spontaneus stimulation group. C. Molecular functions of grouped proteins.

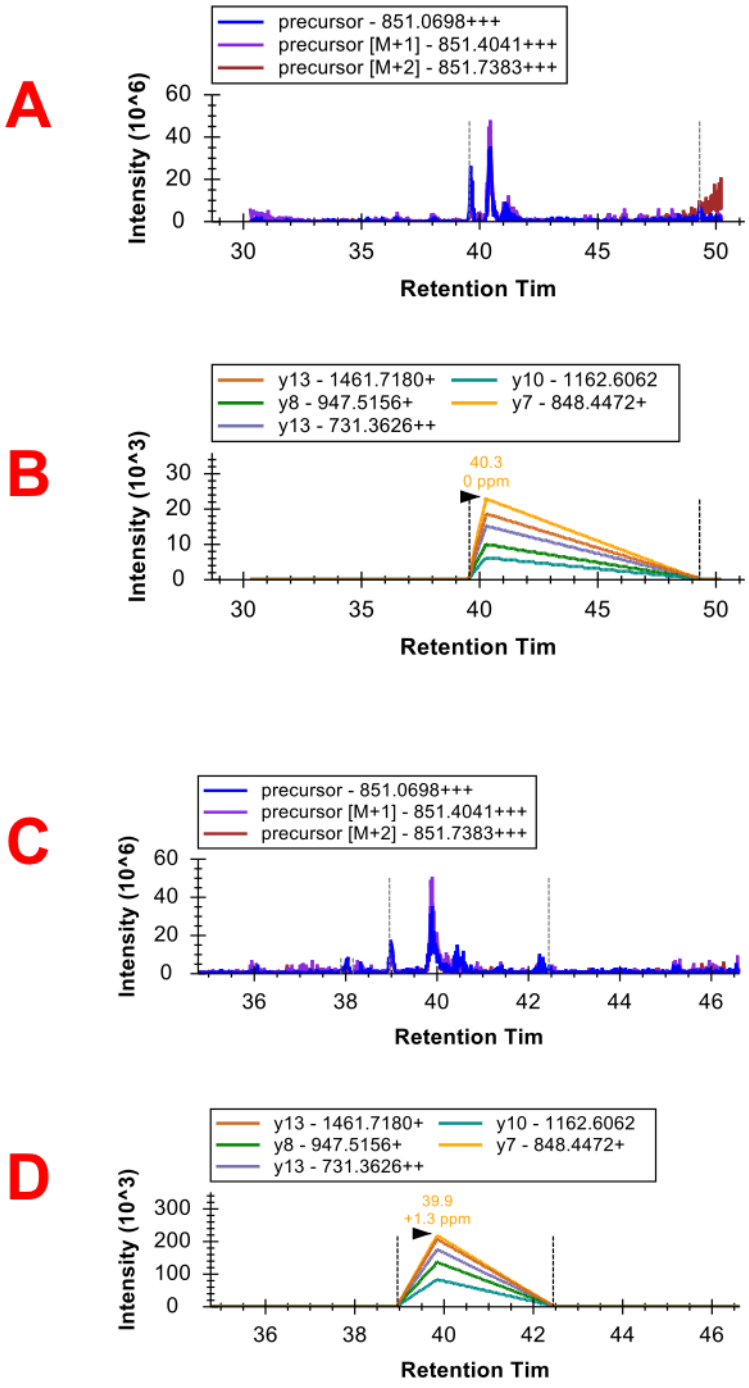

Figure 6. Targeted quantitation of SCG1 by PRM.

A, B. Extracted MS1 and MS2 chromatogram of SCG1 peptide from ProSpon. C, D. Extracted MS1 and MS2 chromatogram of SCG1 peptide from ProAcute.

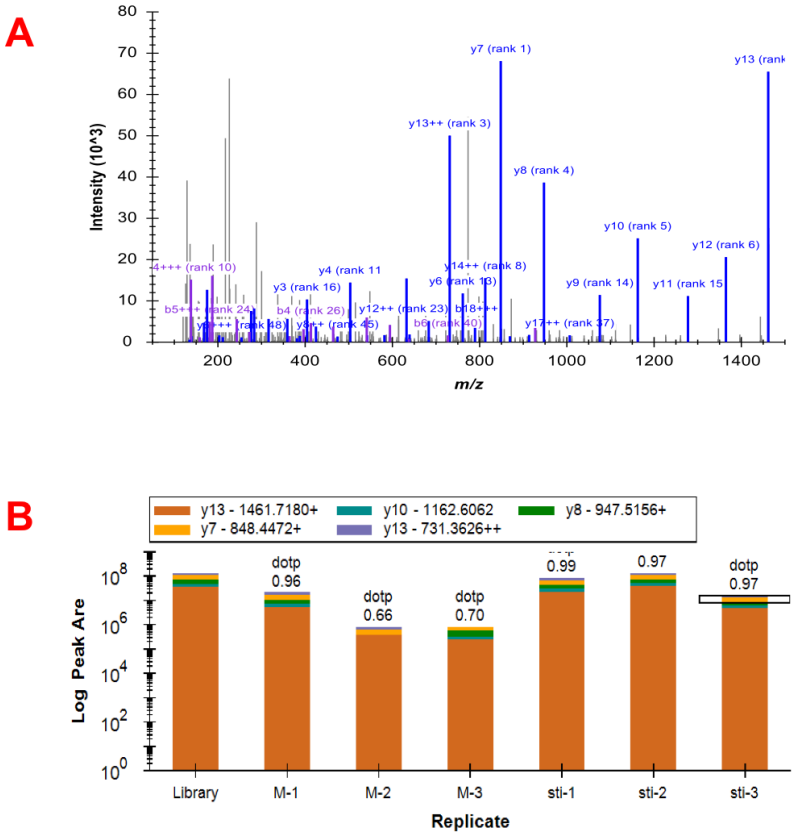

Figure 7. PRM quantitation of SCG1 by its product ion of signature peptide.

A. MS2 fragmentation of SCG1 peptide matched from spectrum library. B. PRM quantitation by its product ions.

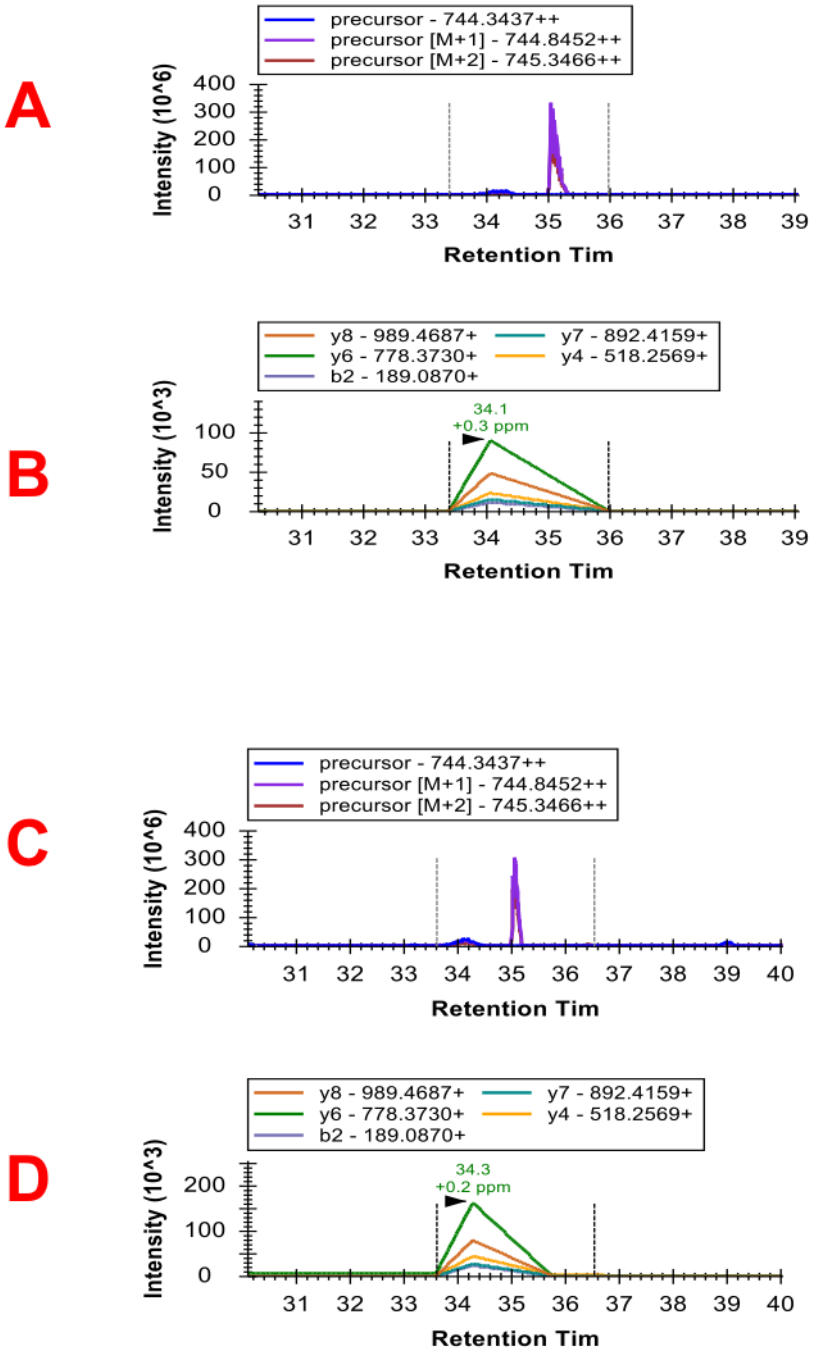

Figure 8. Targeted quantitation of SCG2 by PRM.

A, B. Extracted MS1 and MS2 chromatogram of SCG2 peptide from ProSpon. C, D. Extracted MS1 and MS2 chromatogram of SCG2 peptide from ProAcute.

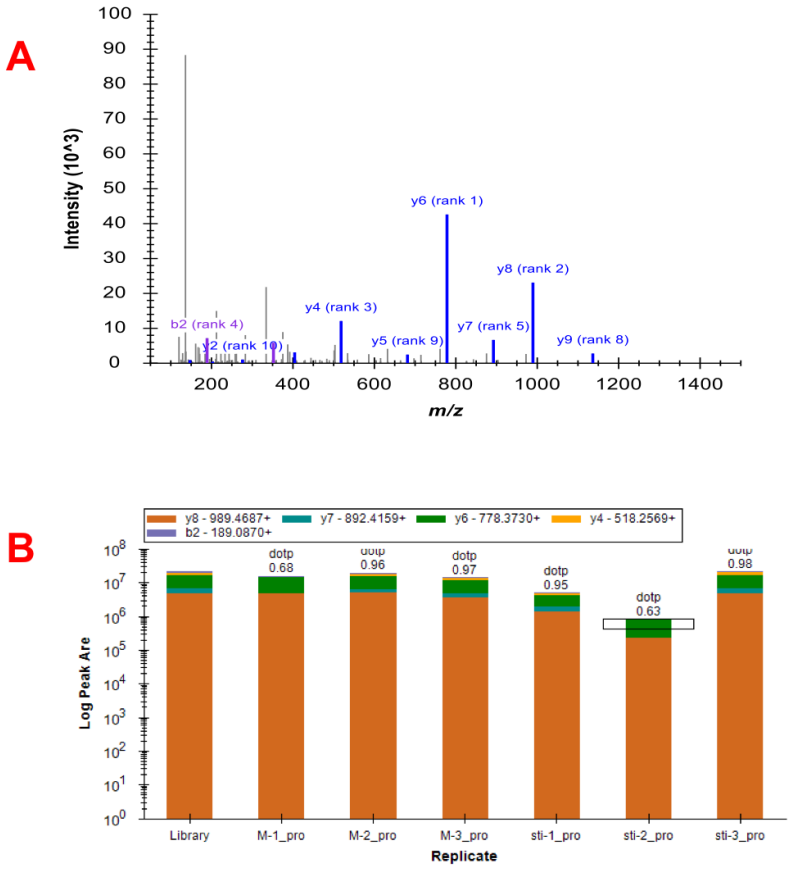

Figure 9. PRM quantitation of SCG2 by its product ion of signature peptide.

A. MS2 fragmentation of SCG2 peptide matched from spectrum library. B. PRM quantitation by its product ions.

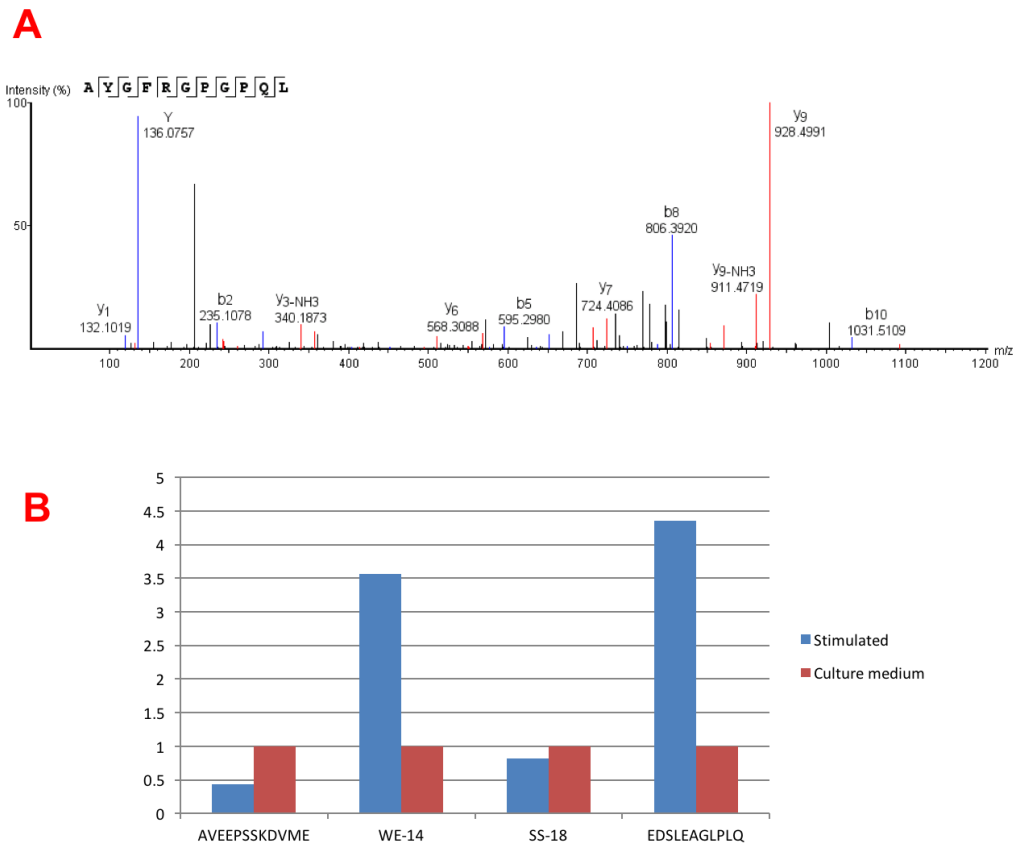

Figure 10. Identification of endogenous peptides.

A. Endogenous peptide AYGFRGPGPQL secreted from acute stimulation. B. Endogenous peptide quantification and comparison between acute and spontaneous stimulation.

Chapter 8

Conclusions and Future Directions

1. Conclusions

In this dissertation, I presented several approaches to address challenges for MS-based bio-analysis including sample preparation, instrumentation and data processing. Immobilized enzyme reactor and monolithic affinity chromatography significantly reduced experimental time and enabled detection of low abundance target analytes against interfering molecules. A new MALDI MS imaging platform was developed and coupled to *in vivo* microdialysis for real-time monitoring of neuropeptide and neurotransmitter secretion in live animal model. In addition to neuropeptidomics, label-free quantification and computational proteomics were employed for secretome analysis and interpretation of signaling pathways.

1.1. Immobilized enzyme reactor (IMER) for proteomic analysis

We demonstrated a one-step construction of IMER for highly efficient proteomic digestion in minutes. With the implementation of multi-proteases, protein coverage was further improved. IMER columns have been coupled to a variety of mass spectrometers including LC-ESI-Q/TOF, LC-ESI-Q-Orbitrap, MALDI-TOF/TOF and MALDI-LTQ-Orbitrap. Even for complicated proteome mixture, IMER digestion showed great benefits with significantly reduced time consumption while maintaining good identification rates. Due to the ability of fabrication in different format, monolithic enzyme reactor was also prepared in stage tips for high performance enzymatic digestion. IMER-LC-MS/MS offers several advantages when compared with in-solution digestion, including: 1) Because of the short digestion time, the problem of peptide degradation was minimized, thus reducing a major source of method variability and bias. 2) Due to minimized secondary processes, target peptides containing tryptophan residues are less of a problem than in the case of in-solution digestion. Thus, sequence coverage of proteins were

improved so as to expand proteomic identification. 3) It can be readily used when sample amount is limited.

1.2. Monolithic affinity chromatography

By changing the binding agents of the monolithic column, we immobilized antibodies for affinity enrichment and purification. With anti-RFamide antibodies immobilized, we developed monolithic affinity chromatography for separating and enriching targeted neuropeptide families. MALDI MS detection and database search results indicated that the targeted RFamide family neuropeptides have been specifically retained in the eluting fractions but not in the washing fractions. We also demonstrated its application to isolation and enrichment of target neuropeptide arginine vasopressin from a mouse pituitary gland extract. The specific capture and release of single target analyte highlighted the remarkable potential of monolithic platform.

1.3. Interfacing separation to MALDI MSI for *in vivo* analysis

Multi-faceted separation tools, such as LC, CE and ion mobility were integrated to MALDI and ESI MS. MSI platform combines the advantage of MALDI detection which can be incorporated with upstream separation and downstream online monitoring. It is flexible to a variety of applications without loss of spatial and temporal resolution. Small molecule neurotransmitters and metabolites were separated by different mechanisms and detected by MSI platform. Comprehensive investigation yield 208 small molecule metabolites identified in circulating body fluid. *In vivo* microdialysis was also coupled with MSI platform for direct analysis of crustacean endogenous neuropeptide degradation profile. Due to the ability to maintain the temporal resolution of microdialysis collection, dialysate was continuously collected onto the MALDI sample plate, enabling real-time characterization of neuropeptide profiles. Relative concentration changes could be reflected directly from imaging signal intensities, which potentially detoured

the limitation of MALDI MS quantitation. Moreover, this analytical platform is widely applicable to study other biological event in a highly dynamic fashion.

1.4. Secretome study of neuroendocrine carcinoid tumor cell line

Secretion from dense core vesicles from neuroendocrine cells were characterized by quantitative MS at both protein and peptide levels. Similar proteomic and peptidomic compositions were identified within acute stimulation group and culture medium collection. Moreover, relative abundances of secreted proteins and peptides correlated very well with each other. Identification and quantification of secreted proteome in dense core vesicles provided strong evidence for existence of spontaneous exocytosis. This documentation of spontaneous exocytosis is a significant discovery in basic endocrinology as it addresses the nature of basal secretion in many studies and shows potential implications in clinical research for cancer treatment.

2. Ongoing work and future plans

Microfluidic devices have been demonstrated to be highly efficient tools in chemical/biochemical synthesis, nano-scale analysis, imitating development of bio-systems, and tissue engineering due to their significantly reduced sample consumption, improved analysis speed, enhanced separation efficiency and detection sensitivity compared to conventional strategies [1-3]. We have fabricated custom-designed poly(dimethylsiloxane) (PDMS) chip devices. Microfluidic devices consisted of PDMS with channel features sealed onto derivatized silicon substrates. The PDMS pieces were formed by molding Sylgard 184 onto a photolithographically patterned SU-8 master. The PDMS prepolymer was then poured onto the master and cured at 70°C overnight. The inlet reservoir was punched by an AcuPunch of 1.5 mm diameter to allow further sampling. For plasma treatment, the PDMS was subjected to oxygen plasma for 30 s at 100 W with an oxygen plasma system to form irreversible attachment between PDMS microchip and substrates. Prior and between use, PDMS pieces were rinsed with methanol and water and dried with nitrogen. Figure 1 shows the channel feature of our chip device. Dimension of serpentine channel was 200 um wide x 50 um deep. Length of the channel is about 15 cm.

2.1. Microfluidic platform for chemical stimulation and real time analysis of secretion from neuroendocrine cells.

Exocytosis is one of the fundamental cellular process in cell-to-cell trafficking. Secretion of neurotransmitters and hormones are controlled by calcium regulated exocytosis which plays an important role in cell signaling. There has been considerable interest in drug and therapeutic development that targets secretion from neuronal cells. Efforts have been made to apply novel analytical tools and devices so as to provide mechanistic insight with enhanced throughput [4-6].

Carcinoid tumor BON cells, an important pancreatic tumor model cell line, release neurotranmitters, neuropeptides, and other hormones upon stimulation and provide appropriate responses to acute stress [7]. Based on previous research on neuroendocrine BON cell secretion, granin-proteins and their derived peptides can be targeted to record for stimulation process. Upon stimulation, cell secretion runs through the channel and got collected on the substrate glass slide. After drying the PDMS chip can be peeled off and matrix can be applied to the glass slide for MSI analysis.

2.2. Microfluidic digestion system for rapid proteolysis.

Considering the mass range limit of MALDI MS, most detectable analytes would be in the peptide range. In order to capture large protein secretion, on-chip digestion can be performed on the microfluidic system. Polydopamine has been suggested for covalent modification of various inorganic and organic substrates [1, 8]. Surface modification can be achieved by injecting polydopamine solution to the microchannel for self-polymerization. Further injection of protease solution would result in the formation of enzymatic surface due to the presence of catechol hydroxyl-groups on the polydopamine layer (Figure 2).

In summary, future work will focus on employing microfluidic platform to monitor stimulation process of signaling molecules secreted from neuroendocrine cells. Integration of MSI collection technique enables recording of secretion order and secretion amount of individual signaling molecules. Surface modification will be performed to achieve rapid on-chip digestion so that large proteins can also be monitored by MSI detection. Thus, this miniaturized system would enable the identification of signaling candidates and mimic the secretion process in the extracellular environment.

References:

1. Cheng, G., et al., *Nanostructured microfluidic digestion system for rapid high-performance proteolysis.* Lab Chip, 2015. **15**(3): p. 650-654.
2. Jun, Y., et al., *Microchip-based engineering of super-pancreatic islets supported by adipose-derived stem cells.* Biomaterials, 2014. **35**(17): p. 4815-4826.
3. Croushore, C.A. and J.V. Sweedler, *Microfluidic systems for studying neurotransmitters and neurotransmission.* Lab on a Chip, 2013. **13**(9): p. 1666.
4. Neher, J.R.a.E., *Emerging Roles of Presynaptic Proteins in Ca++Triggered Exocytosis.* Science, 2002. **298**: p. 781-785.
5. Ges, I.A., et al., *A microfluidic platform for chemical stimulation and real time analysis of catecholamine secretion from neuroendocrine cells.* Lab Chip, 2013. **13**(23): p. 4663-73.
6. MORGAN, R.D.B.A.A., *Secretory Granule Exocytosis.* Physiol Rev, 2003. **83**: p. 581-632.
7. Bader MF1, H.R., Kumakura K, Vitale N, *Exocytosis: the chromaffin cell as a model system.* Ann N Y Acad Sci, 2002. **971**: p. 178-83.
8. Lee, H., et al., *Mussel-inspired surface chemistry for multifunctional coatings.* Science, 2007. **318**(5849): p. 426-30.

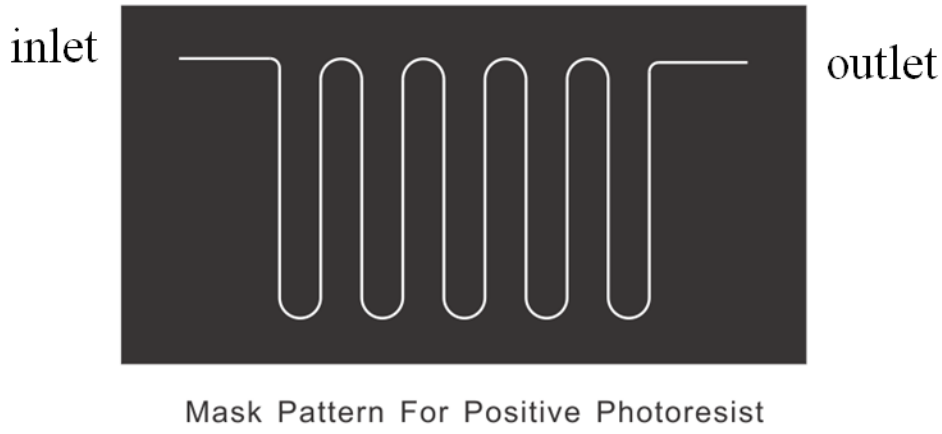

Figure 1. Mask design for microchip fabrication.

Microfluidic device consisted of PDMS chip with channel features and a glass slide sealed underneath.

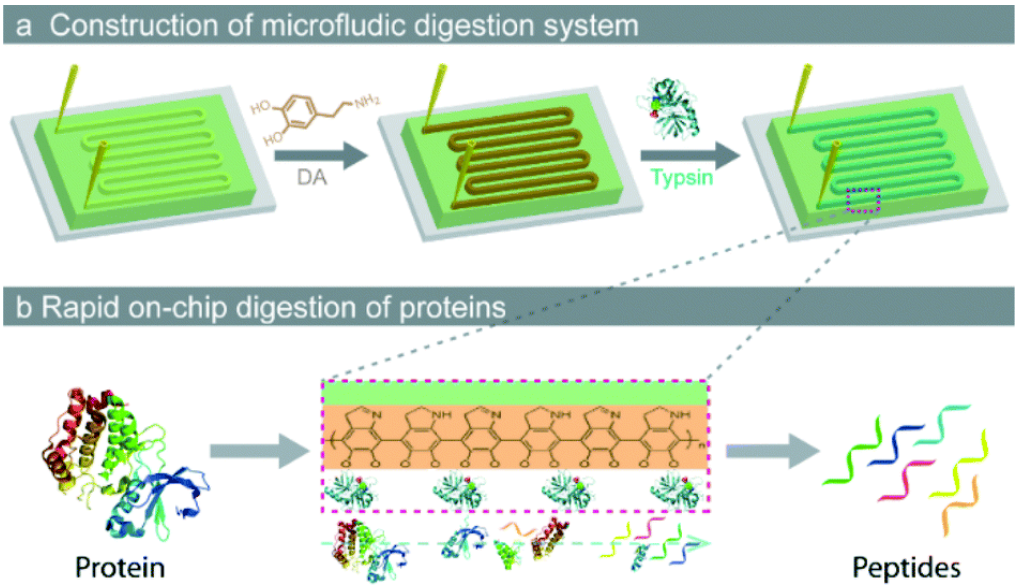

Figure 2. Microfluidic protein digestion system and rapid on-chip digestion of proteins.

Adapted from Cheng, G., et al., Lab Chip, 2015. 15(3): 650-654.

Appendix

List of publications and presentations

Publications:

- **Jiang S**, Liang Z, Hao L, Li L, Investigation of signaling molecules and metabolites found in crustacean hemolymph via *in vivo* microdialysis using a multi-faceted mass spectrometric platform, *Electrophoresis*, 2015, 00, 1-8.
- **Jiang S**, Zhang Z, Li L, A one-step preparation method of monolithic enzyme reactor for highly efficient sample preparation coupled to mass spectrometry-based proteomics studies, *Journal of Chromatography A*, 2015, 1412, 75-81.
- **Jiang S**, Zhang Z, Wang J, Li L, Purification of peptides and targeted biomarkers from biological subject by monolithic affinity chromatography. *In preparation*.
- **Jiang S**, Stallop L, Zhang X, Li L, Beebe D, Real time mass spectrometric analysis of secreted proteins and endogenous peptides by microfluidic device integrated with LC MS/MS and MALDI mass spectrometric imaging. *In preparation.*
- Liang Z, **Jiang S**, Li L, Monitoring neuropeptide degradation via *in vivo* microdialysis by trace-level mass spectrometric imaging. *In preparation.*
- Zhang Z, **Jiang S**, Li L, Semi-automated liquid chromatography-mass spectrometric imaging platform for enhanced detection and improved data analysis of complex peptides, *Journal of Chromatography A*, 2013, 1293, 44-50.
- Zhong X, Zhang Z, **Jiang S**, Li L, Recent advances in coupling capillary electrophoresis-based separation techniques to ESI and MALDI-MS, *Electrophoresis,* 2014, 35, 1214-1225.

Presentations

- Oral presentation (1st author): at the 2015 American Society for Mass Spectrometry (ASMS) Annual Conference entitled “Identification of metabolites in crustacean hemolymph via *in vivo* microdialysis by capillary electrophoresis coupled to MALDI mass spectrometric imaging platform”.
- Poster presentations (1st author): entitled "Integration and application of separation strategies to multiplex imaging mass spectrometry for complex neuropeptide analysis" at the 2014 ASMS conference.
- Poster presentations (1st author): entitled "Development and application of monolith-based approaches coupled to mass spectrometry for enhanced proteomics and peptidomics" at the 2013 ASMS conference.